Nagy András Lajos

Oil degradation and engine wear due to alternative fuels

Doctoral dissertation

Supervisor

Dr Zsoldos Ibolya, Department of Materials Science and Technology, Széchenyi István University

2022

Doctoral School of Multidisciplinary Engineering Sciences

Table of Contents

Declaration of originality

I hereby declare, that the following thesis was written by myself, the presented results, images and graphs are a product of my work, unless stated otherwise.

Some parts of the thesis include verbatim copies of previously published, personally authored scientific articles.

Acknowledgement

As many other things in life, scientific research is a team effort. I'd like to thank the following people, colleagues and friends for their support, their contribution, their guidance and constructive criticism throughout the years, and for helping me along the way.

Funding

Abstract (EN)

Throughout my PhD research I have been studying engine oil degradation from the perspective of a mechanical engineer. Oil aging can be crucial in the wake of alternative fuel technologies, as fuelling affects physical, and chemical properties, as well as the longevity of the lubricant. Ensuring fuel-oil-compatibility is an essential factor for successful bridge technologies towards a carbon-neutral future.

The following doctoral dissertation presents the steps I've taken and findings I've encountered during investigating engine oil aging under real-life and laboratory conditions. I have researched the scientific literature of biogenic and synthetic liquid fuels for passenger cars to form a basis for my investigations. I delved into engine oil composition, aging, and degradation to understand the underlying processes. I've conducted friction and wear experiments to explore the effect of synthetic fuels on the tribology of mechanical systems. I studied data available from previous engine dyno experiments to grasp the effects of oil aging and degradation. To ensure repeatability and reliability I developed an artificial aging apparatus for engine oils, and conducted numerous artificial aging experiments with various parameter setups. As a follow up, I designed and conducted a field study with 12 vehicles, gathered 47 oil samples and analysed vehicle utilization and oil condition data. I interpreted and correlated my findings, and validated the output of my aging procedure. My research has led me to the following new scientific results:

- I have found evidence, that the presence of oxymethylene ether, a proposed alternative fuel affects engine oil aging under laboratory conditions, resulting in elevated wear rate and a transition in the dominant wear phenomenon from abrasion to surface fatigue (pitting) in a ball-on-disc model study.
- I demonstrated the applicability of my aging apparatus and methodology to produce artificially aged engine oil samples with comparable chemical properties to an in-use sample from a gasoline engine after 7 000 km of mixed utilization.
- I correlated vehicle utilization properties e.g. use patterns and the number of cold starts to oil degradation mechanism e.g. oxidation and fuel dilution in a fleet with similar motorisation.

Abstract (HU)

Doktori kutatásom során mérnöki szemmel vizsgáltam meg a motorolajok öregedésének folyamatait. A kenőolajok degradációja az alternatív tüzelőanyagok térnyerésével központi kérdéssé válhat, mivel a tüzelőanyag befolyásolja az olaj fizikai, kémiai tulajdonságait és élettartamát. A kenőolajok és tüzelőanyagok összeférhetőségének biztosítása elengedhetetlen a karbonsemleges jövő felé vezető úton.

A doktori értekezésemben bemutatom a valós és laboratóriumi körülmények között végzett motorolaj öregítési vizsgálatok lépéseit, valamint az elért eredményeket. Kutatásomat a biogén és szintetikus eredetű folyékony személygépjármű hajtóanyagok szakirodalmának tanulmányozásával alapoztam meg. Megismertem a kenőolajok összetételét, illetve öregedési és degradációs folyamatait. Golyó-tárcsa tribológiai vizsgálatokon keresztül feltártam a szintetikus tüzelőanyagok mechanikus rendszerekre gyakorolt hatását. Korábbi motorfékpadi kísérletek eredményeit tanulmányozva tártam fel a motorolaj elhasználódásának összefüggéseit. A megismételhetőség és megbízhatóság biztosítása érdekében saját kenőolaj öregítő berendezést fejlesztettem, amivel számos öregítési kísérletet hajtottam végre, különböző paraméterek mellett. Ezt követően 12 jármű részvételével flottakísérletet állítottam össze, melyből 47 levett olajminta tulajdonságait vizsgáltam a jármű-használati adatok tükrében. Az eredmények értelmezése és korrelációja után validáltam a mesterséges öregítés végtermékét. Kutatásom során az alábbi új tudományos eredményeket állapítottam meg:

- Bizonyítékot találtam arra, hogy az oximetilén éter, mint szintetikus alternatív tüzelőanyag hatással van a motorolaj laboratóriumi öregítésére, amely golyó-tárcsa kísérletek során megnövekedett kopássebességhez és a domináns kopásfolyamatot abrazívból a gödrös kopás irányába módosítja.

- Bemutattam a fejlesztett olajöregítő berendezés és eljárás alkalmasságát olyan mesterséges használt olaj minták előállítására, melyek egy 7 000 km futású benzin üzemű járműből származó használt olajjal összemérhető kémiai tulajdonságokat mutatnak.

- Összefüggést találtam a járműhasználati paraméterek, pl. jelleg, hidegindítások száma, és a kenőolajöregedési jellemzők, pl. oxidáció és hígulás között egy közel azonos motorizációjú flotta esetén.

Abbreviations

This section summarizes abbreviations found in the thesis in the order of their appearance. Product names (e.g. SRV5), sample identifiers, and common abbreviations (e.g. E10, SD or LCD) are not included in the list.

WLTP	Worldwide Harmonized Light-Duty Vehicles Test Procedure
SCR	Selective Catalytic Reduction
DI	Direct Injection
PAO	Poly-Alpha-Olefin
ZDDP	Zinc-Dyalkilditiophosphate
SAE	Society of Automotive Engineers
OEM	Original Equipment Manufacturer
API	American Petroleum Institute
DOHC	Double Overhead Camshaft
RON	Research Octane Number
DISI	Direct Injection Spark Ignition
GC-MS	Gas Chromatography Mass Spectroscopy
SPI	Stochastic Pre-Ignition
ULSD	Ultra-Low Sulfur Diesel
ASTM	American Society of Testing and Materials
TAN	Total Acid Number
TBN	Total Base Number
DPF	Diesel Particulate Filter
GC	Gas Chromatography
FTIR	Fourier Transformed Infrared (Spectroscopy)
IC	Internal Combustion
EHD	Elasto-Hydrodynamic
DLC	Diamond-like Carbon
LOME	Linseed Oil Methyl-Ester
CIDI	Compression Ignition Direct Injection
FAME	Fatty Acid Methyl-Ester
NEDC	New European Driving Cycle
CNG	Compressed Natural Gas
DME	Dimethyl-Ether
HC	Hydrocarbons
PM	Particulate Matter
PN	Particulate Number
KOME	Karanja Oil Methyl-Ester
RME	Rapeseed Methyl-Ester
WEO	Waste Edible Oil

OMDME	Oxymethylene Dimethyl Ether
DMF	Dimethyl Furan
EGR	Exhaust Gas Recirculation
HFRR	High-Frequency Reciprocating Rig
WSD	Wear Scar Diameter
CoF	Coefficient of Friction
HD	Hydrodynamic
PVD	Physical Vapor Deposition
ISO	International Standardization Organization
DSLR	Digital Single Lens Reflex
SEM	Scanning Electron Microscope
VI	Viscosity Index
DIN	Deautscher Institute für Normung
ICP-OES	Inductively Coupled Plasma Optical Emission Spectroscopy
FID	Flame Ionisation Detector
GUI	Graphical User Interface
PWM	Pulse Width Modulation
SUV	Suburban Utility Vehicle
GPS	Global Positioning System
IQR	Interquartile Range
PCA	Principle Component Analysis
OME	Oxymethylene Ether
AAT	Antiwear Additive Test
EPT	Enhanced Pressure Test
AWSD	Averaged Wear Scar Diameter
WOT	Wide Open Throttle
KV40	Kinematic Viscosity at 40°C
KV100	Kinematic Viscosity at 100°C
ST	Soot
OCI	Oil Change Indicator
OAh	Oil Age in hours
DMC	Dimethyl Carbonate
TDC	Top Dead Center

1   Introduction

This thesis summarizes the results of independent and joint research activities in the field of internal combustion engine tribology. The main focus of the presented research activities is engine oil aging in conjunction with fuel dilution. Most research activities – including friction and wear experiments, artificial engine oil aging, data analysis and post-processing – were carried out at the Department of Internal Combustion Engines and Propulsion Technology of Széchenyi István University (University of Győr). Preliminary oil aging experiments and oil analysis were performed by MOL-Lub Kft. In-depth oil analysis was carried out by the Austrian Competence Centre for Tribology (AC2T GmbH).

1.1   Motivation

Environmental concern is the main driving force of automotive powertrain development of the early 21st century. The process of approval of motor vehicles entering the market in the EU dictates stringent limits for passenger cars and light-duty vehicles. In addition to conventional emission measurements on a chassis dynamometer according to the Worldwide harmonized Light vehicles Test Procedures (WLTP) [1], newly approved vehicles are subjected to emission testing under realistic driving conditions [2]. To meet the current emission target, vehicles manufacturers have to implement numerous novel technical solutions regarding engine construction, engine operation and exhaust gas aftertreatment.

Downsizing can still be considered as a common engine development trend [3], with small 3- and 4-cylinder engines being the base motorization in most manufacturers line-up. Traditional optimization of core engine components could still improve the overall weight and mechanical losses of the whole package. Improving components through a conventional mechanical focused engineering approach can have a large impact on efficiency, but modern powertrains have achieved the point where such improvements cannot contribute to a significant level of emission reduction, at least not in an economical way [4].

Advanced powertrain technologies e.g. variable compression ratio [5], [6], over-expansion cycles [7], [8] and water injection [9] are gradually appearing in series production vehicles, [10], [11], [12]. The application of these techniques can lead to

decreased exhaust gas temperatures and increased efficiency, resulting in reduced NO_x and CO_2 emissions. Novel exhaust gas aftertreatment technologies e.g. low-temperature SCR [13] and Gasoline Particulate Filters [14] are also applied in new vehicles in order to meet tailpipe emission targets. The introduction of biologically sourced and synthetic components into the fuel itself could further help to reduce local and global emissions of CO_2, NO_x and solid particles [15], [16].

Powertrain hybridisation offers reduced harmful emission by shifting the operation range of the internal combustion engine to avoid operating conditions with low efficiency and high harmful emission – idling and low-load, typically [17], [18]. Furthermore, reducing the operation time of the internal combustion engine in slow moving traffic and metropolitan areas in general decreases local emissions. The use of 48-volt mild-hybrid technology is wildly spread in the industry, since it offers a good balance between development and production costs and emission reduction [19]. In addition, electrically aided turbochargers can also be implemented, which lead to improved drivability and thermal efficiency in the lower load regions [20]. Combining these advanced technologies can yield significant reduction in both fuel consumption and harmful exhaust components [21], [22].

The widespread utilization of alternative fuels and hybridisation can present new challenges to automotive lubricant development. Previously absent species of combustion by-products and fuel components could affect oil aging and induce increased wear on the contact pairs and bearing surfaces of an internal combustion engine. For a successful introduction of carbon-neutral biogenic and synthetic fuels, their compatibility with the existing vehicle fleet in terms of chemical and physical properties has to be assured. Biofuels and synthetic fuels, which require little to no modifications to in-use vehicles can be considered as drop-in alternatives. The thermodynamic behaviour, emissions, cost of production and effect on the fuel system of such non-fossil fuels are a vital part of their assessment. Long-term effects of alternative fuels on the internal combustion engine as a complex tribosystem must be considered as well.

With many nations planning a phase-out of pure internal combustion engine drivetrains in new vehicles during the next decade, the automotive industry and energy sector faces a fundamental transformation. Despite the heavy lobby against the internal

combustion engine, the world's present passenger car and commercial vehicle fleet operates mainly on some form of traditional fuel. Developed countries may be able to afford gradually replacing every conventional car and truck with a so called "zero-emission" vehicle in a 15 to 20-year period, but developing countries will need more time for the transition. To aid the transition and ease its financial burden, the development of synthetic and biofuel technologies is a necessary bridging solution to a lower emission future.

1.2 Goal and hypotheses

The goal of my PhD research was to establish a methodology to evaluate the long-term effect of alternative fuels on engine oil aging and the consequent alteration in friction and wear. In order to lay out the key scientific aspects of my research, I have formulated the following hypotheses:

Hypothesis #1: Alternative fuels can contribute to an accelerated degradation of engine oils, which will have an effect on friction and wear of engine bearings and load bearing surfaces.

Hypothesis #2: An artificial aging method can be used to simulate in-use engine oil aging and produce aged samples with comparable physical and chemical properties to real-life used oil.

Hypothesis #3: Engine oil aging is heavily influenced by vehicle use, which, in some way, can be traced back to the recurrence of severe operating conditions.

2   Fundamental of friction, wear and lubrication

This section gives a brief introduction to the most common friction and wear phenomena inside internal combustion engines, as well as to the engineering surface, the scene of all tribological phenomena. Furthermore, this section introduces the reader to the composition of modern engine oils, and the degradation mechanisms of oils as a result of in-use effects. The majority of moving elements in an automotive powertrain exhibits friction and wear during operation. A high coefficient of friction is generally considered to be a main contributor to increased fuel consumption and CO_2 emission. Hence, the application of a lubricant is preferred, where possible. The presence of a lubricating fluid reduces asperity contacts and introduces favourable friction and lubrication regimes. Using a lubricant also contributes to controlling and reducing wear on the load bearing surfaces.

2.1   The engineering surface

The engineering surface is the collection of adjoined layers sheathing the bulk material. These layers emerge as a result of various manufacturing processes, oxidation, adsorption of lubricant additives and contamination with dirt. For most engineering applications the mechanical properties of a part or material correspond to the bulk. However, the engineering surface can show distinct mechanical, physical and chemical properties, which play a significant role in governing the tribological process in rolling and sliding contacts. According to Schmaltz [23], the engineering surface depicted on Figure 1 can be divided into 3 layers:

- deformation layer,
- oxidized or reaction layer,
- adsorption layer.

The deformation layer consists of the same base material as the bulk, but have undergone some amount of recrystallization. The deformation layer is a product of the manufacturing process, usually associated with machining, grinding and polishing; however, this layer can also develop and transform due to the shear stresses during sliding contact. A common property of the deformation layer is a finer grain structure, which results in a significant increase in hardness compared to the bulk. The deformation layer has a thickness of more than 5 μm.
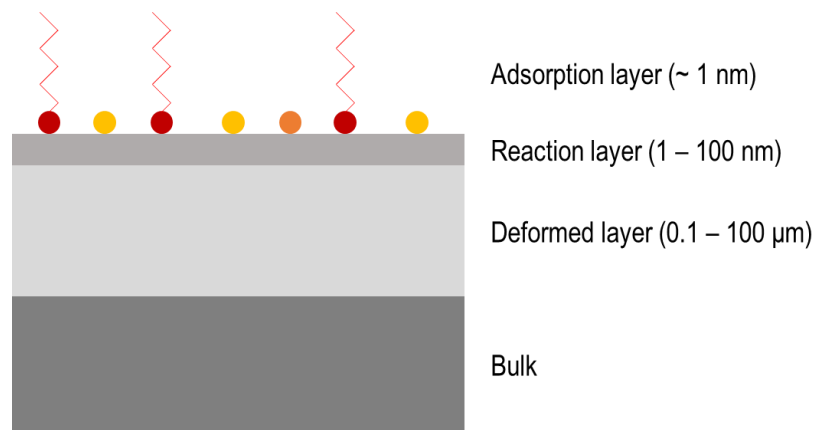
Figure 1. Layers of the engineering surface according to Schmaltz [23]

The oxidized layer or reaction layer forms on top of the deformation layer in the presence of oxygen, if the material of the deformation layer is chemically active. Most technical applications rely on ferrous and nonferrous metals as the base stock for manufacturing, which are prone to oxidation. Depending from the material, the oxide can exhibit hardness values an order of magnitude higher compared to the bulk. As a result, worn down oxide particles can participate in the tribological process and lead to increased abrasion. The oxidized layer has a typical thickness of 1 to 10 nm.

The reaction layer is also chemically active, hence foreign compounds – i.e. surface active additives from a lubricant – can bond to it, forming an adsorption layer on the outer perimeter of the engineering surface. Some sources distinguish between an adsorption layer and a contaminant layer, which is formed through the unintentional pollution of the surface by dirt and debris. The contaminant layer can exist in place or on top of the adsorption layer. The presence of an adsorption layer is favourable in many applications as detailed in Chapter 2.4.1, whereas unwanted pollutants can introduce increased wear. The adsorption layer has under 1 nm thickness.

For the sake of simplicity, the "engineering surface" is referred to as "surface" in the following.

2.2 Friction and lubrication regimes

The state in which a lubricated system is operating at any time is influenced by multiple aspects. The main contributing conditions are sliding speed, contact pressure, temperature, type of lubricant and surface roughness. Depending from these factors a lubricated sliding pair can exhibit one of three main states of lubrication:

- boundary lubrication,
- mixed lubrication,
- hydrodynamic lubrication.

A common method of portraying the lubrication regimes of a sliding surface pair is the Stribeck curve. Figure 2 presents an idealized Stribeck curve of a model tribological system. The Stribeck curve depicts the coefficient of friction as a function of the Hersey number, a dimensionless parameter formed from the sliding speed (v), contact pressure (P) and dynamic viscosity (η), or as a function of λ, the ratio of lubricant film thickness (d) to the reduced surface roughness (R_{xy}):

$$Hersey\ number = \frac{\eta v}{P}$$

$$\lambda = \frac{R_{xy}}{d}$$

As suggested by the above expression, surface roughness has a significant influence on the dominant friction and lubrication regime of a tribosystem. Although the above definition utilizes a reduced roughness of both surfaces in contact, the general practice for characterizing the lubricant retention capability of a surface is through the Abott curve. Figure 3 presents the Abott curve and the related areal functional S_k parameters of a plasma spray coated cylinder surface. The Abott curve or Abott-Firestone curve is the cumulative distribution curve of heights, which can be interpreted both for roughness profiles and surfaces. S_k parameters according to ISO 25178 [24] are derived from the R_k parameters defined for profiles by ISO 13565-2 [25]. S_k parameters describe the core roughness (S_k), as well as the reduced peak (S_{pk}) and valley roughness (S_{vk}) of a profile, with the corresponding lower (S_{mr1}) and upper (S_{mr2}) material ratio. A high S_{vk} and low S_{mr2} value hints at better oil retention capabilities.

Boundary lubrication is governed by a thin surface layer of contaminants, oxides and lubricant additives which are embedded into the surfaces of the sliding pair. This regime of lubrication is dominated by asperity contacts and characterised by a relatively high coefficient of friction. The boundary lubrication regime is depicted on the left side of the Stribeck curve. A system is considered to exhibit boundary lubrication if λ < 1 is calculated or measured.
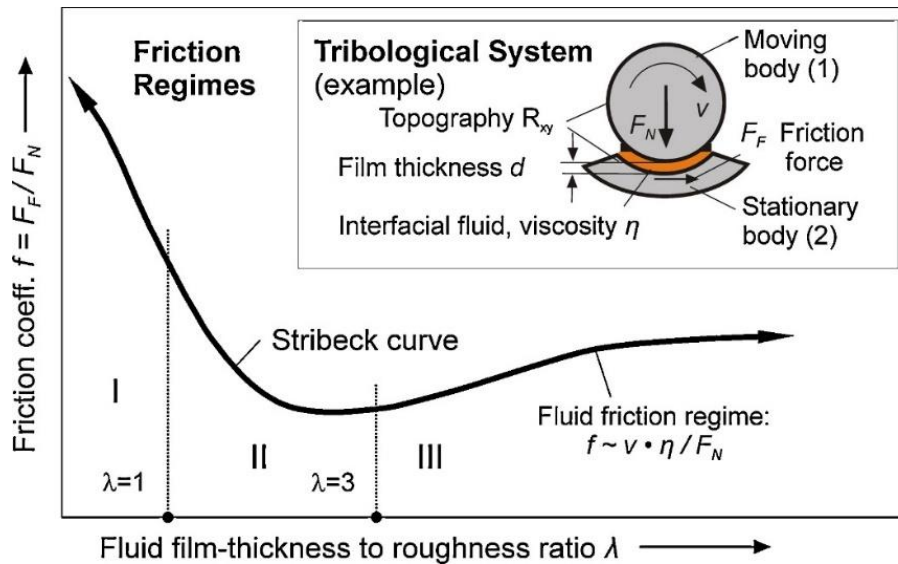
Figure 2. Characterisation of friction regimes using the Stribeck curve [26]

Mixed lubrication involves a partially formed hydrodynamic oil film on the surface, but contact between surface asperities is still possible, thus resulting in a mixture of fully separated and directly contacting regions on the mating surfaces. This lubrication regime enables a reduced coefficient of friction compared to boundary lubrication. The mixed lubrication regime is depicted in the middle region of the Stribeck curve. A system is considered to exhibit mixed lubrication if the measured or calculated value of λ lied between 1 and 3.

Sk	0.704	µm
Spk	0.189	µm
Svk	3.79	µm
Smr1	7.89	%
Smr2	76.4	%
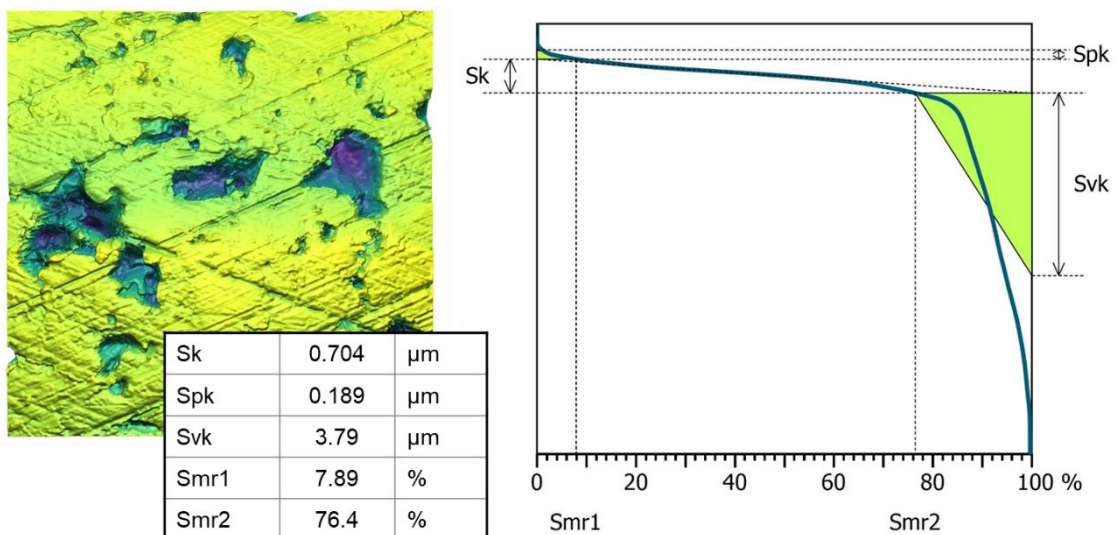
Figure 3. Areal functional parameters derived from the Abott-Firestone curve of a honed plasma spray coated cylinder surface. The large voids in the coating contribute to a relatively high S_{vk} value compared to the S_{pk} and S_k roughness

Hydrodynamic lubrication is characterized by the fluid film, which is formed between the contact surfaces. The fluid film separates the two surfaces completely, thus

eliminating the possibility of asperity contacts. The coefficient of friction is determined by the viscosity – i.e. the internal friction – of the lubricant. Hydrodynamic lubrication is depicted on the right side of the Stribeck curve. A system is considered to exhibit hydrodynamic lubrication if λ > 3 is measured or calculated.

Hydrodynamic lubrication is the preferred lubrication regime in case of sliding bearings, geared transmissions, chain drives and most other contacting surfaces in an internal combustion engine. In order to achieve hydrodynamic lubrication, the following criteria has to be met:

- the lubricant is able to adhere to the mating surface,
- the mating surfaces move with different velocities,
- the macro-geometry of the mating surfaces forms a wedge.

Adherence is achieved with appropriate surface roughness and oil viscosity, as well as with selected oil additives to increase cohesion. A difference in velocity is inherently given by a number of lubricated subsystems of an engine, where one of the mating bodies is stationary e.g. the cylinder wall, or the main bearing shell of a crankshaft. A wedge-shaped geometry is also present in case of the crankshaft or timing shaft bearings. Other subsystems e.g. the piston ring – cylinder wall pair utilize special surface geometry designs to achieve a wedge and facilitate lubricant film formation.

It should be mentioned, that some subsystems of an internal combustion engine can utilize purely hydrostatic lubrication. Since hydrodynamic lubrication implies higher demands on the lubricating medium, hydrostatic lubrication is not discussed in detail in this thesis.

2.3   Common wear mechanisms in internal combustion engines

Depending on the lubrication and surface quality, different wear mechanism can occur between the surfaces of a sliding pair. The four most common manifestations of wear between sliding surface pairs of machines and engines as summarized by Zum Gahr [27] are:

- abrasion,
- adhesion,
- surface fatigue (pitting),

- tribochemical reactions,
- erosion and cavitation.

Abrasive wear (Figure 4 a) can occur in systems of two surfaces with distinct surface hardness, or in the presence of a third body (foreign particle) with significantly higher surface hardness as the surfaces of the sliding pair. During the abrasion process asperities of the harder surface penetrate into the softer counterpart due to the normal load, and a given amount of material is displaced due to the sliding motion. A tendency of a material to exhibit abrasive wear can be correlated to its hardness and plasticity, but additional factors e.g. lubrication and surface roughness also influence wear mechanisms in a complex system.
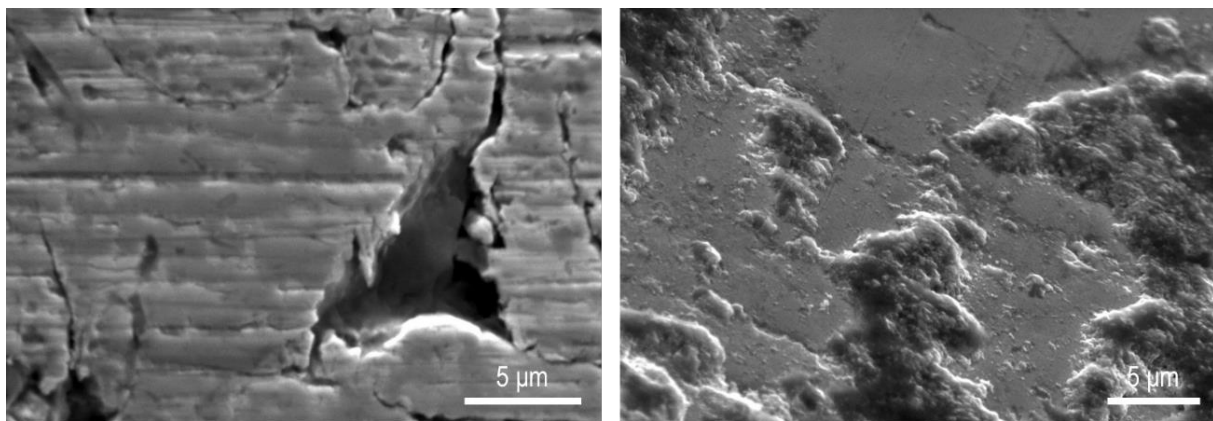
a) Abrasive wear: broader and thinner longitudinal marks on chrome steel liner coating

b) Adhesive wear: Fe and oil residue deposited on Cr-coated piston ring

Figure 4. Typical adhesive and abrasive wear marks on internal combustion engines parts (scanning electron microscope images by the author)

Depending from the hardness difference, environmental factors and the frequency of engagement abrasive wear processes can exhibit the following sub-mechanisms:

- micro-cutting: the penetrating asperity removes material from the softer body
- micro-ploughing: the penetrating asperity displaces material on the surface
- micro-fatigue: material removal due to repeated material displacement
- micro-cracking: material removal on brittle surfaces due to sub-surface crack formation and propagation

The two most common abrasive sub-mechanisms in lubricated metal-metal contacts are depicted on Figure 5.

a) micro-cutting	b) micro-ploughing
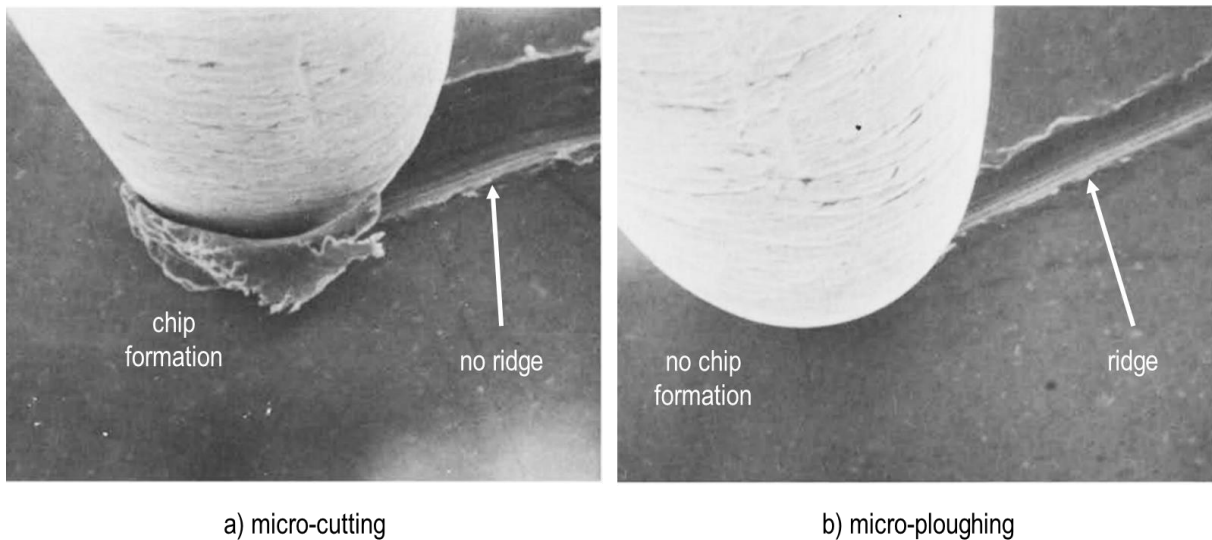
Figure 5. Sub-mechanisms of abrasive wear from a model study by Hokkirigawa and Kato [28]

Adhesive wear (Figure 4 b) can occur due to mechanical interlocking or atomic forces binding the contacting surfaces together during the sliding motion. The adhered region of the surfaces gets torn apart as the parts move forth, which results in dales and material deposits on the surfaces. Certain materials have a higher tendency to develop adhesive wear under high normal load and starved lubrication or dry running conditions. The main contributing factor to the tendency of a material to adhesive wear is its shear strength. In general, materials with lower surface hardness and shear strength tend to exhibit higher rates of adhesion.

Fatigue wear (Figure 6 a) is characterized by crack formation and propagation on the surface layer due to fatigue, which is the result of a high cyclic load being exerted on the surface. Surface fatigue usually occurs under boundary and mixed lubrication, where higher shear forces act on the surfaces in contact. Machine elements with high concentrated contact pressures like ball bearings or gears tend to be more prone to fatigue wear.

A tribochemical reaction is a chemical reaction of surfaces of the sliding pair with each other, the interfacial medium (i.e. lubricant) or the environment, which occurs while cyclic tribological stress (contact pressure, heat and relative motion) is exerted on the surfaces (Figure 6 b). The reaction products wear away and reform in each cycle as a result. This chemical reaction consumes the contacting bodies and the interfacial medium, which leads to a loss of material – i.e. wear – on the participating surfaces.

a) Lapped 100Cr6 steel surface after HFRR oil test

b) Debris on a WC/Co hard metal surface after repeated scratch testing in HCl
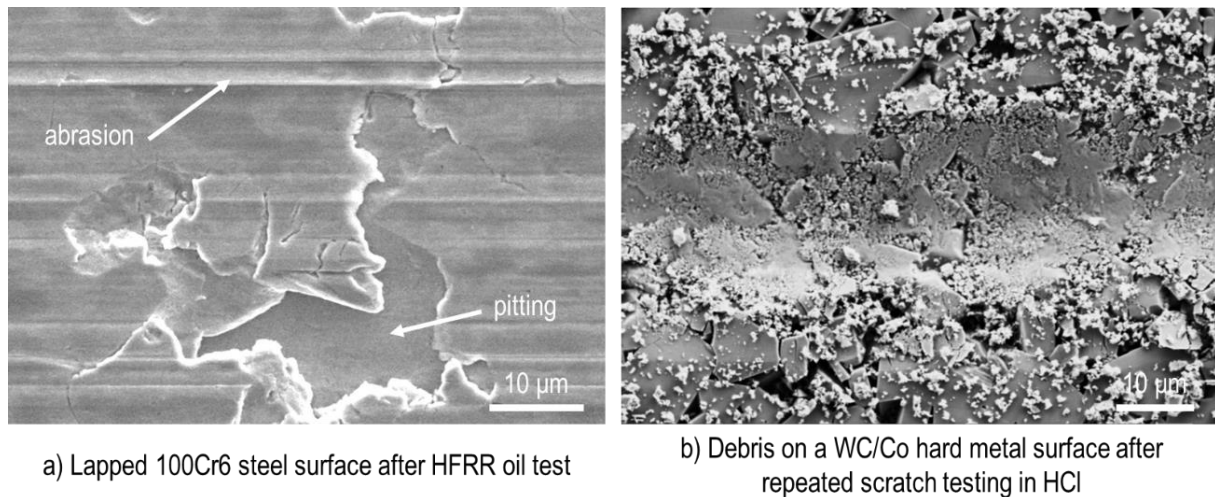
Figure 6. Typical appearance of fatigue wear (pitting), and tribochemical wear as presented by Gant et al [29]

Erosion is the process of material removal from a solid surface through a flowing gaseous or liquid medium. Most commonly, erosion is the phenomenon shaping river beds, coastlines and mountain ranges. Cavitation can appear at the interfaces of systems where fast-moving pressure waves are able to travel in a liquid medium. Due to the severe drop in local pressure behind the pressure front (e.g. the inner wall of a pipe) the fluid can start to boil and form small bubbles. As the pressure wave passes, the newly formed bubbles rapidly collapse and exert a striking load on the nearby interface, which over time can lead to the removal of material. As this thesis focuses on the wear of bearing surfaces, erosion and cavitation are not considered further.

2.4 Composition and properties of modern engine oils

Lubricating oil dilution, consumption and degradation of internal combustion engines is a known issue since the dawn of the automotive industry and still a permanent threat in the age of charged direct injection (DI) engines and hybrid powertrains. The lubricant in an engine serves multiple purposes, which demands a complex formulation in order to fulfil its function. Aside from friction and wear reduction the oil protects engine parts against corrosion and oxidation, removes third bodies from sliding pairs, transfers heat away from core engine components and helps in achieving appropriate sealing and reducing vibration.

An engine oil is composed of a base oil and an additive package [30]. Modern engine oils are mostly poly-α-olefin (PAO) based, which is a synthetic compound. The base oil itself has inferior properties as an engine lubricant, hence the addition of a selection

of chemical compounds (additives) is necessary to achieve the desired physical and chemical properties. Additives aim at enhancing a specific property of the formulation. A certain property can be achieved through multiple different chemical compounds, but the reaction of these compounds with each other must be considered during the formulation of the lubricant.

Based on Torbacke et al [31], lubricant additives can be categorized into two groups:

- surface active additives, that act on liquid-liquid, liquid-solid or liquid-gas interfaces, and
- bulk active additives, that take effect within the liquid.

2.4.1   Surface active additives

Surface active additives provide corrosion and wear resistance on solid surfaces, and also assist in reducing friction. These additives consist of a polar moiety and a hydrocarbon chain. Surface active additives interact with surfaces, that have available electrons to form a bond through physisorption, chemisorption or a chemical reaction. Most commonly utilized surface active additives in engine oils are:

- corrosion inhibitors,
- friction modifiers,
- antiwear additives
- defoamers.

Corrosion inhibitors are mainly film-forming additives that bind to the surface by physisorption or chemisorption in order to reduce the surfaces chemical reactivity with the environmental medium. Adsorbed corrosion inhibitors form a protective film, thus preventing metal surfaces from getting into contact with water, oxygen or acidic compounds formed during engine operation. Commonly used corrosion inhibitor additives consist of long chain amines, sulfonates, phosphites and carboxylic acids.

Friction modifiers are added to engine oils to reduce friction in the mixed lubrication regime (Figure 7 b). Friction modifiers adsorb to the contacting surfaces under moderate temperatures and loads through physisorption. However, severe load will lead to the desorption of the additive. Friction modifiers can bond to themselves and form multilayers in the lubricant (Figure 7 a), which facilitates the separation of

asperities. Friction modifier layers also yield easily to tangential load, which both contribute to the reduction of friction between the surfaces. Frequently used friction modifier compounds involve saturated fatty acids with 13 to 18 carbon atoms.

a) Stylized multi-layers of friction modifier additive, with easily shearable bonds between hydrocarbons

b) Active regions of extreme pressure (EP), antiwear (AW) and friction modifier (FM) additives
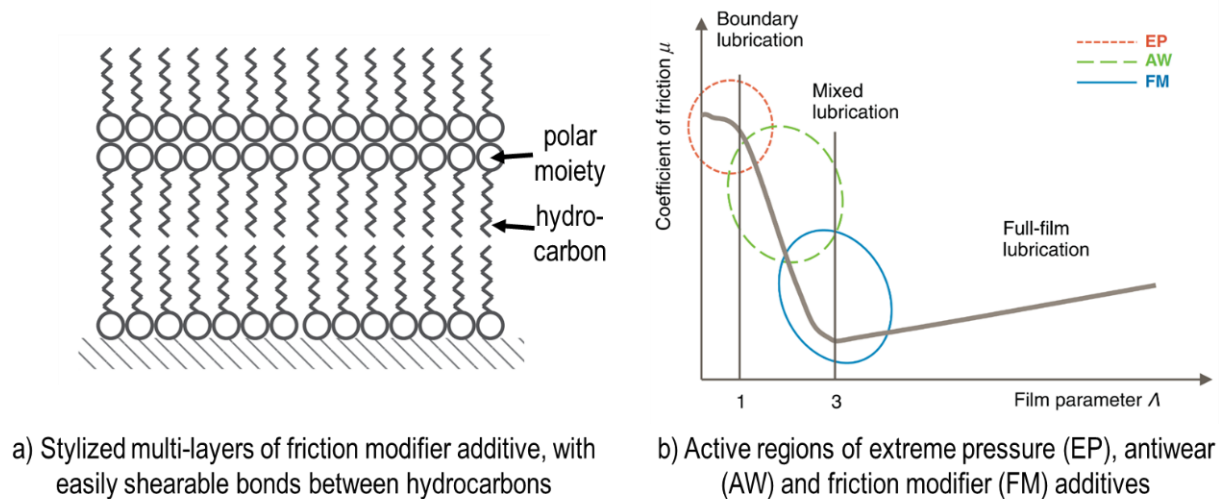
Figure 7. A stylized representation and area of activity for friction modifier additives as presented by Torbacke at at. [31], where Λ is the ratio of oil film thickness to the combined roughness of contacting surfaces

Antiwear additives alter the surface of metals in order to reduce wear in the mixed lubrication regime. Antiwear additives bond to the surface primarily through chemisorption at a comparably higher activation temperature and load than friction modifiers. The predominantly used antiwear additive in engine oils is zinc dialkyldithiophosphate (ZDDP), that simultaneously acts as an antioxidant and detergent additive as well.

Defoamers prevent the formation and growth of foam – i.e. air trapped in the lubricant – in engine oils. Foam formation hinders the oil pumps ability to transport the lubricant, which can lead to the starvation and damage of lubricated contacts. The crumbling of air bubbles near to solid walls can also lead to material removal through cavitation. Defoamers facilitate the rupture of the lubricant film surrounding the entrained air by decreasing its thickness. Consequently, these additives hinder the effect of some detergents, dispersants and viscosity modifiers. Defoamers often consist of silicone oils or polymethacrylates.

2.4.2 Bulk active additives

Bulk active additives are larger macromolecules, which engage with other compounds and materials in the lubricant. Bulk active additives are either physically active through

steric action – intramolecular interaction without bonding – or chemically active. The most common bulk active additives in engine oils are:

- viscosity modifiers,
- pour point depressants,
- dispersants,
- detergents,
- antioxidants.

Modern engine oils function over a wide range of temperatures, hence a means of providing appropriate viscosity at all relevant operating temperatures is necessary. Viscosity modifiers employ steric action to increase the viscosity of the base lubricant. Viscosity modifiers are large, long chain molecules with short hydrocarbon branches, which expand due to thermal energy. Their activation is proportional to temperature, thus introducing a negligible change in viscosity in low-temperature environments and exerting a more pronounced thickening effect at higher operating temperatures (Figure 8 a). Today's viscosity modifiers are either olefin copolymers or ester polymers.

Pour point depressants influence a lubricants physical properties in the low temperature regime by hindering wax crystallization through steric action. The application of pour point depressants ensures appropriate cold flow and pumpability of an engine oil by lowering its pour point (Figure 8 b). This effect is frequently achieved with alkylated wax naphthalenes or polymethacrylates.
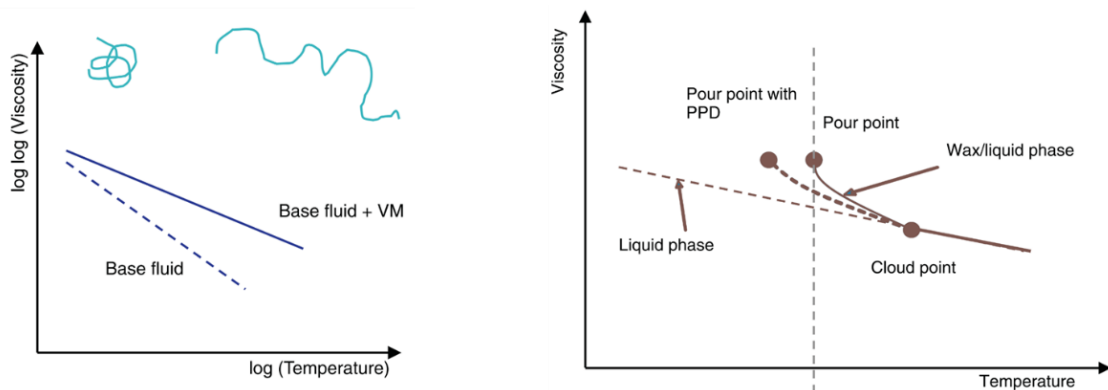
a) Temperature dependence of base fluid viscosity with and without viscosity modifiers

b) The effect of pour point depressants (PPD) on the phase of the lubricant

Figure 8. Influence of viscosity modifiers and pour point depressants on viscosity over temperature as presented by Torbacke at at. [31]

Dispersants are used to improve filterability and prevent blockages in the oil system by capturing and retaining foreign particles in the lubricant. Dispersants are similar to surface active additives in their structure, with a weak polar moiety to bond to polar contaminants and a hydrocarbon chain to exert steric repulsion. Hence, dispersants are able to encapsulate dirt or wear debris, prevent particle agglomeration and limit sediment build-up (Figure 9). High molecular polyisobutene succinimide is a commonplace dispersant additive.
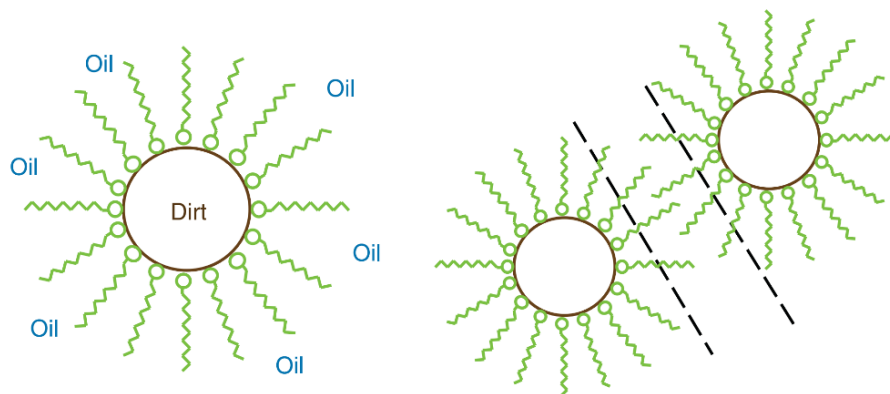
Figure 9. Dispersant additives encapsulate dirt with their weak polar moieties and exert steric repulsion to avoid agglomeration as presented by Torbacke at at. [31]

Detergents in engines oils act as a basic reserve to neutralize acidic combustion by-products. Detergents consist of an oil soluble alkaline salt (e.g. calcium or magnesium), which is enclosed by surfactants with a short hydrocarbon chain and a strong polar moiety (Figure 10). Detergents can be neutrally based or overbased. Neutrally based detergents find use as surface cleaning agents, whereas overbased detergents are widely used in internal combustion engine oils. Certain detergents can also act as antioxidant additives.
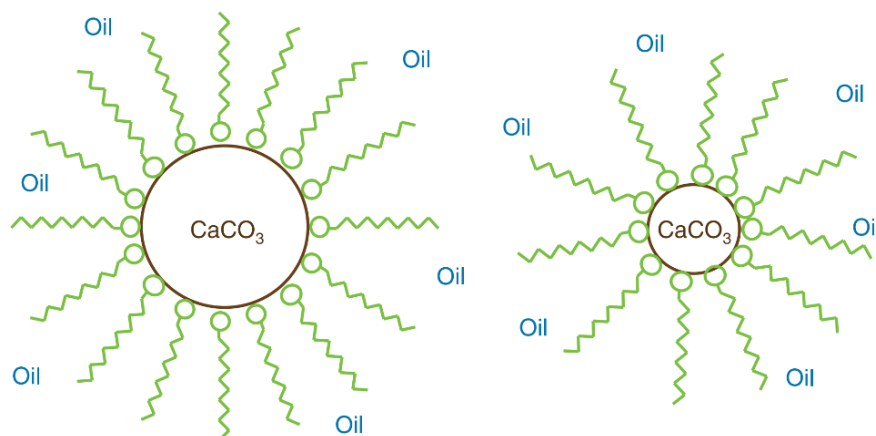
Figure 10. Stylized detergent molecule consisting of an overbased core, which is consumed over time through neutralizing acidic contaminates in the engine oil as presented by Torbacke at at. [31]

Antioxidants decelerate the rate of oxidation in engine oils, hinder varnish formation and limit soft metal corrosion. The oxidation process can be broken down into three main phases: initiation, propagation and termination. During the initial oxidation phase the collision of oxygen with hydrocarbons results in the formation of highly reactive radicals and carboxylic acids, that can attack metal surfaces. During the propagation phase the previously formed radicals react with hydrocarbons to form new radicals. This chain reaction can be terminated by a radical-radical reaction or with the introduction of an antioxidant. Antioxidant behaviour can be achieved through:

- aromatic amines or hindered phenols by converting radicals to alcohols or ring-stabilized radicals,
- hydroperoxide decomposers (e.g. ZDDP) by transforming hydroperoxydes into alcohols,
- salicylic acid derivatives by deactivating metallic surfaces.

2.4.3 Engine oil classification

Commercially available engine oils are generally characterised by their SAE viscosity grade and API service category. OEMs – original equipment manufacturer, i.e. vehicle and/or engine manufacturer – set additional requirements, which are defined by internal standards and assure the compatibility of a lubricant with the OEMs selected products. Depending from the climate an engine can be operated with a single-grade or multi-grade lubricant. A single-grade lubricant is designed to operate under nearly constant environmental conditions, whereas multi-grade lubricants are made to ensure the engines functionality even under severe fluctuations of environmental temperature during their service life (Figure 11). Functionality over a broad temperature range with kinematic viscosity values in an acceptable region is achieved by viscosity modifier additives. OEMs predominantly advise the use of multi-grade engine oils in modern internal combustion engines.

The SAE grade of a multi-grade engine oil is given with a pair of numbers, the first referring to the oils low temperature or "winter" viscosity, whereas the second represents the viscosity of the lubricant at 100°C. The exact temperature to measure the winter viscosity, as well as the determination of the oil grade based on the measured viscosity is given in the SAE J300 standard [33].
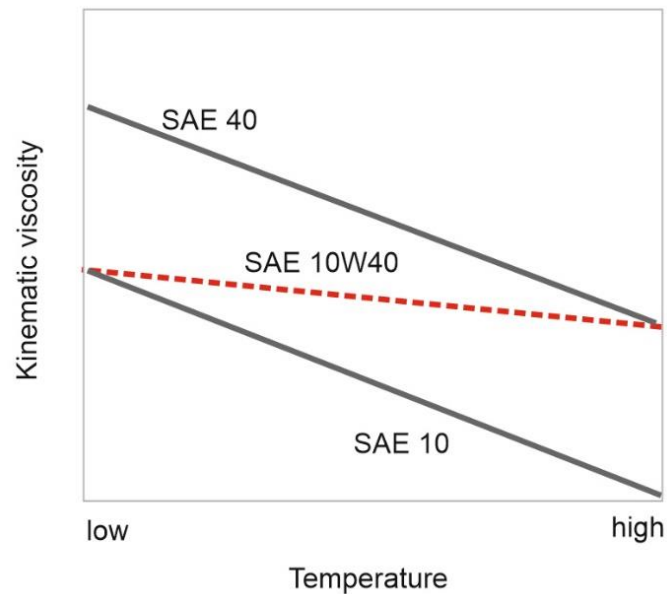
Figure 11. The function of kinematic viscosity over temperature of single-grade (e.g. SAE 10 and SAE 40) and multi-grade (e.g. SAE 10W40) engine oils [32]

The API service category differentiates between gasoline and diesel engines and prescribes functional properties of the engine oil e.g. protection against low-speed pre-ignition, high-temperature deposit protection, sludge and varnish control, as well as compliance with on-highway and on-road exhaust emission limits and compatibility with novel exhaust gas after-treatment systems.

In terms of diagnostic oil properties, a number of features can be evaluated to gain insight into the condition of a lubricant [34]. The most commonly investigated physical and chemical properties of an engine oil are:

- density and kinematic viscosity,
- solid contaminants e.g. soot and wear metals,
- oxidation, nitration and sulfation,
- total base number, neutralisation number, or total acid number,
- residual additive content.

A selection of standardised test methods is available for the determination of engine oil properties, involving financially feasible solution for regular testing and condition monitoring e.g. Fourier-transform infrared spectrum analysis, and more advanced methods for truly in-depth oil chemistry analysis e.g. optical emission spectroscopy and mass spectroscopy.

2.5 Engine oil degradation

Engine oil aging is the degradation of initial oil properties and functionality due to various chemical reactions [34], which occur as a result of high temperature, high shear load and reactive species in the environment e.g. oxygen or ethanol. During the service life of a lubricant the increasing amount of solid contaminants in the fluid can also lead to altered physical properties and decreased wear resistance [35]. These effects cannot be fully mitigated, hence a continuous condition monitoring and regular oil change in the lubricated system is necessary to assure long-term reliability and functionality.

2.5.1 Oxidation

Oxidation and thermal degradation is the main contributor to engine oil aging. Present-day engine oils include numerous additives with oxidation inhibiting properties, which moderate the formation of polar compounds – e.g. aldehydes, ketones, oxygenated polymers, or carboxylic acids. These polar reaction products can lead to deposit and sludge formation, or can exhibit corrosive properties. Sediments, sludge (Figure 12 a) and resin could block the main oil gallery, or hinder oil collection through the recirculation channels, which can cause severe engine malfunction or failure.

a) Gelling and sludge formation, presumably due to missed oil change

b) Contamination with engine coolant, presumably due to a cylinder gasket failure
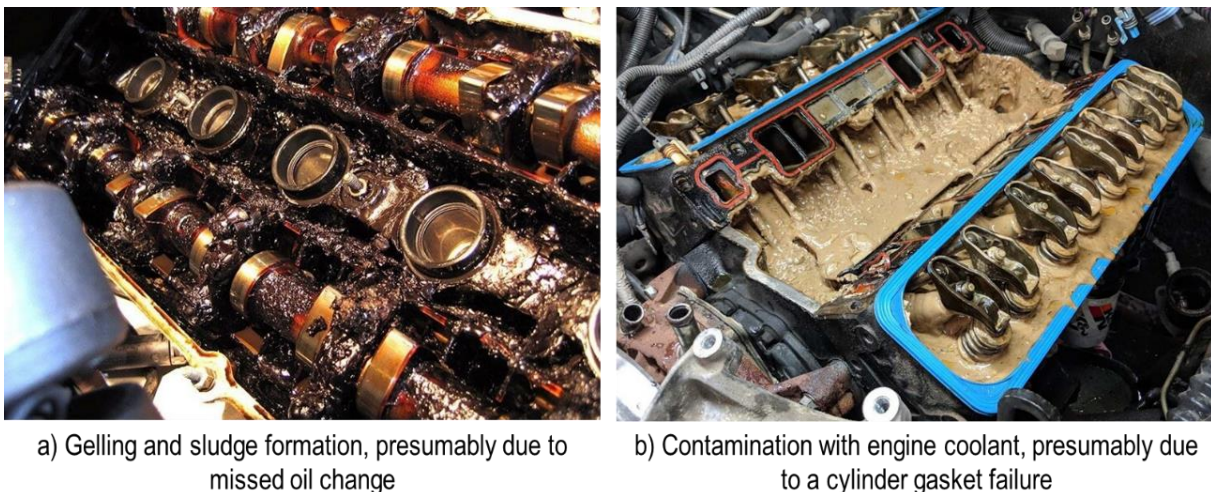
Figure 12. Aging and degradation of engine oil due to overloading [36] and contamination [37]

The base oil used to produce a specific formulation is highly influential regarding an engine oils oxidation resistance. Base oils, that contain predominantly saturated compounds have a lower tendency to oxidation. The rate of oxidation will increase with rising temperature, which can also lead to the formation of peroxides and free radicals in the engine oil, which in turn can contribute to acid and sludge formation. Oxidation

can also lead to an increase in viscosity due to polymerization between the base oil molecules.

In certain use cases the lubricant can also undergo chemical reactions with nitrogen or sulphur, resulting in the nitration or sulphation of the oil. Although neither as common, nor as severe in passenger car engines as oxidation, these reactions also alter the composition of engine oil and over time can degrade the lubricity.

2.5.2   Contamination and depletion

Sulphuric acids can form from water and sulphur inside the combustion chamber. The water content of the fuel, the humidity of the air inside the combustion chamber and the sulphur content of the fuel and lubricant can influence the amount of such acids. Acid formation can also occur due to hydrolysis of ester compounds – e.g. viscosity modifier additives – in the presence of water inside the combustion chamber. Water can also affect the lubricant through selective solubility resulting in the removal of specific additive compounds. Severe cases of contamination with water can lead to emulsification (Figure 12 b) and a catastrophic failure of the engine.

Friction modifier and antiwear additives function via binding to metal surfaces and forming a protective layer. These additives can also bind to metallic wear particles that flow in the engine oil, which yields the reduction of the effectiveness of such additives. Dispersant additives provide a means of keeping particles away from the sliding pairs through encapsulating wear debris and foreign bodies, which prevents them from subsiding. These together with detergents serve as cleaning agents, reducing the amount of sediment formation and the risk of clogging inside oil delivery lines. Some additives like zinc dialkyldithiophosphate (ZDDP) have a high volatility which can lead to their evaporation at higher temperatures.

2.5.3   Fuel dilution in engine oils

State of the art passenger car and commercial vehicle engines implement direct injection fuel systems with high injection pressures and varied injection timing strategies. Injecting fuel directly to the combustion chamber offers a more precise control over mixture formation and the combustion process which together with turbocharging allows for higher specific power, higher torque and an overall higher efficiency. However, utilizing direct fuel injection can lead to a higher amount of fuel

impingement and condensation on the cylinder wall and piston top surface under partial load and low-temperature operation.

Dilution of the lubricant with fuel is a possible consequence of fuel impingement, which can lead to fuel transport trough the piston ring pack into the crank case. This seemingly negligible amount of fuel will eventually blend with the engine oil, which can lead to a decreased viscosity and accelerated oil degradation. Defective injectors, bad fuel spray orientation and increased gaps between the piston, piston rings and cylinder wall due to wear may cause increased fuel transport into the crankcase. Fuel dilution can cause lubrication issues, although in normal operating conditions without any fuel line malfunction the fuel content of the engine oil should stay at a manageable level due to evaporation at higher operating temperatures. The unburnt hydrocarbon content of the exhaust gas which is influenced by late injection timing and exhaust gas recirculation can contribute to a similar phenomenon. Figure 13 gives an overview of fuel transport paths in the cylinder-piston tribosystem.
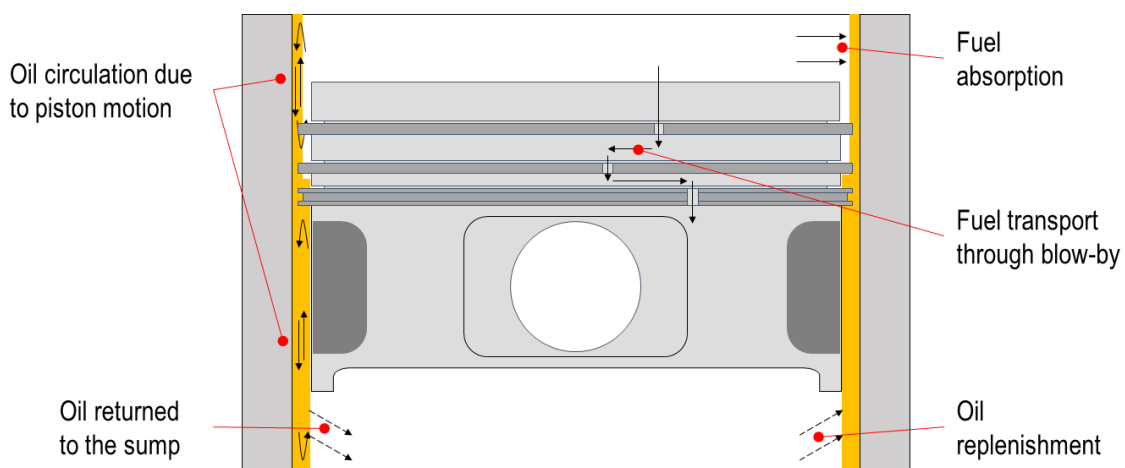
Figure 13. Overview of fuel absorption and transport processes taking place in-cylinder and on the cylinder liner according to Shayler et al. [39]

Sagawa et al [38] investigated the factors which contribute to increased fuel dilution of the engine oil in direct injection and multi-point injection gasoline engines. Measurements were carried out on a 2 litre four-stroke four-cylinder DOHC engine under varied load conditions. Commercially available RON 90 and 100 gasoline fuels as well as a RON 96 research fuel were utilized for the investigations. Dilution levels increased with decreasing operating temperature, elevated engine load, elevated engine speed and increasing fuel density. Late injection timing was also reported to have a negative effect on lubricant dilution.

Costa et al [40] conducted friction and wear experiments on lubricant samples including ethanol as a contaminant. A ball-on-disc environment was utilized under varied speed and temperature conditions to obtain Stribeck curves of base and formulated oils. The addition of ethanol lowered the viscosity of the lubricant, which yielded a thinner elasto-hydrodynamic film and a shift towards mixed lubrication at lower speeds. The contamination promoted the formation of a boundary layer in the case of the base oil.

Hakeem et al. [41] investigated oil dilution in a turbocharged direct injection spark ignition (DISI) engine. Experiments were carried out on a chassis dynamometer at -18°C to accumulate fuel into the lubricant using transient cycles based on Federal Test Procedure 75 and US-06 procedures supplemented with a simulated highway driving phase at constant 88 km/h speed and on-road testing under highway driving conditions separately. SAE 5W-30 grade lubricant and an E10 ethanol-gasoline blend was used for the experiments. Oil samples were taken at specific stages of the dyno tests, and in 45 min intervals throughout the on-road testing, and analysed using gas chromatography (GC-MS). Light fuel hydrocarbons were not found in the oil after the accumulation, mid-range hydrocarbons were present after the accumulation, but evaporated from the lubricant after engine warm-up, whereas heavy fuel hydrocarbons were present even after the conclusion of the highway tests. An equilibrium fuel dilution of around 4% by weight was established (Figure 14).
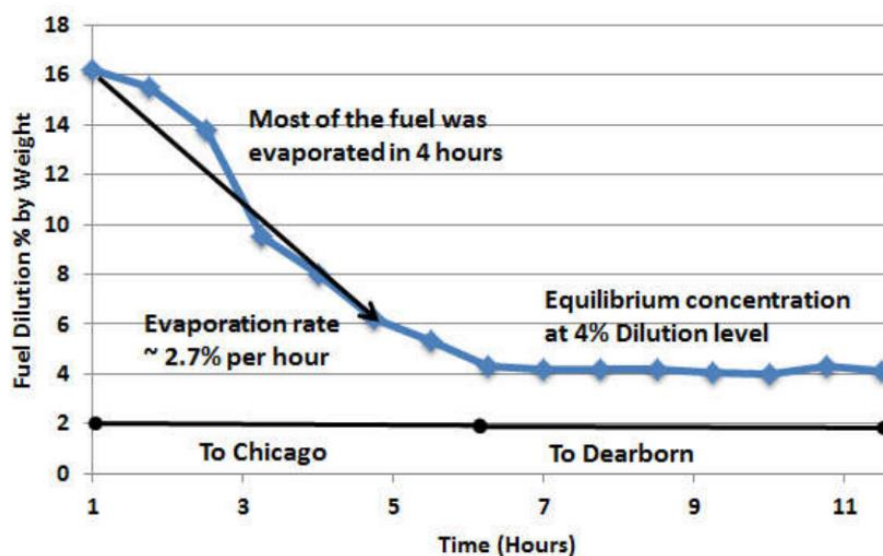
Figure 14. Fuel in engine oil measurement results during a field test under cold environmental conditions by Hakeem et al. [41]

Hu et al [42] investigated fuel dilution in the lubricant of a turbocharged direct injection gasoline engine in relation to injection timing and duration. Engine dynamometer tests were performed with a cyclic load profile. A RON 93 gasoline and a SAE 5W-30 grade synthetic lubricant were utilized during testing. The maximum achieved fuel dilution in oil was reported to be around 9%, which caused a significant drop in oil viscosity. Long injection durations under high engine speed were found to increase the amount of fuel in oil, which is believed to be in relation with fuel droplet size and wall impingement.

Haenel et al [43] analysed the impact of engine oil composition and the dilution of engine oil with fuel on the stochastic pre-ignition (SPI) phenomenon in a series production inline 4-cylinder turbocharged direct injection gasoline engine. Spark timing, throttle position, injection timing, injection mass, valve timing and enrichment were varied under steady-state load conditions with regularly repeated baseline measurements to gather significant results despite the unpredictable nature of SPI events. It was found that lubricant formulation can have a large impact on SPI occurrence. An engine-aged lubricant was shown to increase the number of SPI events by a factor of 2. Directly diluting the lubricant with fuel yielded no significant change in SPI occurrence.

Lacey et al [44] investigated the effect of oil drain interval on mineral based engine oil quality. Laboratory oil analysis conducted on engine oil samples from a wide variety of vehicle manufacturers within the normal service interval showed advanced additive and base stock degradation after 4800 to 8000 km of use. Oil samples showed acceptable properties after 4800 km to 6400 km and in some cases up to 9600 km of operation. The variance in results could be attributed to vehicle design differences, lean lubricant quality and rejuvenation by addition of fresh oil.

Watson and Wong [45] experimented with ultralow sulfur diesel (ULSD) and B20 and B100 biodiesel diluted CJ-4 and CI-4+ oil samples in order to describe the effect of fuel dilution to the lubricant. A benchtop thin plate oxidation method similar to ASTM D6594 was utilized to characterized mixtures of oil diluted with 0%, 5% and 10% of ULSD and biodiesel. After 160 hours of oxidation the mass loss of the thin plate as well as TAN, TBN and viscosity of the mixture were measured. Findings showed that 10% B100 biodiesel causes a significant increase in TAN alongside a decrease of TBN. Mass loss also increased with increasing biodiesel content.

He et al [46] conducted experiments with ULSD and B20 in order to compare lubricant dilution and lubricating property degradation in conjunction with late in-cylinder fuel injection for diesel particulate filter (DPF) regeneration. Measurements were carried out on a heavy-duty Cummins engine equipped with DPF and an oxidative catalytic converter as well as a passenger car with a 2-liter diesel engine. Test cycles simulating normal operation and DPF regeneration were utilized. Oil samples were analyzed through gas chromatography (GC) and infrared spectroscopy (FTIR). An increased accumulation rate and a nearly constant concentration of biodiesel inside the lubricant was reported for the commercial vehicle engine. It was also found that B20 has a positive effect on DPF clogging, although biodiesel tends to accumulate in larger quantities in the oil over time.

Fuel dilution and oil aging can have diverse effects on the internal combustion engine on a system level, which could induce complex processes and impact several components. A procedure for the integrated analysis of the long-term effects of fuel in engine oil and fuel induced oil degradation is yet to be established.

Reliable long-term operation of an engine can only be assured if the lubricant is in appropriate condition. Oil dilution caused by water adsorption and fuel contamination, oxidation through the crank case gases, wear particle and soot contamination altogether alter the properties of the lubricant and lead to the depletion of additives and to the aging of engine oil. Alternative fuels represent a new challenge in the chemical engineering of lubricants, and their impact on the chemistry and lubricating properties of oils must be taken into consideration. Kurre et al. [47] reviewed engine oil contamination, degradation and engine wear related to biofuels, and concluded that biofuels reduce soot emission, which is one of the main contributors to oil degradation and wear in an IC engine. Khuong et al. [48] reviewed lubricant dilution with bioethanol. Due to its higher vaporization heat and boiling point, bioethanol tends to dilute engine oil more compared to gasoline. Bioethanol dilution decreases the viscosity of oil, which can however increase over time due to oxidative processes in the contaminated lubricant. The contamination increases corrosion and wear, and affects deposit and sludge formation in the lubricant. These negative effects can be counteracted with additives in the lubricant.

Friction and wear test rig experiments were carried out by Costa et al. [40] to investigate the effects of ethanol contamination on lubricants during engine use. Two base oils and a formulated oil without friction modifiers were mixed with 2% of anhydrous and hydrated ethanol separately. The ethanol contamination was found to lower the viscosity of the lubricants, thereby reducing elasto-hydrodynamic (EHD) film thickness. Coefficient of friction (CoF) was similar with all investigated lubricants with and without ethanol contamination. Ethanol was found to promote boundary layer formation in the base oil, while it hindered the process with the formulated lubricant.

The performance of bioethanol diluted engine oil was investigated by Banerji et al. [49] regarding friction and wear of cast iron against DLC sliding pairs on a ball on disc test rig. It was reported that using a 1:1 blend of E85 and SAE 5W-30 synthetic lubricant, the CoF and amount of wear (Figure 15) were reduced compared to results with the pure lubricant. The ethanol in the diluted oil facilitates the decomposition of the antiwear additive zinc-dialkyl-dithiophospate (ZDDP) into zinc sulphide and zinc pyrophosphate, which then form a protective tribolayer on the surface of the cast iron specimen.
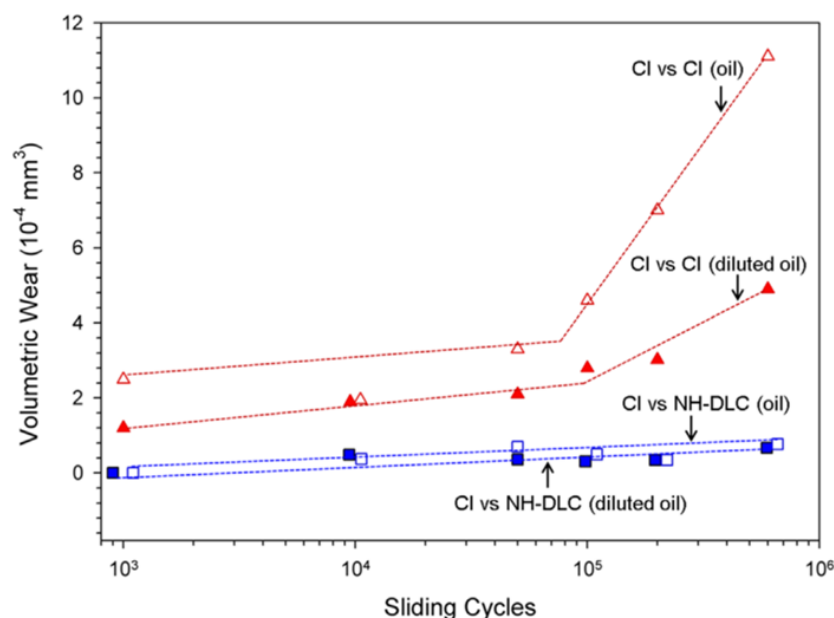
Figure 15. Volumetric wear of cast iron (CI) and non-hydrous diamond-like carbon (NH-DLC) samples in unidirectional sliding experiments lubricated with neat and diluted engine oil by Banerji et al. [49]

Khuong et al. [50] investigated the effect of bioethanol-gasoline blends on the friction and wear characteristics of a commercial fully synthetic lubricant. SAE 5W-40 engine oil was diluted with 6% v/v E10, E20, E30 and E85 respectively. Fuel-oil blends were

subjected to four ball wear tests under boundary lubrication according to ASTM D4172. A decrease in viscosity, increase in total acid number (TAN) and an overall degradation in friction and wear properties of the lubricant were reported. Additional oxidative and corrosive wear marks were observed on the surface of specimen after testing with contaminated oils, as opposed to pure oil.

Chemometric data evaluation was carried out by Besser et al. [51] to investigate the effects of ethanol in gasoline on the engine oil. Oil samples were artificially altered through oxidation in laboratory conditions, as well as using chassis dynamometer tests on a passenger vehicle with a 125 kW turbocharged DISI engine fuelled with E5 ethanol-gasoline blend. The engine was equipped with a modified oil sump for accelerated alteration through the addition of acetic acid to the lubricant. Aminic antioxidants and ZDDP depleted faster during artificial alteration, whereas the result of dyno test showed slower ZDDP depletion, but an increased degradation of phenolic antioxidants.

Singh et al. [52] conducted friction and wear experiments to investigate the behaviour of engine oil diluted with a dual biofuel – 70% aamla (phyllanthus emblica) biodiesel, 30% eucalyptus oil. Three different blends of oil-fuel mixture and two samples of used engine oil were compared using ball on disc HFRR and pin on disc test rig experiments. A good agreement of CoF and amount of wear between tests with used engine oils and contaminated fresh oils was reported. The biofuel blend was found to have a positive effect on the lubricating properties of the engine oil in the experiments.

Fang et al. [53] investigated the impact of biodiesel on engine oil through friction and wear test rig experiments. A higher wear of test specimen was reported in relation to the contamination of the lubricant with pure biodiesel. Oxidized products from the biodiesel can react with ZDDP in the oil, causing it to lose its antiwear properties.

The effect of a 20% LOME-diesel blend on the engine oil was studied by Agarwal et al. [54] in a 4 kW single cylinder compression ignition direct injection (CIDI) engine. Oil dilution, moisture and ash content were found to be lower compared to regular diesel operation, however with the biodiesel blend the oxidation of the lubricant was found to be slightly higher than with petrodiesel.

Andreae et al. [55] investigated engine oil dilution on a CIDI engine powered with B20 biodiesel and ultra-low sulphur diesel (ULSD) fuels, using Fourier Transform Infrared Spectroscopy (FTIR) to analyse fuel content of used engine oil. Higher rates of fuel dilution were reported in relation to B20, due to the higher evaporation temperature of FAMEs.

2.6   Section summary

Friction, wear and lubrication are fundamental aspects of machine design. Ensuring longevity and robustness requires prior knowledge of anticipated friction regimes, wear phenomena and lubricant aging properties. The lubricant itself is a vital component of an internal combustion engine, and is responsible for lowering friction, controlling the amount and mode of wear, collecting debris and sediments, and protecting metal surfaces from corrosion. To assure this, modern oils are formulated from a synthetic base stock with functional additives to increase their performance and stability. Harsh operating conditions including heat, contamination and oxidation degrade the oil during its service life. Based on available scientific literature, oil degradation as a result of alternative fuels can be summarized by the following key points:

- Fuel contamination in the engine oil can have various effects on the tribology of the engine. Lubricant dilution with ethanol or biodiesel lowers the viscosity of the oil causing a lower CoF between sliding surface pairs, however the chemical processes taking place in the diluted oil cause further alterations in the performance of the lubricant.
- Ethanol dilution decreases lubricant film thickness and promotes corrosive wear of the interacting surfaces. Furthermore, ethanol promotes the decomposition of certain antiwear additives, shortening the lifetime of engine oils.
- Biodiesel dilution tends to lower friction and wear due to the addition of long-chain FAME molecules, but the acidic nature of the fuel decreases the oxidation stability of the lubricant at the same time. The higher evaporation temperature of fatty acid methyl esters, the main component of biodiesel fuels, implies a higher rate of oil dilution at normal operating conditions.
- Data regarding the effects of synthetic fuels on engine oil aging and additive degradation is only scarcely available.

3   A review on the impact of alternative fuels on internal combustion engines

Alternative fuels play a vital role in the long-term transition to a global sustainable mobility. A large scale transition from fossil fuels to renewable energy sources is only achievable gradually, with the utilization of low-emission and carbon-neutral fuels along the way. Furthermore, there are certain applications, where pure electric propulsion systems cannot present a viable alternative, such as off-road, heavy-duty [56] and marine vehicles or aviation. Figure 16 presents enacted and historic worldwide NEDC-normalized CO_2 emission and fuel consumption targets for light commercial vehicles. Carbon-neutral fuels are essential for commercial vehicles to be able to contribute to reaching the 2030 targets.
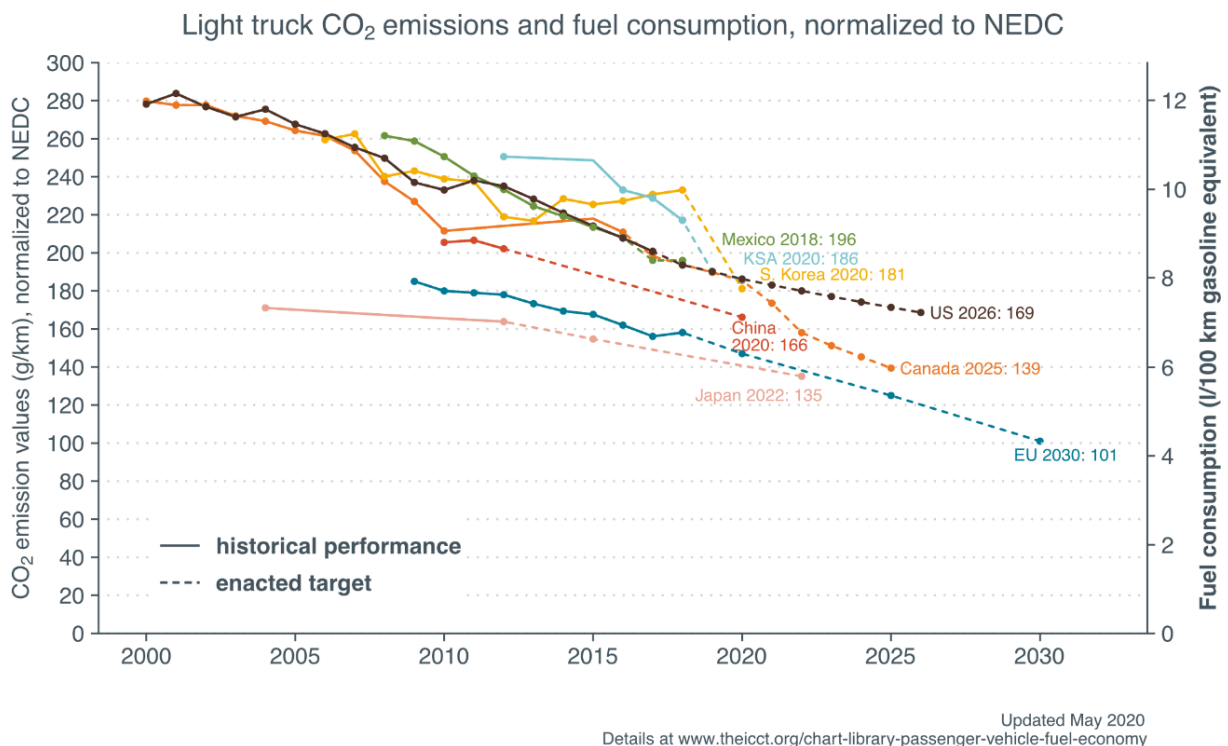
Figure 16. Enacted and historic worldwide NEDC-normalized CO_2 emission and fuel consumption targets for light commercial vehicles [57]

Another aspect which increases the significance of carbon-neutral fuels is their potential use as long-term energy storage for renewable energy power plants [58]. In contrast to classic on-demand energy production, solar and wind power plants can only produce energy during specific weather conditions, and thus cannot be directly driven by energy consumption needs. For their integration in the power grid, an appropriate backup plant should also be established to account for the fluctuations in energy

production and consumption, or means of high capacity energy storage have to be utilized in order to fully harness the available solar or wind energy. Power-to-Gas and Power-to-Liquid technologies offer a possible solution for this matter. Using H_2 produced through electrolysis with green electricity and CO_2 from biological waste or air capture, a suitable gas or liquid can be produced and used as fuel in the existing vehicle infrastructure. Hence, it is vital to determine the compatibility of novel fuel formulations with all related infrastructure on both the production and consumption side.

3.1 Biofuels

Biofuels can be considered as the first step towards replacing fossil fuels and reducing atmospheric CO_2 levels.

First generation biofuels are made from food crops grown on cultivable land through the transesterification of vegetable oil or the fermentation of crops containing sugar and starch. Because of the conflicting nature of food versus fuel production, first generation biofuels are not favoured as a replacement for petrofuels [59].

Second generation biofuels are made from biomass, a by-product of agriculture. This makes them more favourable, due to the fact that the feedstock is a waste product, not suitable for human consumption or for the feeding of livestock. Second generation biofuel production processes require more energy compared to the first generation, due to the number of preparation steps and chemical processes necessary to achieve the desired result [60].

Third generation biofuels are derived from algae, meaning that no cultivable land or freshwater is needed for their production. Production costs for third generation biofuels are higher compared to previous generation, however novel technologies in the field could provide feasible methods for mass production. It is possible to extract lipids from algae using ionic liquids through a process with significantly lower energy demand and therefor production cost [61], as for the previous generations.

Fourth generation biofuels are also derived from algae; however, the algae are genetically engineered to enhance its relevant properties, e.g. faster grow rate, more efficient nitrogen use or lower sensitivity to the environment [62]. Fourth generation biofuel production offers increased yield and decreased expenses, although it poses

an elevated environmental risk. Contamination of the natural environment with fast growing species that use feedstock very efficiently could possibly lead to the devastation of indigenous species [63]. Algae-based biofuel production could emerge as a low-maintenance, low-cost, organic carbon capture technology, but is still in its early research phase.

The products of biofuel production depending on the feedstock and procedure used are mainly methanol or ethanol for bioethanol and fatty acid methyl esters (FAME) for biodiesel. Ethanol is suitable as a propellant for both spark ignition and compression ignition engines, therefore it is blended into petrofuels worldwide. FAME compounds are able to self-ignite under the same pressure and temperature as fossil diesel, hence biodiesel is used in compression ignition engines.

3.2 Synthetic and carbon-neutral fuels

Synthetic fuels are transport fuels derived from CO_2 and H_2 through processes such as the Fischer-Tropsch synthesis or methanol synthesis. The CO_2-feedstock for the synthesis is produced through liquefaction of natural gas, coal or from biomass. The product of the process is a chemically pure compound, compared to the composition of fossils and biofuels. The three main group of fuels produced from synthesis gas are hydrocarbons, alcohols and ethers [64]. Synthetic fuel production can be competitive with petrofuel production for certain processes [65].

Carbon-neutral fuels or renewable electrofuels as referred to by Ridjan et al. [58] are essentially synthetic fuels made using renewable energy for the synthesis. Compared to synthetic fuels, electrofuels rely on atmospheric CO_2 [66] or biomass as feedstock. Production cost estimations for electrofuels yield higher rates compared to biofuels [67], however the advantages of carbon-neutral fuel production and synthetic fuels have to be taken into account as well.

3.3 Physical and chemical properties

Gaseous fuels such as compressed natural gas (CNG) are playing a significant role on the market. CNG is capable of powering dedicated gas engines or dual fuel engines which can operate with both gasoline and natural gas. Through synthetic fuel production, it is possible to manufacture methane, the main component of CNG. Natural gas needs to be compressed to around 200 times the atmospheric pressure

(20 - 25 MPa), in order to contain comparable amounts of energy per unit mass to gasoline. The combustion of CNG forms few pollutants compared to conventional gasoline or diesel, which makes it ideal as a clean fuel. The low viscosity of CNG however can cause high friction and severe wear on the components of the fuel system.

Dimethyl ether (DME) is a promising synthetic gaseous fuel for compression ignition applications. As opposed to natural gas, DME turns into liquid at around 5 times atmospheric pressure (0.53 MPa) at 25°C, and has similar energy density to ethanol. The main advantage of DME is the soot free combustion due to the lack of direct C-C bonds in its molecules, which makes it a favourable alternative to petrodiesel. Density and viscosity of liquefied DME are very low, which can cause severe wear and leakage from the fuel system.

Due to the physical properties of gaseous propellants, the fuel system of a previously mono-fuel gasoline or diesel powered engine must be converted, in order to accept CNG or DME. Thus these fuels cannot be considered drop-in alternatives for use with the existing vehicle infrastructure.

Table 1. Physical and chemical properties of various liquid fuels
(corresponding sources listed in the header)

	Gasoline [EN 228]	Diesel [EN 590]	Bioethanol [68], [50]	Biodiesel [69], [70]	OMDME[*] [71]	DMF [68]
LHV[1] (MJ/kg)	42.9[+]	42.68[+]	26.9	34 – 45	17.5 – 22.4	33.7
Density (kg/m^3)	720 – 775	820 – 845	790.9 - 799	815 – 913	860 – 1130	889.7
Kin. Viscosity (mm^2/s)[x]	0.37 – 0.44[+]	2.00 – 4.50	1.47 – 1.71	1.3 – 19.2	1.08 – 2.63	0.57
RON[2]	> 95		110			119
CN[3]	10 – 15[+]	> 51	8	40 – 63.5	29 – 104	9
Oxygen (% w/w)	< 2.7	0	34.78	11.3 – 13.4	42.1 – 49	16.67
Sulphur (mg/kg)	< 10	< 10	varying	varying°	0	0

[*] depending on the number of CH_2O groups in the liquid
[+] not regulated
[x] at room temperature
° depending on the feedstock
[1] Lower Heating Value
[2] Research Octane Number
[3] Cetane Number

A broad variety of combustible liquids were investigated by researchers in terms of usability in IC engines. Vegetable oil based biodiesels, alcohols and oxygenated synthetic compounds are the most promising alternatives, offering comparable engine operation in terms of performance and reduced soot and CO_2 emissions. Table 1 gives an overview of the core physical and chemical properties of the most commonly researched liquid fuel alternatives.

3.4 Combustion and exhaust emissions

Performance and emissions of compression ignition direct injection (CIDI) and direct injection spark ignition (DISI) engines play a vital part in the assessment of alternative fuels. A comprehensive review has been written by Tamilselvan et al. [69] on the topic of performance, combustion characteristics and exhaust emissions of biodiesel powered engines, summarizing that biodiesel fuels produce lesser CO_2, HC, particulate matter (PM) and particulate number (PN) emissions, contain no sulphur and can be utilized in up to 20% blends without any alteration to the engine. Due to their lower heating value, engine brake power slightly decreases, along with a slight increase in fuel consumption. Manzetti et al. [72] reviewed the emission profile of bioethanol-gasoline blend powered vehicles, and concluded that besides regulated exhaust gas content, a variety of unregulated organic component emission was reported by scientist investigating bioethanol emissions. Thangavelu et al. [73] reviewed CIDI engine performance and emissions in relation to bioethanol. A conclusion of increased combustion efficiency, increased fuel consumption with higher blends (E60-E80), a reduction of HC and CO and increased acetaldehyde and formaldehyde emissions was reported.

Pandey et al. [74] investigated the performance and emission of a 580 kW 12-cylinder military CIDI engine during operation with karanja-oil methyl ester (KOME), and reported a decrease in CO_2, hydrocarbon (HC) and soot emission, and a slight increase in NOx compared to petrodiesel operation.

Devitt et al. [75] investigated the viability of rapeseed methyl ester (RME) as an alternative to diesel fuel in the United Kingdom. Measurements were conducted on a CIDI engine using RME. A 6.6% drop in brake power, 10% increase in fuel consumption and a more than 7% reduction in CO_2 emission were recorded.

Zare et al. [76] examined the influence of oxygenated waste edible oil (WEO) on engine performance and emission. Experiments were carried out on a 162 kW 6-cylinder turbocharged common rail CIDI engine in steady-state and transient cycles on a dynamometer. Different blends of WEO, petrodiesel and triacetin, a highly oxygenated additive were investigated. A decrease in brake power, PM and PN were reported with increasing oxygen content of the fuel. NO_x emissions were higher with the oxygenated fuels. Further investigations with oxygenated WEO under cold-start and hot-start conditions on the previously used testing equipment [77] revealed higher NO_x, PM and PN with the oxygenated blends during cold-start. PM and PN were reported to be lower during hot-start with oxygenated WEO blends as opposed to pure petrodiesel.

Iannuzzi et al. [78] evaluated the performance and emissions of poly(oxymethylene) dimethyl ether (OMDME) – diesel blends using a single cylinder CIDI engine. Blends of 5% and 10% OMDME in diesel were compared to pure diesel. A decrease of nearly 35% in soot emission was reported in relation to the 10% OMDME blend. NO_x emissions showed no significant increase. Thermal efficiency and fuel consumption remained nearly identical to pure diesel operation.

Xiao et al. [68] studied the combustion and emission characteristics of dimethylfuran (DMF)-diesel blends on an 85 kW 4-cylinder CIDI engine under static loading conditions on an engine test bench. Blends of 10 wt% and 30 wt% DMF in diesel were compared to regular diesel. A decrease in PM and a variation in particulate size distribution was reported with increasing DMF content. A slight variation in cylinder pressure and heat release rate were also experienced.

An investigation on the combustion and emission characteristics of biodiesel – OMDME blends was carried out by Li et al. [71] on a naturally aspirated single cylinder CIDI engine. Palm oil biodiesel (B100), regular diesel and a blend of 15% OMDME and 85% biodiesel (BP15) were used under constant loading conditions. Exhaust gas recirculation (EGR) and injection timing were varied throughout the experiments. Due to the higher volatility of OMDME, shorter ignition delay was reported with BP15. Soot emission decreased with both B100 and BP15 compared to diesel. This allowed a higher amount of EGR to be utilized, which produced a significant drop in NOx emissions compared to diesel.

Costagliola et al. [79] investigated the performance and emissions of a 132.4 kW DISI engine powered with different blends of bioethanol and gasoline. The experiments were carried out on a chassis dynamometer using steady-state and transient driving cycles representing city and highway conditions. Regulated emission components and volatile organic compounds were registered. CO emission and PN decreased, whereas HC emission and PM increased with bioethanol content. Higher amounts of VOC were reported with all bioethanol blends during slower driving cycles.

López-Aparicio and Hak [80] evaluated the use of bioethanol fuelled buses through ambient air and on-road exhaust gas composition measurements in the region of Oslo using 21 public buses powered by 198 kW 5-cylinder DISI engines running on E95 bioethanol. Measurements were conducted during three periods, representing spring, summer and winter weather conditions. An increase in local and ambient acetaldehyde concentrations was experienced through the evaluation period. A high local acetic acid emission was also reported.

3.5 Friction and wear characteristics

In a high-performance or heavy-duty engine with direct injection, lubricating properties of the fuel are key aspects to reliable long-term operation. The high-pressure fuel pump of CIDI engines is often cooled and lubricated with the fuel itself. Standardised testing procedures have been established for petrodiesel fuels to assess their lubricity and to rank their antiwear properties. These experiments are conducted on friction and wear test rigs using a ball specimen on a rotating disc [81] to evaluate the load bearing capacity of the fuel expressed in grams of normal load, or high frequency reciprocating rigs (HFRR) using a ball specimen on a stationary disc [82], [83] to evaluate boundary lubrication properties through the diameter of the wear scar expressed in µm, as a measure of fuel lubricity. According to the US standard [84], the wear scar diameter (WSD) on the specimen after a standardised measurement should not exceed 520 µm, while the EU standard [85] imposes a WSD of 460 µm as upper limit. Biodiesel and synthetic diesel fuels are assessed through the same experimental procedures.

Biofuels containing methylesterified bio-oils (FAMEs) such as linseed oil methyl ester [86] or palm oil methyl ester [87] show a better overall performance than petrodiesels in regards of friction and wear. A lower coefficient of friction (CoF), lower amount of wear and lesser surface damage can be attributed to a high quantity of long-chain ester

molecules found in these compounds [88], [89]. The mixing of petrodiesel with FAME compounds [90] or ethanol [91] can grant better lubricity for the blends.

Biodiesel fuels offer better friction and wear characteristics compared to petrodiesels, but long-term chemical compatibility with metals and elastomers in IC engines has to be taken into account, due to oxidation and the corrosive nature of certain biodiesels, according to Haseeb et al. [92]. Singh et al. [93] concludes that the rate of corrosion is a factor of temperature, water content microbial growth and type of feedstock used for the synthesis of biodiesel. Sorate et al. [94] concluded that the cold flow properties of biodiesels can be enhanced with additives or blending with petrodiesel, and that oxidation during long-term storage can be limited through temperature control.

LOME was investigated by Agarwal et al. [54] in a 4 kW single cylinder CIDI engine to assess its impact on engine tribology. Significantly lower amounts of wear and carbon deposits were experienced after operating the engine on a 20% LOME-diesel blend for 512 hours, compared to pure petrodiesel operation.

Pandey et al. [74] investigated fuel pump wear on a 580 kW 12-cylinder military CIDI engine after 512 hours of operation on KOME. Pump wear was found to be lower as opposed to testing with regular diesel.

Hu et al. [95] investigated the corrosion resistance of copper, mild steel, aluminium and stainless steel in rapeseed methyl ester (RME), and found that Cu and Fe can serve as catalysts for the decomposition of rapeseed methyl ester, simultaneously causing severe corrosion of said metals.

Cursaru et al. [96] conducted static immersion tests of aluminium, copper and mild steel specimen in regular diesel, sunflower biodiesel and a blend of 20% biodiesel in petrodiesel. The corrosive nature of sunflower biodiesel was reported, with the severity of corrosion and fuel degradation depending on temperature. Formation of peroxides and acids in the biodiesel intensifies at higher temperatures. Cu is more susceptible to corrosion in sunflower biodiesel compared to Al and Fe.

Synthetic oxygenated compounds such as OMDME, oxymethylene ethers (OMEs) and DMF can exhibit similar characteristics to petrodiesel. With increasing chain length, a

similar viscosity to conventional diesel fuel can be achieved [97], [98]. Information on the actual lubricity of such compounds is scarcely available.

Hu et al. [99] investigated the lubricity of 2,5-dimethylfuran using a four ball test rig. Different blends of DFM and diesel were tested under the same condition. A significant decrease in the CoF and lower amount of wear were observed with increasing concentrations of DMF. A tribochemical alteration of the blend was also reported, with hydroxyl and carboxyl groups forming in the fuel during the four ball tests.

Sukjit et al. [100] conducted experiments with various oxygenated compounds on a high frequency reciprocating rig according to [83], in order to assess the lubrication properties and tribological mechanisms associated with such liquids. A strong dependence of lubricity from the functional group of the investigated compounds was reported, with ketone, ether, ester, hydroxyl, aldehyde and carboxyl ranging from worst to best. Humidity was also found to influence lubricity due to water adsorption: increasing water content deteriorates the ability of the fluid to form a lubricating film on the surface.

Gasoline and ethanol lubricity is of rising interest due to the elevated injection pressure in DISI engines. There are no international standards for gasoline or ethanol lubricity measurement in effect as of December 2017, though many investigations have been conducted to assess the lubricating properties of these fuels [101], [102]. Gasoline has a lower viscosity compared to diesel fuel, resulting in a thinner hydrodynamic (HD) film and lower friction in the full HD regime [103]. This could pose a threat of lower load bearing capacity and high wear under heavy load in high-pressure application.

Ethanol lubricity depends heavily from water content: anhydrous ethanol has worse lubricating properties than gasoline, whereas hydrous ethanol can perform significantly better [104]. Ethanol-gasoline blends can exhibit better lubricity compared to pure gasoline [105], but the added alcohol impacts the effectiveness of lubricity modifiers.

Gustavsson et al. [106] conducted HFRR tests on experimental and commercial PVD coatings as well as 100Cr6 on cast iron in gasoline, diesel, white spirit, RME and E85 (85% bioethanol, 15 % gasoline). They concluded that coated specimen exhibited a higher CoF in RME compared to other fuels, and uncoated specimen experienced higher wear in RME and E85 compared to gasoline and diesel.

The effects of E22 ethanol-gasoline blend and E100 bioethanol on the wear of electric fuel pumps were studied by Rovai et al. [107] on a pump test rig. Abrasive wear was reported in conjunction with E22, whereas E100 operation produced mainly corrosive damage to the pump unit.

3.6 Section summary

Regarding the emissions, friction and wear of internal combustion engines related to alternative fuel technologies the following assumptions can be made, based on the available research data:

- Biodiesels and synthetic fuels present a good alternative for petrofuels in terms of engine performance and exhaust emissions. The decrease in engine performance can be compensated in modern engines with modifications to injection duration. With reduced soot emissions from biodiesel and OMDME, the injection timing can be modified, EGR can be utilized without the restrictions of additional soot formation or higher efficiency exhaust gas after treatment units can be integrated into the exhaust system in order to reduce NO_x emission.
- Bioethanol provides good performance, however acetaldehyde, formaldehyde and acetic acid emissions associated with organic compounds found in bioethanol possess harmful properties.
- Fourth generation biofuels could provide a cost-effective means of environment-friendly fuel production.
- Besides the short-term effects regarding the friction and wear of machine components in biofuels and synthetic fuels, the long-term processes of corrosion and oxidation of materials in the fuel, as well as chemical and tribochemical alterations in blends of petrofuels, biofuels and synthetic fuels must be taken into account.

4 Materials and methods

This section presents the utilised materials and methods in general to establish a basic understanding of the workflow and instrumentation used for measurements and experiments discussed later on.

Friction and wear testing methods are introduced in Chapter 4.1. Most methods presented are based on existing standards or previously published works of independent researchers. Some aspects were modified after preliminary testing, to achieve better reproducibility.

Sample types, sample preparation methods, as well as sample pre- and post-processing procedures are detailed in Chapter 4.2. The amount and type of wear are determined partly through standardised methods. Volumetric wear measurements, as well as wear scar characterization were done through internal procedures.

Engine oil analysis steps are discussed in Chapter 4.3. Detailed oil analysis was carried out at the Austrian Excellence Centre for Tribology. The resulting oil properties were jointly analysed and published.

A self-developed novel engine oil aging apparatus is presented in Chapter 4.4. The instrumentation and control system setup are described, along with measurement results regarding repeatability. Apart from the basic concept, all aspects of the aging apparatus were developed from scratch.

Chapter 4.5 introduces the design of a comprehensive fleet study, the sample collection method and the means of vehicle speed data acquisition. This investigation was conducted to establish a reference for artificial aging experiments.

Statistical analysis and Principal Component Analysis are introduced in Chapter 4.6. and 4.7. The presented method was used for chemometric data evaluation of oil analysis results and the analysis of vehicle speed readings.

4.1 Tribometrology

Measuring certain properties of a system can be accomplished on multiple levels of complexity. Czichos [26] differentiates between 6 levels of complexity for tribometrology, ranging from a simple, but abstract model study, to the ultimately realistic but time consuming and expensive field testing. Figure 17 presents the levels of tribology testing, highlighting the main aspects of each level. The presented work is mainly based on model studies, with a short introduction to ongoing specimen tests presented in.
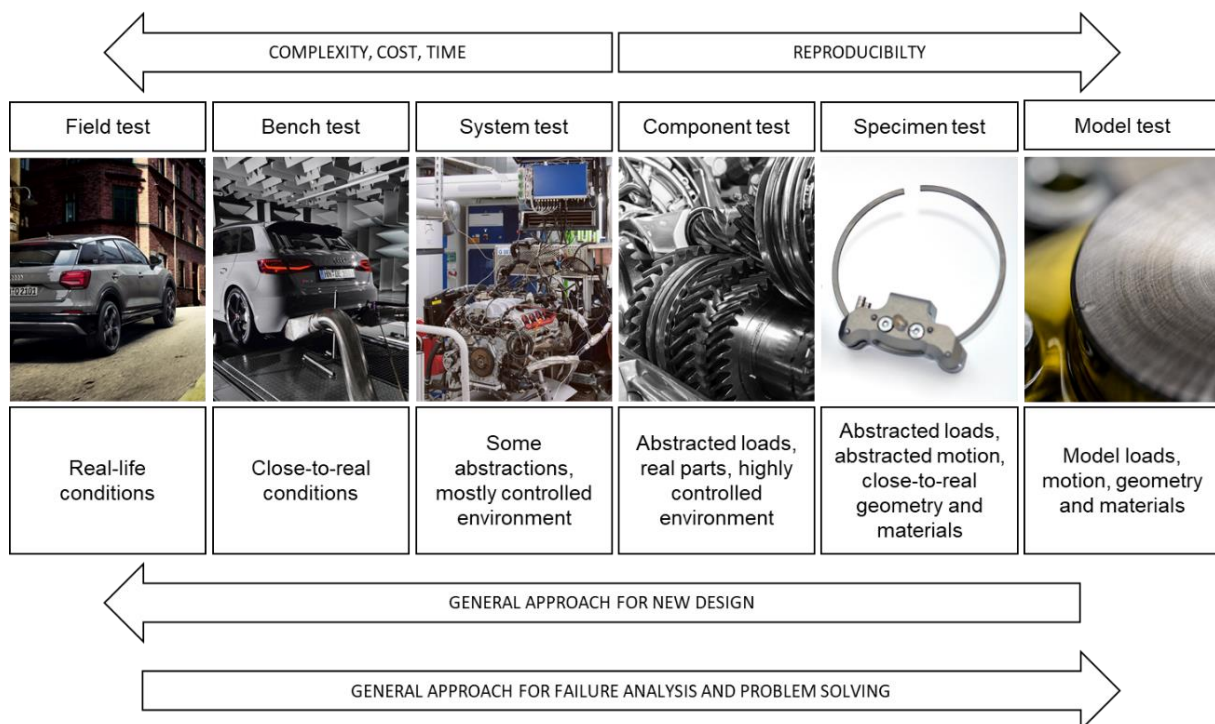
Figure 17. Levels of tribology testing according to Czichos [26]
(photos illustrating field and bench test are from Audi MediaCenter, the rest by the author)

Conducting friction and wear measurements on purpose-built instrument – i.e. tribometer – using simplified representations of the parts and surface in question offers a high level of reproducibility and reliability with manageable cost and time requirements, but often lacks direct transferability of results to more complex systems. In contrast, a holistic approach can offer instant interpretation and a solid ground for decision making, but requires an increased budget and introduces additional sources of uncertainty, hence reducing the repeatability and reliability of the results. In most cases, experimenting on a complex system – e.g. a complete engine on an engine test bench – also inherently means a restricted number of repetitions due to budgetary and time constraints.
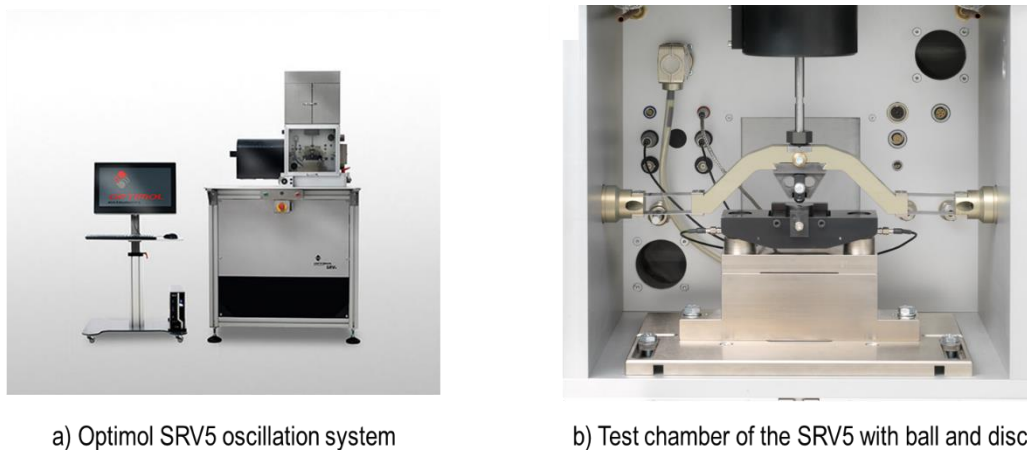
a) Optimol SRV5 oscillation system

b) Test chamber of the SRV5 with ball and disc

Figure 18. Optimol Instruments SRV5 tribometer for friction and wear testing of diverse materials, surfaces and lubricants (courtesy of Optimol Instruments Prüftechnik GmbH)

In order to investigate numerous variations of the system with a constrained budget, an Optimol Instruments SRV5 tribometer (Figure 18) was used as a basis of experiments related to this thesis. An SRV5 tribometer enables the user to apply a vast number of test sample types in a variety of experimental setups. In the initial exploratory research phase, a ball-on-disc setup was selected for friction and wear measurements. A standardised ball and disc sample complying with the requirements set in ISO 19291:2016 [108] was used for the ball-on-disc experiments. The relevant properties of the samples are summarized in Table 2.
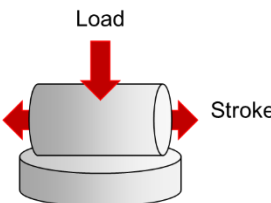
Table 2. Size and material properties of the ball and disc specimen

Specimen	Disc	Ball	
Size [mm]	Ø24 x 7.9	Ø10	
Material	100Cr6 (AISI52100)		
R_a [µm]	0.047 ± 0.003	0.02 ± 0.001	
HRC	62	61.5	
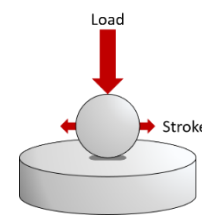
Additional research setups include a cylinder-on-disc arrangement utilizing identical disc samples to the ball-on-disc setup. The most relevant physical properties of the utilized cylinder samples are presented in Table 3. A third experimental setup is composed of a piston ring and a cylinder liner segment, both machined from series production parts of an inline 4-cylinder turbocharger gasoline engine. The investigated surface of the piston ring is coated with zinc phosphate, with surface micro-hardness and surface roughness value listed in Table 4. The cylinder of the engine is also equipped with a coating, which resides on the cast AlSi base material of the crankcase.

Table 3. Size and material properties of the cylinder specimen

Counter-body	Cylinder	
Size	Ø15 mm x 22 mm	
Material	100Cr6 (AISI52100)	
R_a [µm]	0.046 ± 0.003	
HRC	62	

The Fe-alloy cylinder wall coating is deposited through a high velocity thermal coating process, which is consecutively finished by a multi-step honing procedure. The resulting surface includes a certain number of voids in its bulk, which contribute to better lubricant retention and wear resistance. Table 4 also gives informative values of surface roughness and cross-section micro-hardness of the cylinder liner samples.

Table 4. Size and material properties of piston ring and cylinder liner specimen

Specimen	Piston ring	Cylinder liner
Diameter (nominal)	Ø74 mm	Ø74 mm
Overall dimension	56 x 14 x 2 mm	12 x 12 x 6 mm
Material (bulk)	cast iron	AlSi alloy
Material (coating)	zinc phosphate	Fe alloy
S_a [µm]	2.156 ± 0.196	0.258 ± 0.112
S_k [µm]	7.116 ± 1.226	0.170 ± 0.031
HV 0.5 (coating)	~360	282.4 ± 13
HV 0.5 (base)	316.3 ± 14.5	83.6 ± 3.4

All three experimental setups utilize a single degree of freedom, hence provide purely sliding friction between the body – i.e. the disc or the cylinder segment – and the counterbody – i.e. the ball, disc or piston ring segment. Every test run on a tribometer concludes with a primary dataset generated during the test run and a secondary dataset, which is an aggregation of data created before and after the test run. The primary dataset is a collection of time series data, which in the presented experiments involves sample temperature, oscillation frequency, average sliding speed, normal load, mean friction coefficient, absolute friction coefficient and stroke length values over the test period with a 1 Hz sampling frequency. The secondary dataset contains discrete values describing the test setup and boundary conditions, as well as 2D (photographs and microscope images) and 3D (surface topography data) information to illustrate and characterize the surface before and after the measurement. The

collected information is subsequently processed, analysed and visualized using MountainsMap and MATLAB or Python.

4.2 Samples, samples preparation and post-processing

Standardized friction and wear measurement samples for the ball-on-disc and cylinder-on-disc experiments were acquired from Optimol Instruments GmbH. Cylinder liner segments were manufactured from a series production crankcase. The cylinder bank was removed on an industrial metal cutting band saw at PER-KOR Kereskedőház Kft. Liner segments were machined from the prepared bank through wire electric discharge machining at Török Gépipari Kft. In order to avoid corrosion, the finished liner segments were sprayed with a paraffin-based wax. Piston ring segments were cut from series production parts with a Struers Labotom precision cutting machine. To avoid any possible influence due to hardening / softening of the material during machining, the sides of the cylinder segment are chamfered with a grinding machine. As a result, the transition zone is excluded from the contact area. For piston rings, the cut surface lies outside of the contact area. In order to provide appropriate curvature, the sample holder for the ring segment requires a significantly longer ring arc than the cylinder segment.

The first step of sample preparation is establishing a means of sample identification. For this purpose, an alternating head engraving machine was utilized to apply an alphanumeric identifier to the samples. The mechanical engraver was substituted with a fibre laser in the later stage of experiments to ensure better readability with long identifiers as well. Ball samples were not engraved, due to the limited surface area and the troublesome nature of engraving curved surfaces. These samples were handled separately and contained in labelled plastic zip-lock bags to prevent confusion. After applying the sample ID, the samples are stored in engine oil until further use.

Every sample goes through a cleaning procedure before surface analysis, and friction and wear measurement. Samples are spayed with an organic solvent in order to remove the bulk of the corrosion inhibitor (engine oil or paraffin wax). Samples are then placed individually in 50 – 100 ml borosilicate glass beakers and covered with a 1:1 mixture of isopropyl alcohol and acetone. The beakers are placed into an ultrasonic cleaner and the samples are agitated at 50°C for 10 minutes. Cleaned samples are

removed from the solvent bath and blown dry with laboratory compressed air. As a finishing step, the dried samples are placed into a desiccator cabinet until utilization.

a) Ø10 mm 100Cr6 ball

b) Ø24 mm 100Cr6 flat disc
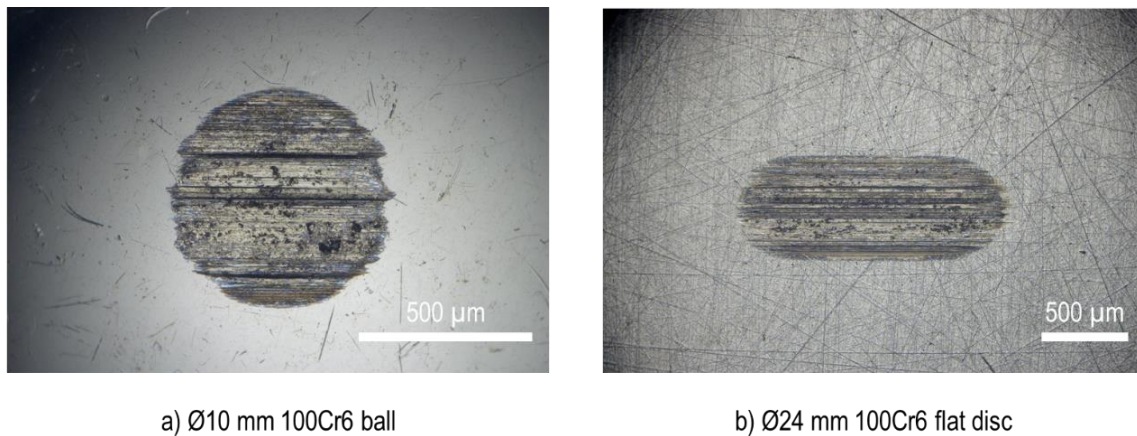
Figure 19. Exemplary microscope image showing the wear scar on a ball and disc specimen after friction and wear testing on the SRV5 tribometer

Before each friction and wear test on the tribometer the initial surface topology of the samples is recorded. A high resolution photo is taken to visualize any imperfection on the surface with a Nikon D5100 DSLR camera equipped with a Nikon AF-S Micro NIKKOR 60mm f/2.8G ED macro lens. Additionally, a high resolution microscope image (as shown on Figure 19) and a 3D confocal scan is also taken of the surface with a Keyence VHX1000 digital microscope equipped with a VH-Z100R lens, and a Leica DCM3D measuring microscope equipped with a 50x / 0.8 Leica HC PL Fluotar lens respectively.

Proceeding the test run on the tribometer, the samples are cleaned and subjected to all previously mentioned optical surface analysis steps. The surface is documented with the digital camera, and each wear scar is recorded with the digital microscope. The digital microscope also allows the measurement of 2D features on the surface, e.g. the diameter or width of the wear scar. A confocal scan of multiple overlapping single scans is taken over a larger area, which is set up to cover at least 2x the projected area of the wear scar in case of the ball-on-disc analysis. For larger wear scars a sampling approach is taken, which involves measuring 3-5 strips of surface topography perpendicular to the wear scar. These perpendicular measurements allow the quantification of a wear scar section area and wear scar depth, and can be used to calculate an approximate integral wear volume.
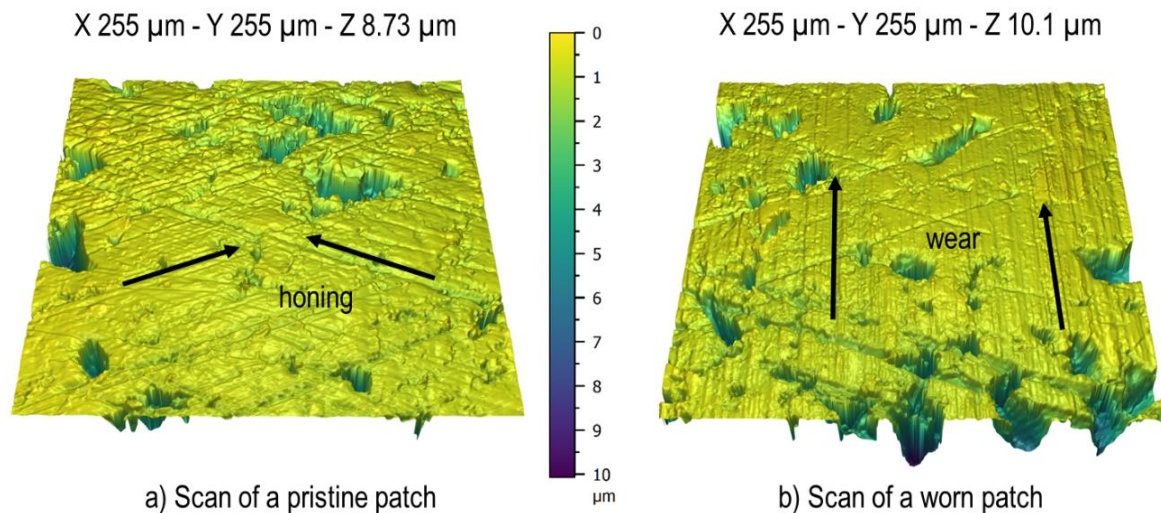
Figure 20. Exemplary confocal scans of a cylinder liner specimen showing the as-manufactured (a) and worn (b) state of the honed thermal spray coating

The collected 3D dataset is post-processed (as shown on Figure 20) in MountainsMap, which usually involves the following steps:

- creating a panoramic (tiled) dataset from multiple overlapping single scans,
- utilizing a levelling operator to remove any inclination from the data,
- retouching the surface – filling in non-measured areas and removing dirt,
- cropping the region(s) of interest,
- visualizing the wear scar with a 3D representation,
- calculating relevant surface roughness and topology parameters.

Results are either exported manually, or batch processed for selected measurement series, and saved in a spreadsheet.

In certain cases, a more in-depth analysis is carried out. Selected samples are further analysed with a Hirox SH4000-M table-top scanning electron microscope equipped with a Bruker Quantax energy dispersive X-ray spectroscope. Samples undergo an additional ultrasonic cleaning step in 99.9% ethanol at 50°C for 10 minutes before SEM imaging. A motorized rotating XY stage is used to manipulate samples, which are fastened by electrically conducting carbon tape to a flat or inclined (45°) aluminium sample holder.

4.3 Engine oil analytics

Physical and chemical analysis of the lubricant is a fundamental step in tribology research. The properties presented in this section were determined by the Austrian Excellence Centre for Tribology. Based on the source of the analysed sample a different set of analytical investigation steps were taken. For in-use engine oil samples, the verification of wear metal content can provide vital information regarding the health of the engine. However, no meaningful result can be derived from this assessment in case of the artificially aged samples studied in this thesis, since no mechanical aging was considered in the degradation process. Hence, the methodology of external analytics is grouped into three depth levels.

4.3.1 General physical and chemical properties

These properties were determined for all investigated engine oil samples, regardless if fresh, artificially aged or in-use.
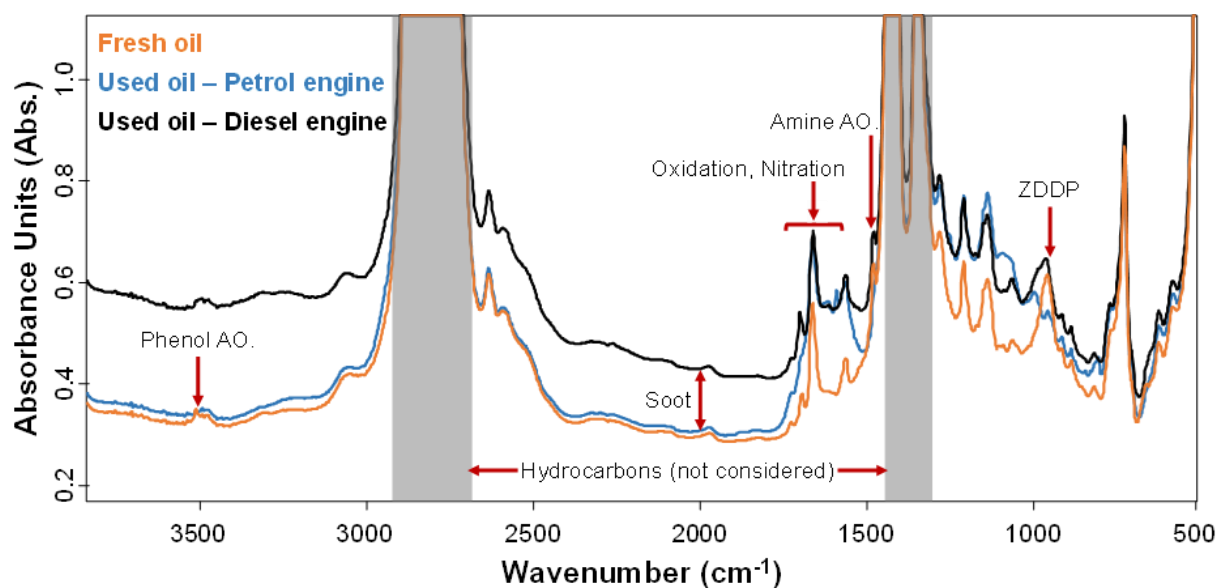
Figure 21. FTIR spectrum of used engine oil samples from a compression ignition (Diesel) and spark ignition (Petrol) engine, compared to the spectrum of fresh engine oil {8}. Changes in peak height and area can be translated to an increase in degradation products and the depletion of additives.

The infrared spectra of samples were captured via a Bruker Tensor 27 measurement device. The height of the measured absorption peaks was used to calculate oxidation (peak at 1720 cm^{-1}), residual content of aminic (peak at 1515 cm^{-1}) and phenolic (peak at 3650 cm^{-1}) antioxidant additives, and residual ZDDP antiwear additive content (highest from the range 1020 cm^{-1} to 920 cm^{-1}). The experimental method is further detailed in [109].

Kinematic viscosity was determined at 40°C and 100°C according to ASTM D 7042-21 [110] using an Anton Paar SVM 3000 instrument. The resulting kinematic viscosity values were used to calculate a viscosity index (VI) according to ASTM D 2270-10 [111].

Engine oil acidity and base reserves are characterized by the total base number (TBN), which was determined through potentiometric titration on a Basic Titrino 794 with a Metrohm auto-sampler. The process was conducted according to DIN ISO 3771 [112].

4.3.2 Conventional engine oil analysis

In addition to the previously detailed analyses, in-use engine oil samples were also subjected to the following diagnostic measurement techniques.

The captured infrared spectra were used to determine nitration using the adsorption peak height method at 1630 cm^{-1}, whereas sulfation and soot content were calculated according to ASTM E 2412-10 [113].

To assess the amount of water in the lubricant a coulometric Karl-Fischer titration according to DIN 51777 [114] was conducted on the samples with a KF Coulometer 756 assisted by a Metrohm Oven Sample Processor.

An element analysis was also performed using inductively coupled plasma optical emission spectroscopy (ICP-OES) on a ThermoFischer iCAP 7400 ICP-OES Duo. Samples were prepared with microwave assisted digestion after the addition of nitric acid as described in [109]. The elemental composition of the engine oil reveals internal and external contaminants e.g. wear metals and dirt, and it can give insight into the depletion of additives.

4.3.3 Advanced analysis

Selected in-use engine oil samples were also subjected to mass spectroscopy on a ThermoFischer TSQ Quantum XLS mass spectrometer, equipped with a Trace GC Ultra gas chromatograph, a flame ionization detector (FID) and a TriPlus autosampler. Gasoline content was determined according to ASTM D3525-20 [115], whereas diesel content measurements were based on ASTM D3524-14 [116]. Both quantitative and qualitative assessments were carried out as outlined in the previous methods. As

detailed in {6}, measurement parameters were altered to achieve better sensitivity with the available sample quantities:

"The parameters were adapted as follows: A column of 100% dimethyl polysiloxane was used with 15 m length, 0.25 mm diameter and 0.25 µm stationary phase thickness, instead of the 5–10 m length, 0.53 mm diameter and 0.88–2.65 µm stationary phase thickness as described in the standard. The oven was heated from 40° to 255°C at a heating rate of 16 °C/min, while a carrier gas (helium) flow rate of 10 mL/min was used. Sample evaluation was done according to the standard via determination of the area of the fuel component of interest. A calibration curve in the respective concentration range for calculation and the results were reported as sum parameter of all fuel components in mass percent."

4.4 Thermo-oxidative engine oil aging

In order to reduce cost and time needed for investigating several oil formulations with diverse fuel samples regarding thermal and oxidation stability a laboratory procedure was established based on Singer et al [117]. The newly developed method simulates the conditions of high temperature and constant gas flow inside the internal combustion engine. In contrast to commercial solutions, the procedure integrates a programmable, variable, cyclic load structure similar to real-life vehicle use to induce chemical alterations in the lubricant.
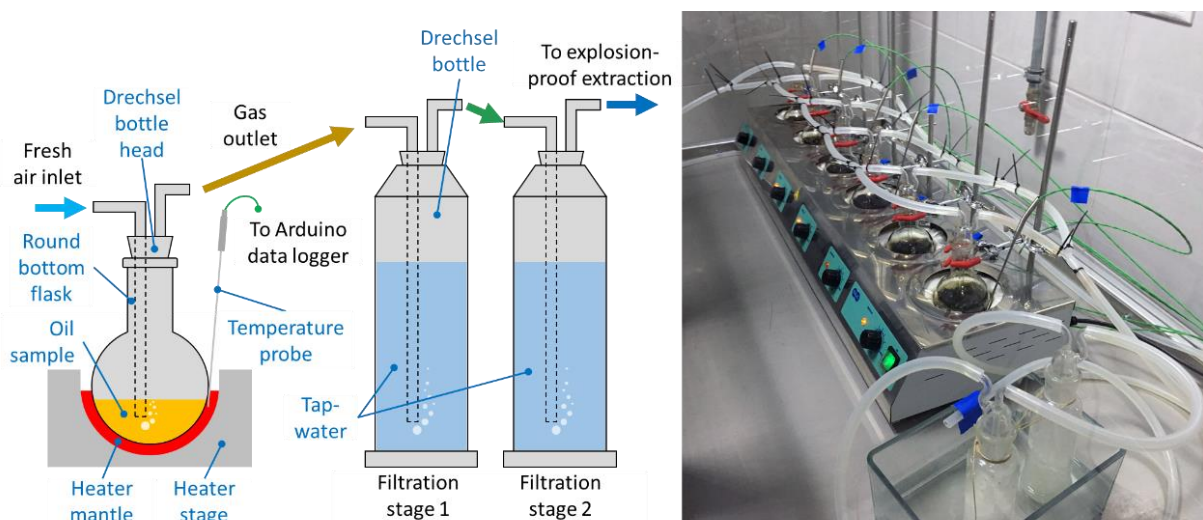

Figure 22. Thermal-cycling rig for controlled engine oil aging experiments (original setup)

A thermal-cycling rig (Figure 22) was designed with 6 individual heater stations for the simultaneous aging of different samples. The unit is based on a FALC BE-6 6-station

laboratory heater originally designed for Soxhlet extraction. The heater stations are able to accept flasks up to 500 ml and utilize a ceramic mantle for direct heat transfer. Each mantle is connected to an individual power regulator circuit and has a maximum power throughput of 180 W. The original design does not incorporate any means of temperature measurement or closed loop control for the mantle surfaces or the liquid inside the flasks. Six discrete power cut-off switches allow the selection of the maximal allowable power throughput of each mantle in five stages. A target temperature range is given for each stage by the manufacturer of the apparatus.

The initial aging setup involved six 250 ml round bottom flasks with six Drechsel bottle heads – a glass bottle head with two glass tubes running through, one connecting the head directly to the environment, the other extending into the flask – to allow for pressurized air to be lead through the contents of the flask. The inlet of each bottle head was connected with silicone tubing to a laboratory pressurized air supply system which was restricted from 7 bars to around 1,1 bar pressure. This ensures a continuous air supply for air circulation through the oil samples. The exhaust gas – a mixture of air, evaporated oil fractions and suspended fine droplets – was fed through two Drechsel bottles filled with tap water for filtration purposes. The setup is placed inside a purpose-built cabinet, which consist of an aluminium profile frame, polycarbonate side and top panels and a stainless-steel vat for spillage collection. The cabinet is connected to an explosion-proof gas extraction unit.

Since the FALC BE-6 has no built-in temperature control or any means of direct temperature feedback for the heater mantles, an Arduino data logging system was designed to monitor sample temperature. This setup also allows for future automation of the rig with precise temperature control, automated cyclic start and stop, and electronic air flow monitoring and control for each heater stage. In order to determine the temperature of the mantles, a K-Type thermocouple was wedged between each flask and its corresponding mantle for the first test run as a rudimentary approach. The thermocouples were connected through six MAX31850 thermocouple amplifiers to an Arduino MEGA board. The controller board is equipped with a data logger shield, which provides a real time clock and an SD-Card interface. These are necessary for precise time series data collection and time-based aggregation of measurement values. The device can handle SD memory cards with FAT16 and FAT32 file systems, enabling temperature log files of up to 4 GB in size. A 2,8" TFT-LCD screen with capacitive

touch provides a basic GUI for user input and feedback of current temperature and state information about the running experiment. The initial setup of the aging rig implemented no closed-loop temperature control.

4.4.1 Physical system development

A suitable solution to determine sample temperature during aging is necessary in order to realize precise temperature control. The initial setup utilized a one-neck flask design, which was accommodated with a Drechsel bottle head. This arrangement allows fresh air to enter the flask, flow through the sample, and exit the flask, but connecting a temperature sensor and maintaining ease of access for filling, emptying and sampling proved to be difficult. The external thermocouples were substituted with fine-wire thermo-couples (Ø0,25 mm), which were guided through the silicone tubing on the inlet side of the Drechsel bottle heads. This allowed the measurement of temperatures inside the flasks but introduced noticeable noise into the temperature measurement due to the incompatibility of the thermocouple amplifiers with the higher resistance of the fine-wire thermocouples.
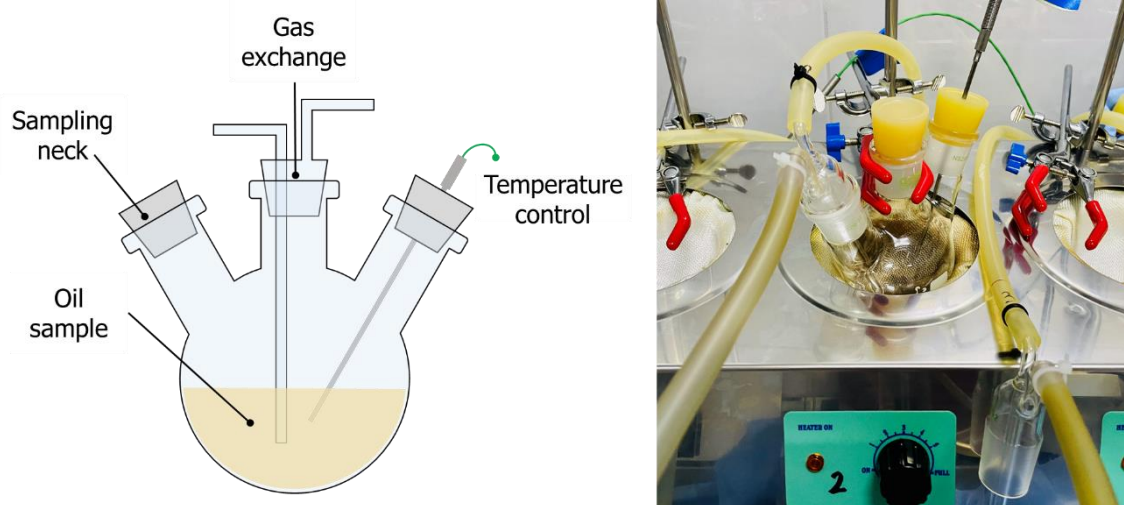
Figure 23. Revised thermal-cycling rig for controlled engine oil aging experiments, with three-neck round bottom flasks and improved control system

Since it was not possible to feed common size thermal sensors through the bottle heads, the one-neck round bottom flasks were substituted with three-neck flasks (Figure 23) with identical ground glass joints. The left joints of the flasks were occupied by silicone rubber caps. Regular Ø1,5 mm K-Type thermocouples were fed through the caps. The middle joints were occupied by caps as well, which can be easily removed for sample taking and contaminant dosing. A Drechsel bottle head was

connected to the right joint of each flask, allowing laboratory air to circulate through the sample lubricant. These modifications enabled the introduction of a precise closed-loop control system for sample temperature supervision.

In addition to the implementation of a closed-loop system, the admixing of the oxidizing agent (laboratory air) was also re-evaluated. In order to control the amount of air passing through the lubricant samples, individual flow meters were introduced into the tubing preceding the inlet of each bottle head. The flow meters utilize a single-tube rotameter principle to determine the volumetric flow of the gas passing through them. The flow meters are calibrated to instrument air – compressed air for pneumatic control systems – and are able to measure flows ranging from 1 l/min to 10 l/min.

4.4.2 Control system development

Temperature control is realized through six power width modulated (PWM) bidirectional triode thyristor (AC dimmer) circuits. These circuits communicate via SPI (Serial Peripheral Interface) on a two-wire bus with the Arduino control board. The control software of the aging rig is implemented in the Arduino language, a programming language similar to C. The main software loop consists of the following components:

- read and store values (in memory) from each K-Type thermocouple amplifier with 1 Hz,
- run PID algorithm and set output value for each AC dimmer every 5 seconds,
- refresh temperature values on screen every 5 seconds,
- output temperature values to memory card every 60 seconds.

Temperature values are read out in series through SPI with a sampling rate of 1 Hz. In order to avoid ambiguous readings and measurement errors, the control system uses five consecutive measurements to calculate an average temperature value. This value is given to the PID algorithm, which calculates the control terms according to the setpoint temperature and the received average temperature value for the corresponding thermocouple. The calculated terms are then used to determine the duty cycle, which is passed through the PWM output to the AC dimmer circuits. The most recent average temperature values are displayed on the LCD screen. The temperature values of each sample are stored on the SD-Card every 60 seconds.

Since PID control algorithms function efficiently around their setpoint, a logical control is implemented at the start of each heating cycle. The maximum allowable PWM output is set for the active heating mantles while the corresponding sample reaches a temperature of 20°C below the setpoint. After reaching this temperature value, the controller switches to the PID algorithm in order to reach the desired temperature.

A lower and upper heating boundary is implemented due to fire safety considerations. If any of the samples are unable to reach the setpoint during a given time period, the corresponding mantle is shut off permanently. To avoid overheating, the PWM output of the corresponding mantle is set to zero in case of a sample registering temperatures over 180°C. As opposed to static setpoint laboratory hotplates, the control system of the aging rig can be programmed to follow a given function of setpoint temperature over time. This enables the implementation of a variable temperature aging cycle, which can mimic temperature conditions present in an internal combustion engine during mixed use conditions.
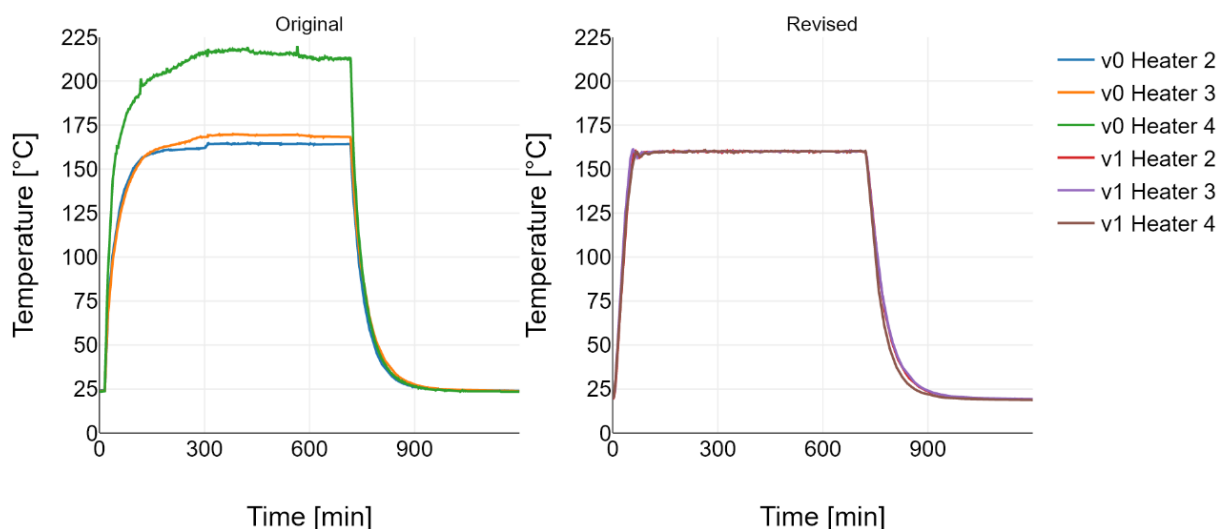
Figure 24. Temperature logs from the original (v0, left) and revised (v1, right) aging rig, with both running identical aging cycles, showing the enhanced precision of the revised physical equipment and control system

A two-stage thermal cycle was utilized in order to test the reliability of the control system on 150 ml oil samples. A cycle time of 24 hours was selected with a total aging time of 96 hours (4 cycles). During the first 12 hours of a cycle a temperature setpoint of 160°C was defined (tempering phase). The heater mantles were shut off during the second stage of each cycle (polymerization phase). A second aging experiment was conducted with the modified setup to determine the performance of the improved aging

rig. A constant air flow rate of 1 l/min was set. Figure 24 presents the improved behaviour of the revised system:

- steeper heating rate, thus a stable setpoint temperature is achieved in less time,
- better precision, reduce temperature fluctuations and offset,
- better repeatability, with nearly identical conditions across all heaters.

4.4.3 Aged sample characteristics

In order to confirm the suitability of the developed aging rig for the simulation of certain aspects of engine oil aging, the samples aged with the modified aging rig were sent to chemical analysis through Fourier-transform infrared spectroscopy (FTIR). Oxidation, nitration, ZDDP anti-wear additive, phenolic antioxidant content and aminic antioxidant content were determined as detailed in Chapter 4.3. Averaged values of all six samples for each chemical property are shown in Table 5. with their corresponding deviations.

Table 5. Averaged values and standard deviation of chemical properties of artificially aged engine oil (v1 aging rig setup, 96-hour cycle)

	Oxidation [A/cm]	Nitration [A/cm]	ZDDP [%]	phenol. AO [%]	amin. AO [%]
Ref. oil	0	0	100	100	100
Avg	4,1	0,6	10,8	82,2	83,0
Dev (abs)	0,1	<0,1	0,2	1,1	0,6
Dev (%)	2,7	4,8	1,6	1,4	0,8

The chemical analysis shows a mild oil degradation except for the ZDDP anti-wear additive content that shows a level of depletion comparable to engine oils with 7000 km mileage or higher [109]. This phenomenon could also be a result of the interaction between the metal sleeve of the thermocouples and the zinc-phosphate additive, which should be investigated and taken into account before further experimentation. In general, the aging experiment with the revised aging rig configuration produces highly comparable sample degradation in terms of oxidation, nitration and additive depletion. The deviation of values is under 2,5% for additive traces and under 5% for oxidation and nitration values. The presented trends are in agreement with the values published in [118].

The presented aging apparatus, methodology and preliminary results support Thesis 2.

4.5 Fleet study

The alteration of key physical and chemical properties – e.g. viscosity – of engine oils can affect performance, reliability and conformity of the engine. The depletion of anti-wear additives can give way to increased levels of wear on the cylinder wall surface and piston rings, which can lead to increased gas leakage and reduced peak pressure and ultimately a decrease in engine performance. Changes in viscosity due to aging can affect the behaviour of certain subsystems – e.g. hydraulic belt and chain tensioners, hydraulic valve tappets – in an internal combustion engine, which can result in unreliable operation. Changes in oil composition can also have an effect on the amount of oil consumption and the quality of exhaust emissions as a result.

A preliminary study for an experimental investigation on the effect of alternative fuel induced oil aging was conducted on a passenger car fleet composed of 12 vehicles. The vehicles were monitored between 09.2019 and 03.2020. The fleet contained a selection of compacts, sedans, estates and SUVs with 2-liter four-cylinder turbocharged DISI (9) and CIDI (3) engines ranging between 130 kW and 221 kW. Vehicles were selected based on historic data and the following considerations:

- engine type should be identical or closely related,
- vehicles with a high rental rate should be included,
- vehicles nearing end-of-life should be excluded,
- the fleet should include gasoline and diesel engines,
- the fleet should include restricted range and general use vehicles.

Only frequently rented vehicles were considered in order to ensure an approximate mileage of 15.000 km (oil change period) during the investigation. Since the study was planned for a period of 6 months, vehicles possibly reaching end-of-life during this timeframe were discarded. Vehicles were grouped into two distinct categories regarding their range of usage:

- Vehicles categorized as short-range were restricted to be used solely inside the perimeter of a given controlled speed zone (i.e., a speed limit of 50 km/h).
- Vehicles categorized as long-range were general-use passenger cars without any special restriction.

Table 6 summarizes key details of vehicles participating in the fleet study. A factory standard oil change was performed on each vehicle before the start of the experiment. The vehicles were filled with a VW 504.00/507.00 compliant SAE 0W-30 grade fully synthetic engine oil. Oil samples were taken at regular time intervals from every vehicle during the monitoring period. An intended sampling period of 1 month and 2500 km was defined for short and long-range vehicles, respectively. It should be mentioned, that certain vehicles were taken for excessively long trips, which lead to missed or late sample collection. In other cases, the driver ignored the request to bring the vehicle in for sample collection. A total of 47 in-use engine oil samples were collected throughout a 6-month time period.

Oil sampling was carried out through the dipstick tube of each vehicle. A moderately rigid medical polymer tubing was fed through the dipstick tube into the oil pan of the sampled engine. Samples were extracted with the help of a 50 ml medical single-use syringe. Each engine was operated at idle for at least 5 minutes before sampling in order to stir the lubricant volume and reduce the risk of clogging the polymer tube with sediments. An amount of 10-12 ml of engine oil was extracted at a time, to avoid the need for oil refill during the sampling period. Used engine oil samples were collected in 8 ml borosilicate vials, which were labelled with vehicle identifier, sampling date and vehicle mileage values.

Additional information regarding daily usage was collected through GPS vehicle fleet tracking. Vehicle speed and mileage values were registered every 5 seconds during each trip. The experiment was conducted with random ordinary drivers, who were not aware of their involvement. To respect general data protection regulations, no GPS coordinates were saved for analysis, nor was any other form of information collected, that could be used to identify individual drivers or to profile their behaviour.

The aim of the fleet study was to create a baseline for engine oil aging in modern high-performance vehicles under ordinary vehicle use conditions. Hence, a fleet comprising various chassis types and differing engine-power classes was commissioned to facilitate generalization of results. However, one main shortcoming of such an experimental design is the low reproducibility. An investigation in a strictly controlled environment – e.g. as presented in Chapter 6. – gives better insight into the nuances of in-use oil aging and show how variations in engine load, engine speed or

environmental conditions influence certain physical and chemical properties of the lubricant.

Table 6. Notable details of vehicles participating in the fleet study {6}

Vehicle	Engine type	Range	Engine power (kW)	Average trip length (km)	Average speed (km/h)	Number of oil samples	Total mileage (km)
1	Diesel	Long	130	32.2	85.4	4	12,700
2	Diesel	Long	140	34.5	89.5	5	11,600
3	Diesel	Long	140	34.9	93.2	2	1,300
4	Petrol	Long	221	18.5	64.2	2	8,000
5	Petrol	Long	185	24.7	76.5	4	14,700
6	Petrol	Long	185	36.0	81.1	5	17,100
7	Petrol	Long	185	38.0	96.9	4	9,200
8	Petrol	Long	221	9.5	50.5	2	5,100
9	Petrol	Long	221	31.3	74.9	4	7,500
10	Petrol	Short	155	1.5	16.0	5	1,700
11	Petrol	Short	155	1.6	12.4	5	1,100
12	Petrol	Short	155	1.6	17.3	5	1,800

4.6 Data analysis through statistics

A common approach to analysing time dependent variables is to calculate general statistic parameters, e.g. arithmetic mean and standard deviation values, which respectively describe the central tendencies and the variance of a given dataset. These characteristic numbers can serve as a first step in analysing and interpreting data. However, certain applications demand further details to appropriately explain a property of an observed phenomenon. One such example is surface roughness, where distinct surface topographies can possess identical average roughness values, meanwhile contributing to vastly different surface effects. Oil retaining bearing surfaces are better characterized by roughness parameters derived from the dispersion of asperities over the total height, rather than a central value and the average deviance of the population from this central value.

In order to visually and quantitatively portray time series values such as coefficient of friction during friction and wear testing, the probability density function and the quartiles of these datasets are calculated. The probability density function presents how likely would an arbitrary value equal a given sample in relation to any other. Using CoF over

time values measured in the study presented later in Chapter 5 as an example, Figure 25 provides a visual interpretation of the probability density function (PDF). The presented curve demonstrates, that during the corresponding measurement the CoF was most likely to take on a value between 0.1 and 0.105. It was also highly possible, that a CoF value between 0.095 and 0.1 gets registered. Yet, it was very unlikely, that CoF values under 0.08 or over 0.14 would be measured during the experiment.


Probability density of coefficient of friction
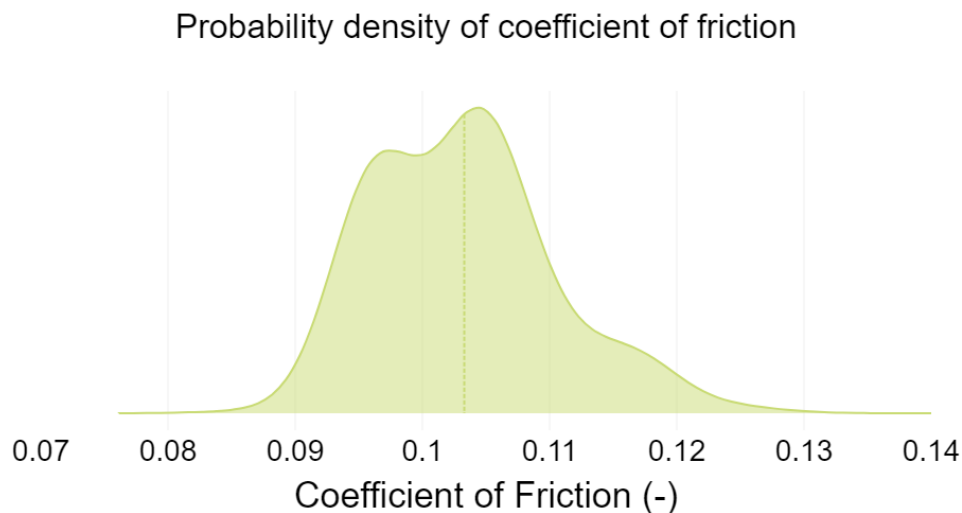
Figure 25. A typical probability density function of coefficient of friction values. The dashed line marks the arithmetic mean of the dataset.

Incorporating the arithmetic mean into the plot also accentuates the importance of using thorough analysis methods, rather than comparing means and deviations. As depicted on Figure 25, the mean of the dataset has a slightly lower probability, than the maxima of the curve. Hence, a randomly selected CoF value from the dataset has a fairly high probability of being slightly larger than the mean. A single PDF can be used to compare the probability of values in a dataset, but is also applicable to compare individual datasets to identify tendencies and patterns during repeated experiments.

Similarly to a PDF, quartiles describe the probability of a value being lower than a sample. The 1st quartile (Q1) is a quantitative indication of the lower 25 % of values, the 2nd quartile (Q2) indicates the lower 50%, and the 3rd quartile indicates the lower 75%. In other words, 25% of all values in a sample are lower than Q1, 50% of all values lie under Q2 – which is also the median of a dataset –, and 75% of all data have lower values than Q3. The distance between Q1 and Q3 is titled the interquartile range (IQR).

4.7 Data analysis through Principal Component Analysis

It is common in the field of engineering, that an experimental design considers numerous influencing factors, while monitoring the behaviour of multiple features over an extended number of observations and elongated amount of time. This approach can lead to robust, well based findings through taking into account most – if not all – actors in a given scenario. However, such holistic approaches can yield an immense amount of data with high dimensionality, which requires advanced analysis methods to be decipherable. The human brain is trained to look for patterns and correlations, but it's limited in the number of degrees of freedom it can simultaneously process. We can easily spot groupings and trends on a 2D or even 3D graph, or perceive patterns on a series of images, but struggle to even imagine anything beyond our reality. This means, that our ability to deduce anything from a high dimensional dataset is limited to 3-dimensional chunks of data. Hence, an established mathematical method for reducing the dimensionality of a dataset can be advantageous when dealing with large amounts of data.

One approach of dimension reduction is Principal Component Analysis (PCA). PCA takes a dataset with **n** features as its input and computes the projection of each feature to a new coordinate system, as well as the position of each observation in the new coordinate system. The new coordinate system or the coordinate system of the principal components is orthogonal and generally has 2 or 3 dimensions when PCA is utilized for exploratory data analysis. Intuitively, PCA can be imagined as encapsulating the data in an ellipsoid, which has its longest axis oriented with the direction of highest variance in the data. This axis represents the first principal component. The secondary axis represents the second principal components, and so on. The orientation of each principal component in relation to the original coordinates – i.e. the investigated features during the experiments – of the dataset gives insight to how each feature influences the variance.

The workflow of a PCA can be summarized through the following steps:

- Data preparation
- Covariance computation
- Eigenvalue decomposition
- Final dataset and visualization

Data preparation involves two essential actions, which ensure a successful and meaningful PCA. First, any missing value of the dataset have to be eliminated, since further calculation steps require a fully populated matrix. This can be accomplished either by dropping observations with missing values, or by interpolating from nearby observations. Subsequently, the data has to be standardized in order for all features to have the same scale. Omitting the standardization of the dataset would lead to a misleading interpretation, since a feature with values between -100 and 100 has an apparently larger variance then a feature with values ranging from 0.1 to 0.9.

The covariance of the prepared dataset is computed in the next step. In probability theory and statistics, covariance is a measure of the joint variability of two random variables [119]. In other words, the covariance matrix describes the correlation of values in the dataset. The covariance matrix is a symmetric matrix that has the variances of the features along its main diagonal and the covariance between each pair of features above and below the main diagonal. As described in [120] the covariance for a pair of features X and Y can be calculated through:

$$cov(X, Y) = \frac{\sum_{i=1}^{n}(X_i - \bar{x})(Y_i - \bar{y})}{n - 1}$$

or in case of a matrix A:

$$cov(A) = \frac{1}{n - 1} \sum_{i=1}^{n}(A_i - \bar{A})(A_i - \bar{A})^T$$

The calculation of the principal components is carried out through eigenvalue decomposition of the covariance matrix. Intuitively, this procedure uncovers the direction of largest variance in the covariance matrix. Eigenvalue decomposition is achieved through the diagonalization of the covariance matrix:

$$cov(A) = VDV^{-1}$$

were **D** being a diagonal matrix composed of the eigenvalues and **V** is the matrix of the eigenvectors. This is possible, since the covariance matrix is a symmetric matrix. The matrix equation can be represented by a single vector equation in the form of:

$$cov(A)\vec{u} = \lambda\vec{u}$$

where **λ** is composed of the eigenvalues and **u** contains the eigenvectors, which can be rearranged to:

$$(cov(A) - \lambda I)\, \vec{u} = 0$$

and solved by determining those **λ** eigenvalues, which satisfy the following statement:

$$det(cov(A) - \lambda I) = 0$$

Substituting back to # gives the corresponding eigenvectors:

$$(cov(A) - \lambda_i I)\, \vec{u}_i = 0$$

The results of the eigenvalue decomposition are **n** eigenvalue-eigenvector pairs, which are interpreted as scores and principal components (PC) respectively.
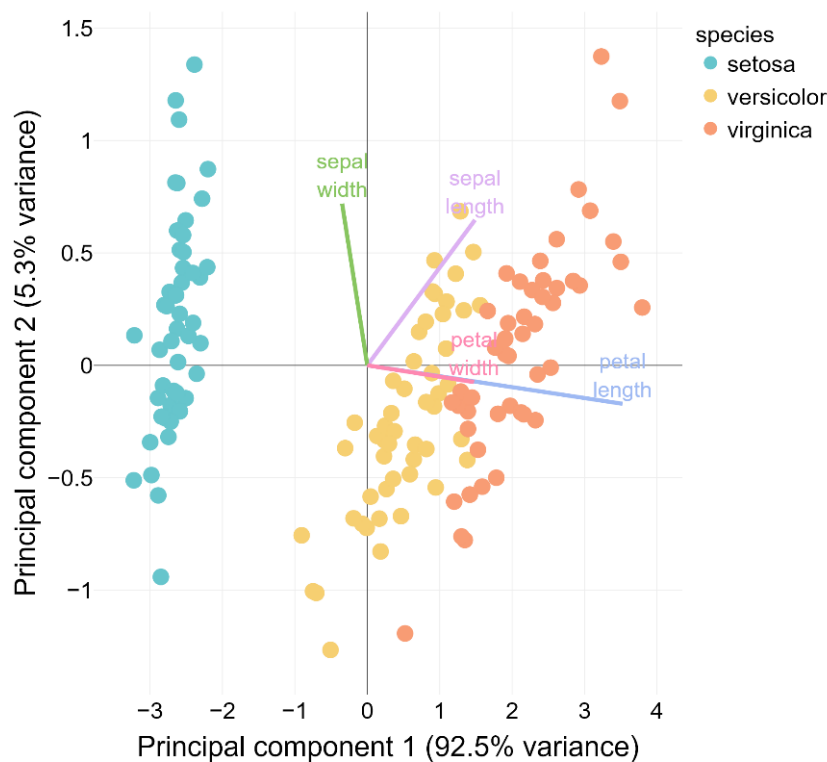
Figure 26. PCA scores of the iris dataset from Fisher [121], supplemented with the calculated loadings for each feature shown as vectors

As stated earlier, principal components show the directions of high variance in the dataset. Scores represent the amount of variance along their corresponding principal components. Figure 26 shows a well-known example for the benefits of principal component analysis based on the iris dataset of Fisher [121], which comprises of sepal width, sepal length, petal width and petal length measurements of numerous

specimens from three iris flower species: *setosa*, *versicolor* and *virginica*. A principal component analysis of the aforementioned 4 features reveals how these species can be clustered, which demonstrates the use of PCA to efficiently highlight the most significant features and differences in large datasets.

The principal components are arranged based on their scores into a descending order, with the 1st principal component (PC1) signalling the direction of highest variance. Since the number of principal components is identical to the number of features in the dataset, this calculation alone does not result in dimension reduction. To reduce the dimensionality a portion of the higher order principal components are neglected. Significant principal components are selected after calculating the amount of explained variance by each PC. The explained variance is determined by dividing the score of a PC by the sum of scores. Practically, the first 2 or 3 PCs are selected to facilitate visualization and interpretation, and the explained variance is calculated to assure the validity of the PCA. A PC1 with low explained variance indicates poor or non-existent correlation between the investigated features in the dataset. The selected PCs are gathered into a feature vector to facilitate further processing. In order to visualize the data in the coordinate system of the principal components the loadings and the final dataset needs to be calculated. The loadings present the contribution of each feature to a PC and are calculated by multiplying the eigenvectors with the square root of the eigenvalues. The final dataset is a projection of each individual observation into the coordinate system of the principal components, by multiplying the transposed feature vector with the transposed standardized dataset.

Consecutively, the observations of the original dataset can be depicted in the space of the PCs along with the projection of each contributing feature for further analysis and interpretation. Taking into account the loadings as well facilitates the interpretation of the score plot depicted on Figure 26. The largest variance (92.5%) of the data, which is shown along PC1 stems from differences in petal size, whereas PC2 corresponds to the differences in sepal size. According to the presented principal component analysis, it could be concluded, that the investigated species of the iris flower can be distinguished by taking a look at the size of their petals.

The described method was applied to the gathered data using Python 3.8 with scikit-learn 0.23.2.

5   Friction and wear testing of contaminated artificially aged engine oil samples

This section presents the results of standardized friction and wear testing on artificially aged engine oil samples contaminated with OME_{3-5} and EN 590 diesel fuel. Aging experiments were carried out by MOL-Lub Kft.

The amount of fuel in engine oil depends from several factors. Different engine specific power, use scenarios and testing methodology yield fuel oil dilution levels ranging from 2.5 wt% [42] to 25 wt% [122]. The type of fuel itself also has an effect on the amount of fuel in the engine oil, since different fuel types have different evaporation rates and characteristics [123]. Based on dilution levels published by [55], [41] and [124] a rounded weighted average of 7 wt% fuel contamination was determined as a basis for laboratory oil aging studies. Two different batches of aged oil samples were prepared containing 7.5 grams of fuel which resulted in a 7 wt% dilution of the sample oil. Friction and wear experiments were conducted on standardized steel specimen using the aged samples in a friction testing rig. Specimen surface alterations were characterized optically and through scanning electron microscopy.

5.1   The applied test method in detail

Data for this study were collected through friction measurements on an Optimol SRV5 high frequency reciprocating rig in a ball-on-disc configuration (see Chapter 4.1 and 4.2). To minimize measurement error and maximize reproducibility the testing of the aged oil samples was carried out according to the ISO 19291:2016 standard [108]. A method based on the procedure described in ISO 12156 [83] was utilized in order to determine the lubricity of fuels used for the dilution and aging of the sample oil. ISO 12156 prescribes the use of a Ø6 mm ball specimen.

The method described in ISO 19291 defines two different load sets. The first load set (Antiwear Additive Test – AAT) consists of a short run-in period and a static normal load period and aims at characterizing the coefficient of friction and the effect of antiwear additives. The second load set (Extreme Pressure Test – EPT) is made up of a longer run-in period and a number of short load steps with sequentially increasing normal load. This load set focuses on the effect of extreme pressure additives. The

effect of varying temperature during testing influences the evaporation rate of fuel from the lubricant as well as the viscosity of the aged sample.

The Antiwear Additive Test procedure should be applicable to investigate the behaviour of the model system in the boundary and mixed lubrication regimes. The oscillating motion realized with the reciprocating rig means a change in the direction of motion at the end of each stroke, where the relative velocity between the specimens is 0 mm/s. At this point the hydrodynamic film breaks and only a boundary layer remains between the specimens. The short stroke contributes to a low average relative velocity of 2 mm/s despite the high oscillation frequency, which implies that the model system operates in the mixed lubrication regime along the stroke. The test system was not equipped with any means of film thickness measurement apparatus, hence the exact friction regime in which the system operates at any given time is only theoretical.

Table 7. Parameter of the HFRR test procedures

Test mode	Lubricity	Antiwear
Sample	various fuels	various aged oils
Sample quantity (ml)	2	0.3
Temperature (°C)	60	50
Stroke (mm)	1	1
Frequency (Hz)	50	50
Load (N)	2	300
Test time (s)	4500	7230

Fuel lubricity measurements and friction and wear experiments with the aged oil samples were carried out according to the test parameters listed in Table 7 which result in an initial mean contact pressure of 0.55 GPa and 2.09 GPa respectively[1]. The contact pressure is however not constant throughout the measurement, since the area of contact gradually increases due to wear. This results in a gradual decrease of contact pressure during the 120 minutes of the experiments. The specified amount from the investigated lubricant sample was applied manually with a pipette before each test run. Coefficient of friction, disc temperature and normal load were registered during the high frequency reciprocating rig (HFRR) experiments.

---

[1] Calculated according to the Hertzian theory considering homogeneous material properties with E = 210 GPa and v = 0.3

To incorporate oxidative effects a two-stage laboratory aging process was carried out on two batches of lubricant with defined fuel content.

Table 8. Properties of fuel and oil samples

Sample name	lean oil	OME$_{3-5}$	EU D
Description	SAE 0W-20	oxymethylene ether 3-5 mixture	regular EN 590 diesel fuel
Density (g/cm^3)	0.839[a]	1.068	0.82 – 0.845[b]
Kin. Viscosity at 40°C (mm^2/s)	46.3[a]	1.19	2.0 – 4.5[b]

[a] manufacturer specification
[b] as specified by EN 590

A fully formulated SAE 0W-20 grade engine lubricant was pre-aged for 72 hours at 170°C in the first stage. The pre-aging occurred in the presence of an iron-acetic anhydride catalyst to facilitate oxidation. Laboratory air was circulated through the flask containing the lubricant. Samples were taken 72 hours after the start of the first phase and fuel was mixed into the flask to achieve a 7 wt % dilution level for the second phase. Further samples were taken at 96 and 120 hours of total aging time. Kinematic viscosity and acidity were checked 72, 96 and 120 hours after the start of the aging process. The aged samples were then subjected to the previously described friction and wear tests. The most relevant physical properties of the used compounds are given in Table 8. An overview of the aged lubricant samples is given in Table 9. Sample names are constructed from the aging batch (B1 and B2) and the aging time (72, 96 or 120 hours).

Table 9. Sample names and properties for artificially aged oils

Sample name	Description	Age (h)	Kin. Viscosity at 40°C (mm^2/s)	TAN
B1-072	lean pre-aged oil, no contaminant	72	43.9	2.7
B1-096	B1-072 with 7 wt% OME$_{3-5}$ after 24 h	96	42.8	4.4
B1-120	B1-072 with 7 wt% OME$_{3-5}$ after 48 h	120	41.9	6.6
B2-072	lean pre-aged oil, no contaminant	72	41	4.56
B2-096	B2-072 with 7 wt% EU D after 24 h	96	40	6.44
B2-120	B2-072 with 7 wt% EU D after 48 h	120	41.4	5.95

Viscosity and acidity measurements reveal the effect of artificial aging in the presence of fuel on the lubricant. The viscosity of the first batch (B1) shows a decreasing trend with a steady increase in the total acid number (TAN), which signifies an advanced

stage of oxidation. Samples of the second batch (B2) show a decrease in viscosity after 96 hours but increase over the viscosity of the pre-aged sample after 120 hours. TAN shows a similar behaviour with rising values at 96 hours which fall back after 120 hours of aging.

5.2 Tribometrology and surface analysis results

Wear analysis was carried out through optical microscopy and scanning electron microscopy (SEM). The surfaces of the ball and disc specimen were investigated under a digital optical microscope. For the ball specimens the diameter of the wear scar was determined as the mean of two diameters measured perpendicular to each other. An increase in wear scar diameter signifies a decreasing lubricity. The surface topology of the wear scars on disc specimens were determined through confocal microscopy measurements. Scanning electron microscopy was utilized to get a better understanding of the worn surfaces microtopology and to identify wear processes and wear debris build-up on the surface of the disc specimen.
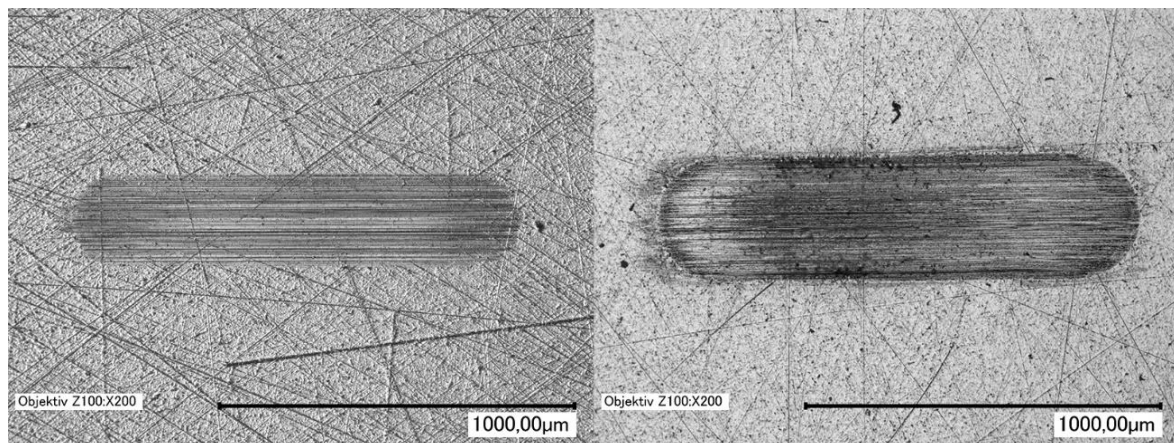

Figure 27. Wear scar on a selected disc specimen after ISO 12156 lubricity test with regular EN 590 diesel fuel (left) and oxymethylene ether 3-5 mixture (right)

According to the ISO 12156 standard, the maximum allowable averaged wear scar diameter (AWSD) of the ball specimen after a standardized fuel lubricity test run should not exceed 460 µm. An AWSD of 278 µm ± 3 µm was established with regular diesel fuel. In contrast, a value of 340 µm ± 29 µm was registered with OME_{3-5}. The increase in the wear scar diameter with OME_{3-5} in comparison to regular diesel fuel could be attributed to the generally lower viscosity of OME_{3-5}. A lower lubricant viscosity hinders the formation of a hydrodynamic film between sliding surfaces at lower sliding speeds, which leads to a higher amount of solid-solid contact and eventually higher surface

wear. In addition to the wear scar measurement on the ball specimen, the worn surfaces of the counterbodies (discs) were also characterized. Figure 27 shows a representative image of the worn surfaces after lubricity measurements with both fuels. While the amount of wear and therefore the lubricity of the two interfacial fluids lies in an acceptable range, the wear mode appears to be very different. The surfaces of the specimen lubricated with regular diesel tend to have abrasive wear marks along the sliding direction with little discoloration, whereas specimen surfaces lubricated with OME_{3-5} show heavy discoloration in addition to signs of adhesive wear in the form of small holes in the worn area. The discoloration can be a sign of tribo-oxidation occurring during the experiments due to the evaporation of the lubricating fluid.

HFRR experiments were carried out to determine the lubricating properties of the samples. The coefficient of friction along the stroke through the measurement was registered for each sample. An absolute integral value was calculated for each stroke in order to incorporate both the extremes at the end of the stroke and the lower CoF mixed lubrication regime in the middle of the stroke. The probability density of the coefficient of friction curves for the fresh oil sample as well as both aged batches at 72, 96 and 120 hours after the start of the laboratory aging process is shown on Figure 28. The deterioration of the oil due to aging can be observed through the probability density curves. Fresh oil ensures a higher coefficient of friction, presumably due to the presence of friction modifier additives. The pre-aging procedure oxidizes the friction modifier and further aging contributes to the polymerization of the lubricant. A 7wt% contamination with OME_{3-5} causes a higher mean coefficient of friction after 96 hours total aging time compared to regular diesel. Both batches draw highly similar results in terms of CoF after a total aging time of 120 hours.

Mean averaged wear scar diameters of the ball specimen and averaged CoF values for the lean and aged oil samples are illustrated in Figure 29. An optical image of a selected wear scar for each oil sample along with the corresponding surface topology illustrated through 2D pseudo-color plots are presented on Figure 30 to Figure 32. Wear scars of the discs were categorized as mild, moderate, severe or extreme according to the depth and lateral extension of the scar and the extent of fatigue wear on the surface.

Probability density of coefficient of friction
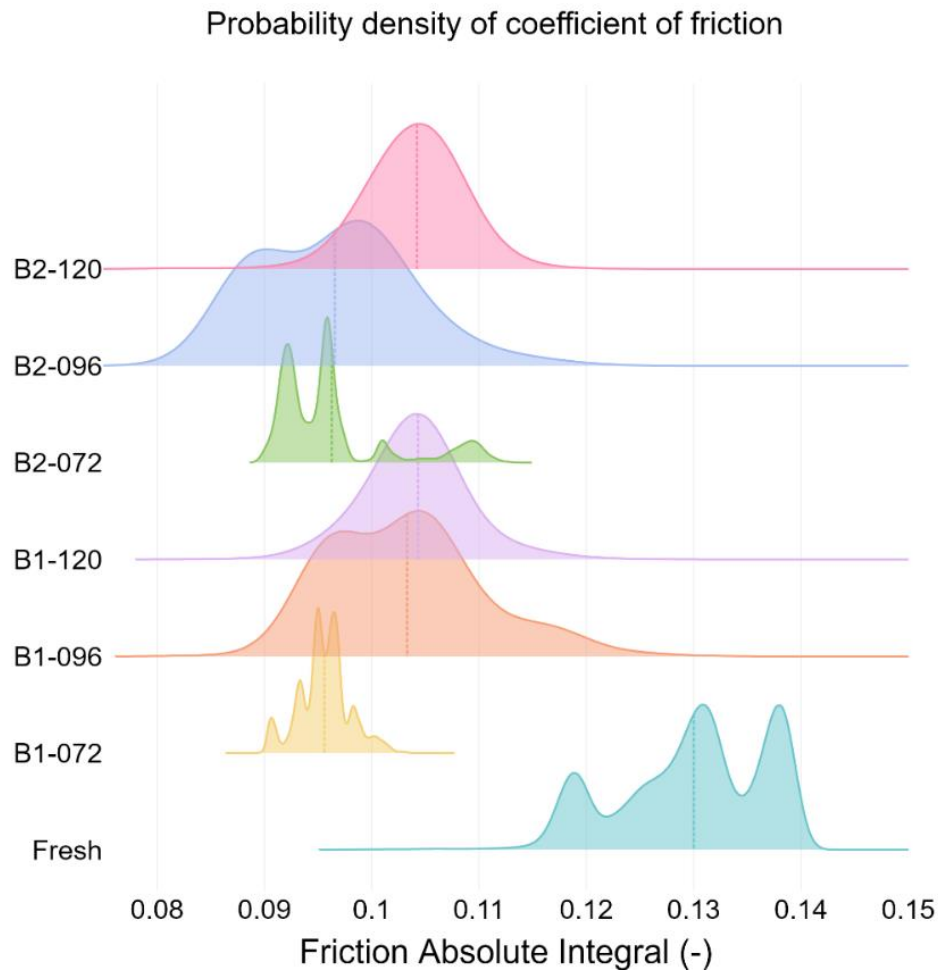
Figure 28. Probability density of the coefficient of friction for the fresh and aged samples, calculated from a total of three measurements for each sample; dashed lines represent the mean value
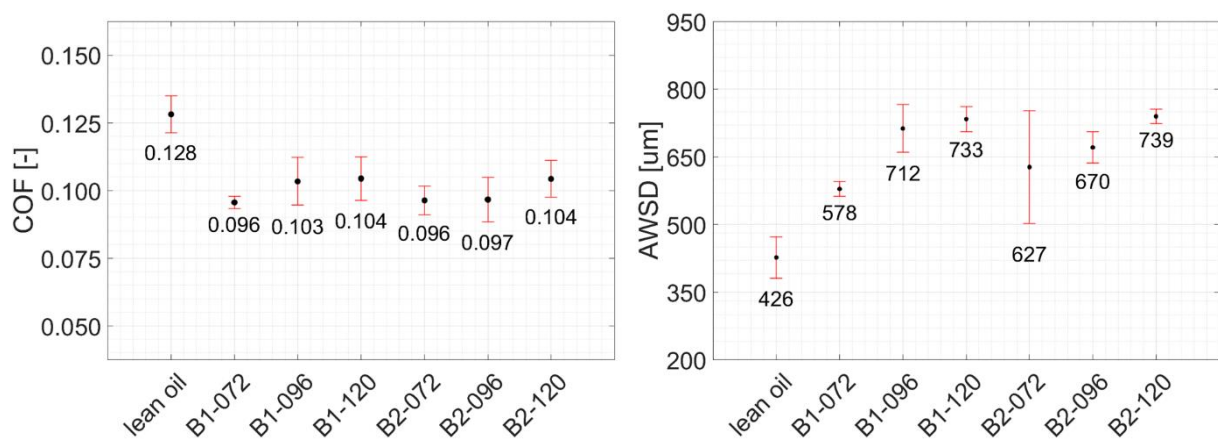

Figure 29. Mean coefficient of friction (left) and mean averaged wear scar diameter (right) for lean (fresh) and aged oil samples

The measurements with lean oil show a higher CoF, which could be attributed to the higher viscosity of the lean lubricant. A slower run-in process can be identified from the generally lower wear scar diameter of the ball specimen. The surface of the disc

specimen (Figure 30) shows mild abrasive wear marks along the stroke with no sign of adhesion. The discoloration could be attributed to additive build-up on the surface. These results are in accordance with the anticipated behaviour and wear mode of a fully formulated low viscosity lubricant in a reciprocating wear test. Both batches of aged lean oil B1-072 and B2-072 show a significantly lower CoF after 72 hours of thermo-oxidative aging as the lean oil.
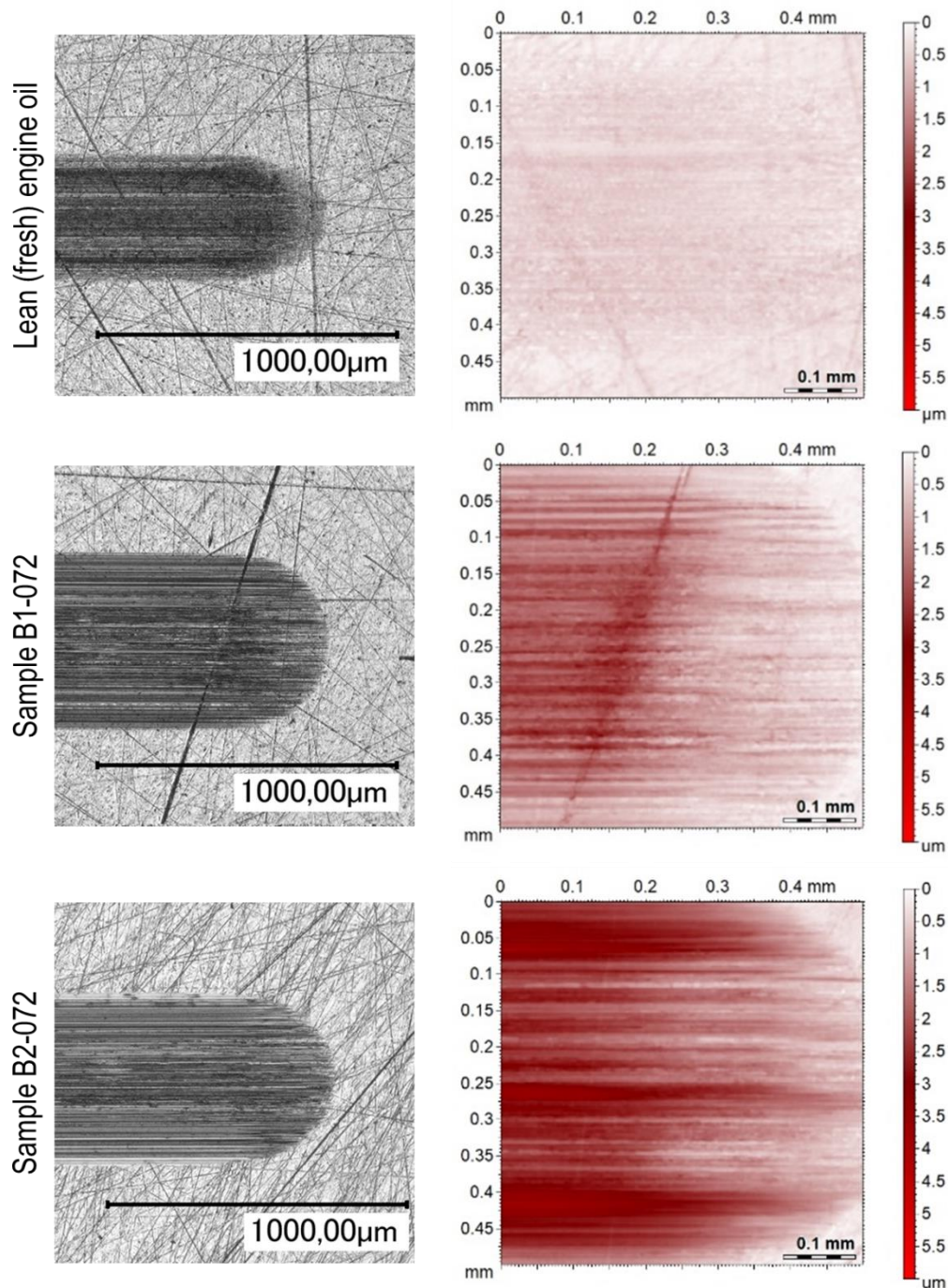

Figure 30. Optical image and confocal scan of a selected wear scar for the fresh and pre-aged (B1-072 and B2-072) oil samples

Increased values of wear scar diameter on the ball specimen were registered. The worn surface of the discs show mild to moderate abrasive wear marks and mild discolouration.

After 96 hours of aging the lubricating properties of the contaminated samples show noticeable variation in the wear process. Contaminating the sample with OME_{3-5} (B1-096) results in an increase in the coefficient of friction and wear scar diameter as well. The wear mode also appears to vary, with a generally deeper wear scar and a significant number of wear pits appearing on the surface of the disc (Figure 31 top row). The worn surface also shows abrasive wear marks and a subtler discolouration.
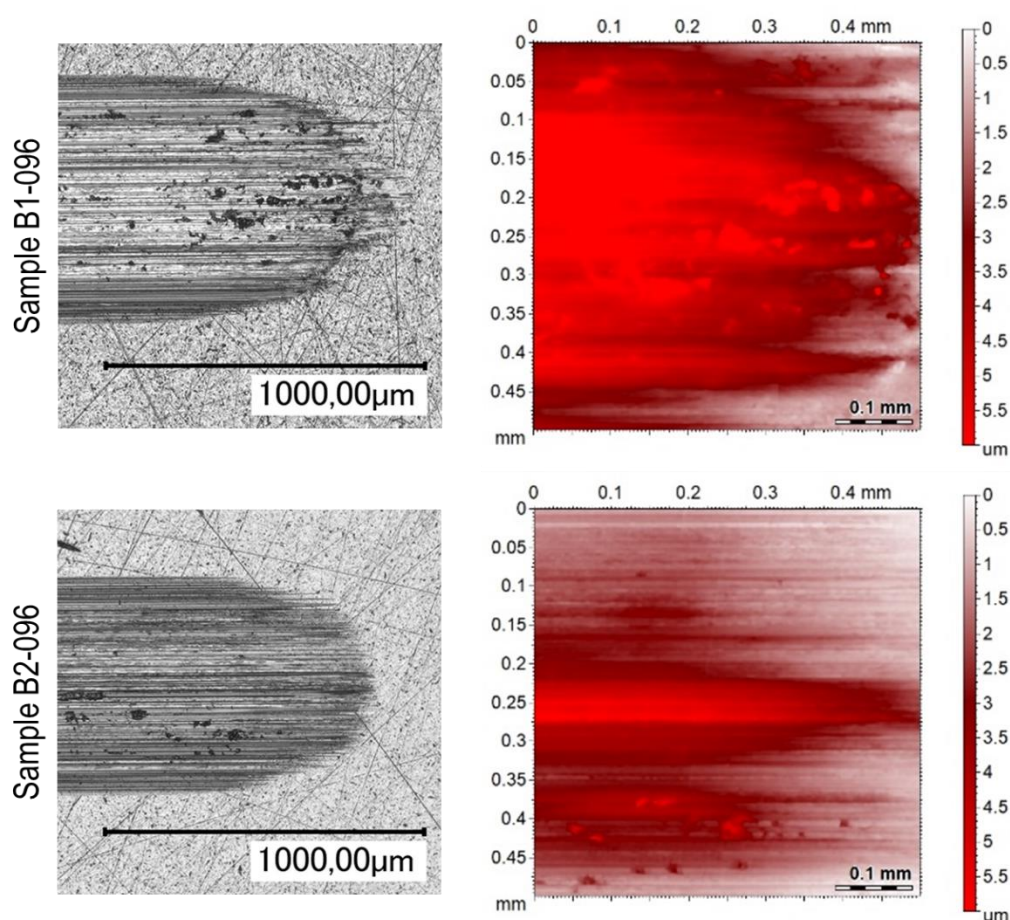
Figure 31. Optical image and confocal scan of a selected wear scar for samples B1-096 and B2-096

Samples contaminated with regular diesel (B2-096) show a slightly lower CoF compared to the other batch at the same stage (B1-096). A less steep increase in wear scar diameter can be registered compared to the samples with OME_{3-5}. There appears to be a mild change in wear mode with some wear pits developing on the surface of the disc specimen in addition to moderate abrasive marks (Figure 31 bottom row).

After 120 hours of aging the difference in the coefficient of friction between the two batches disappears. The overall lubricating properties of the engine oil seem to deteriorate to a level where the type of contamination cannot be clearly distinguished from the friction curve nor from the wear analysis. Wear scar diameter with both batches reaches a maximum value around 750 μm. The surface of the worn discs show severe wear with a mixture of abrasive wear marks and wear pits and mild discolouration (Figure 32).
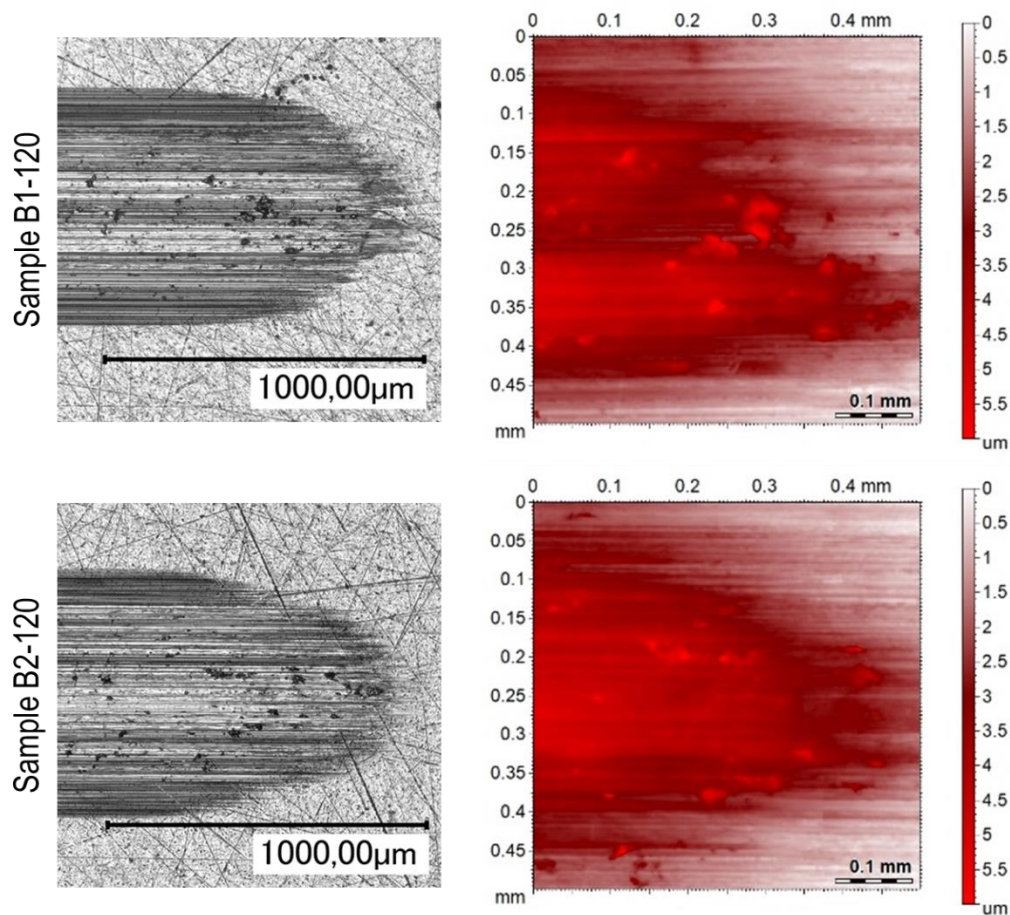

Figure 32. Optical image and confocal scan of a selected wear scar for oil samples B1-120 and B2-120

Further aspects of the wear mode can be determined through SEM micrographs of the worn surfaces of the disc specimen. Figure 33 and Figure 34 shows the micro-topology of a representative specimen from the measurements with samples from B1 and B2 after 96 hours and 120 hours of aging.
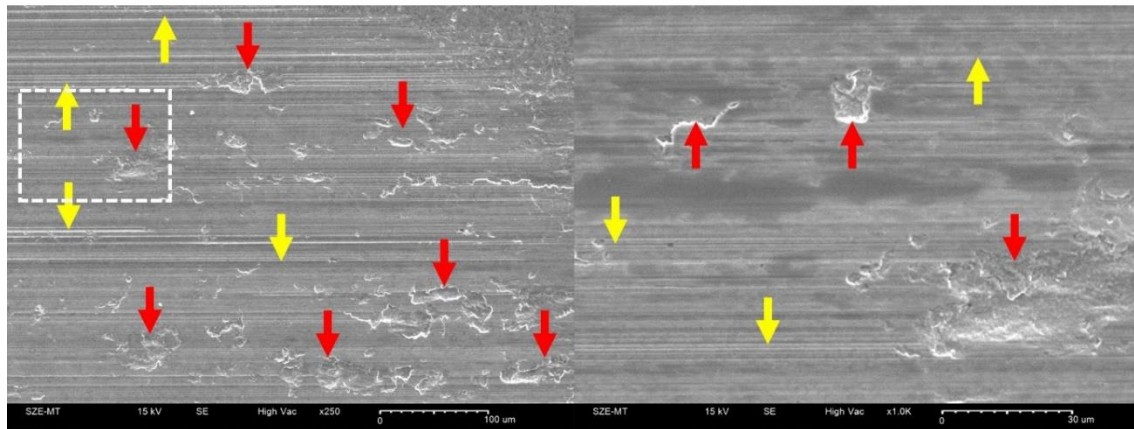
Oil sample B1-096 (contaminated with OME$_{3-5}$)
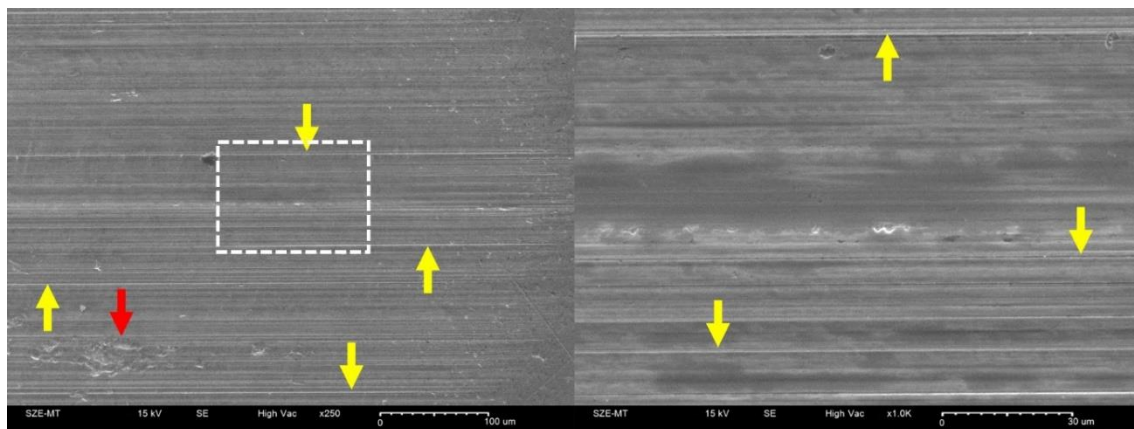
Oil sample B2-096 (contaminated with EN 590 diesel)

Figure 33. SEM secondary electron images at 250x (left) and 1000x (right) magnification, showing surface topography on a worn disc after friction and wear testing. Red arrows highlight pits on the surface, whereas yellow arrows point to abrasive wear tracks.

Numerous wear pits can be found on the specimen surface after friction and wear testing with B1-096 containing 7 wt% OME$_{3-5}$, whereas the sample with the same amount of regular diesel (B2-096) tends to produce milder wear and less surface fatigue. With both samples aged for 120 hours the wear marks on the surface show similar characteristics to each other, with a large number of wear pits appearing on the surface.
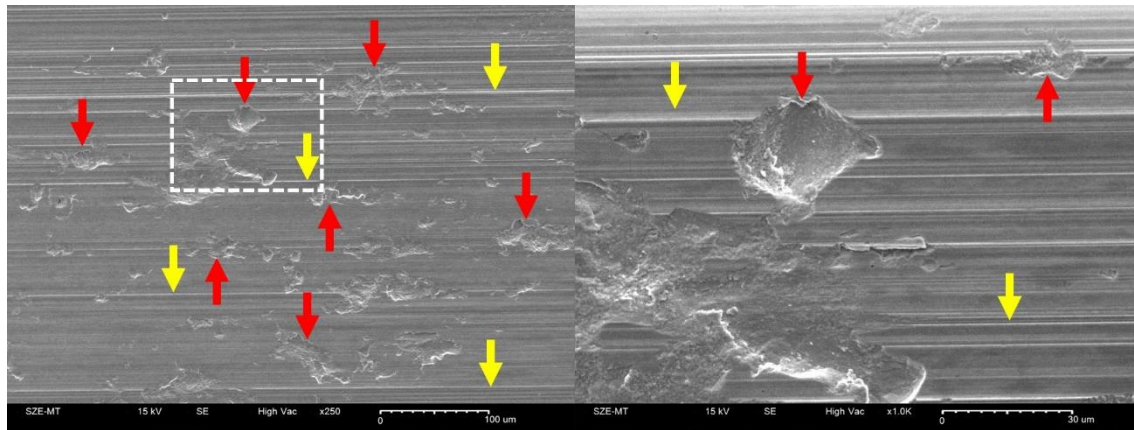
Oil sample B1-120 (contaminated with OME$_{3-5}$)
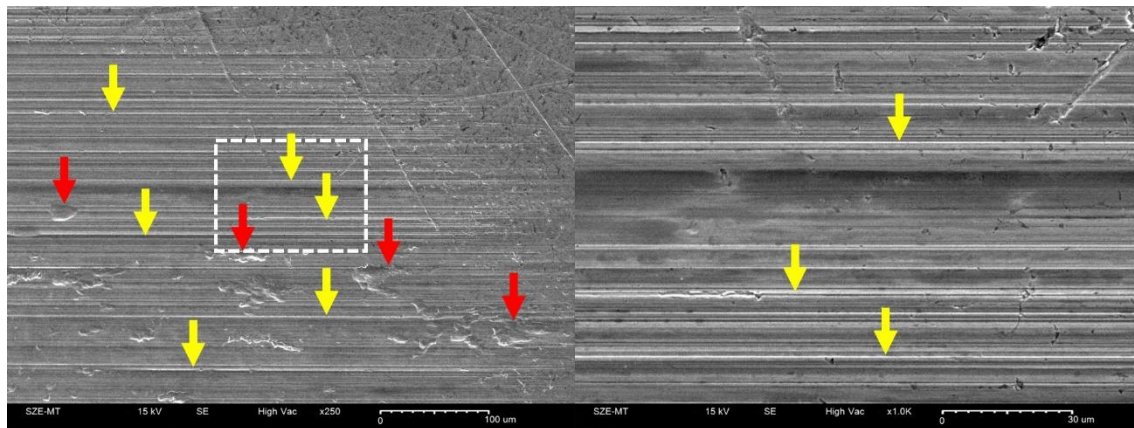
Oil sample B2-120 (contaminated with EN 590 diesel)

Figure 34. SEM secondary electron images at 250x (left) and 1000x (right) magnification, showing surface topography on a worn disc after friction and wear testing. Red arrows highlight pits on the surface, whereas yellow arrows point to abrasive wear tracks.

5.3 Summary and conclusion

The used aging method is designed for the comparison of oxidation stability of different lubricant formulations in the presence of standardised diesel fuel, however it does not account for the possible changes in the behaviour of the mixture due to different contaminant compounds being used. An iron-acetic anhydride catalyst is utilized to accelerate oxidization and to incorporate the presence of ferrous materials during aging. Since the exposure of the catalyst to the contaminant is inevitable in the mixture there is a possibility of unwanted reactions between the two which can lead to uncertainty and reproducibility issues.

Although considering a 7 wt% dilution level with the presented aging method proved to be adequate to show the differences in CoF and wear mode between samples contaminated with OME$_{3-5}$ and regular diesel fuel, further investigation of engine oil dilution levels and oil aging processes is necessary to better approximate real-life oil

degradation through laboratory aging procedures. Undesired reactions during aging due to the catalyst should be excluded through systematic analysis of the aging procedure.

Sample viscosity and acidity in Table 9 show the effect of aging on the chemistry of the engine oil. A change in both viscosity and TAN of aged samples compared to the lean oil is anticipated as a result of the thermo-oxidative aging process. Johnson et al. [125] investigated the oxidation and wear performance of low phosphorus engine oils and demonstrated that the change in viscosity and oxidation during the aging process is not strictly monotonous. Viscosity showed an initial decline and reached a minimum value at 70 hours aging depending from the phosphorus content of the lubricant. At 120 hours, viscosity values showed an overall increase over the initial value. Oxidation showed a decreasing tendency in the first 70 hours of aging and started to rise rapidly afterwards. Varying tendencies of viscosity values can be observed in field test oil samples [126], [127] as well and could be attributed to the depletion of antioxidant and viscosity modifier additives causing an initial drop and the subsequent oxidation of the base oil resulting in the thickening of the lubricant [128]. This phenomenon could explain the diverging results of viscosity and TAN values of B2 samples.

A decline in the viscosity of all samples of B1 and B2 compared to lean oil is anticipated after adding the contaminant [129]. As a result of sample dilution due to fuel addition the effect of oxidation on the viscosity is less noticeable with sample age. The difference in wear behaviour between contaminated samples B1 and B2 could be a consequence of OME_{3-5} accelerating depletion of additives. This could be the cause of elevated wear scar diameters and severe fatigue wear experienced with B1 after addition of the contaminant. A detailed analysis of chemical composition through FTIR spectroscopy or GC-FID chromatography could give better insight into the state and composition of the oil samples.

The probability density curves on Figure 28 show the anticipated behaviour of aging, with a reduction of the CoF of pre-aged samples B1-072 and B2-072 in comparison to the lean oil. The chemical alterations during aging in the presence of fuel appear to change both the ability of the lubricant to form a sufficient hydrodynamic film and the ability of additives to form a protective boundary layer on the surface. This leads to elevated amounts of wear in comparison to lean and pre-aged samples shown on

Figure 29 and a change in wear mode with indicators of localised fatigue appearing in the form of pits on the surface. The elevated wear rate will result in a large AWSD value and hence an enlarged contact area. The comparably low CoF values of contaminated aged samples B1-096, B1-120, B2-096 and B2-120 could be attributed to a decreased contact pressure between ball and disc due to the evolution of the contact area. Based on the presented results of different imaging techniques the number and size of pits on the surface seem to increase with aging time. After 120 hours the lubricating properties of both batches are clearly insufficient.

The effect of oxymethylene ether on a fully formulated engine lubricant was analysed and compared to regular diesel fuel through laboratory aging and friction and wear testing experiments. Two batches of contaminated oil containing 7 wt% fuel were subjected to a thermo-oxidative aging process. Samples were taken from the aged oil after 72, 96 and 120 hours of aging, and were used as lubricant in a high frequency reciprocating rig test procedure utilizing standardized steel ball and disc specimens. The lubricity of the fuels used as contaminant was also determined using a different set of parameters on the same testing equipment. Wear scar diameter and wear mode of the specimen was characterized using optical microscopy and scanning electron microscopy. The following conclusions can be drawn from the conducted experiments:

- oxymethylene ether has a slightly worse lubricity and produces a larger wear scar as regular diesel fuel,
- the wear mode in the experiments with OME_{3-5} appears to be different from diesel fuel, with a heavier discoloration which can be a sign of oxidation during the HFRR experiment,
- the aging process decreases the viscosity of the engine oil after 72 hours, which can be a results of the cracking of long-chain molecules and oxidation of additives in the lubricant, and leads to a decrease of the CoF and an increase in abrasive wear,
- adding 7 wt% OME_{3-5} to the pre-aged oil and aging for another 24 hours results in a mild increase of the CoF which can be attributed to the change in wear mode to fatigue wear and a significantly higher amount of wear in general, which is believed to be caused by the faster degradation of antiwear additives in the lubricant due to the presence of OME_{3-5},

- adding 7 wt% diesel to the pre-aged oil and aging for another 24 hours has subtler consequences as OME_{3-5} and results in a slightly lower CoF as compared to the results with OME_{3-5} and a less severe surface fatigue occurring on the surface of the specimen,
- continued aging of both batches of contaminated engine oil for a total of 120 hours results in identically severe wear and similar CoF.

Further research is needed to narrow down the cause of the sudden increase in the amount of surface fatigue on the specimen in the presence of OME_{3-5} in the aged oil. Ongoing FTIR analysis of aged oil samples and further aging experiments with elevated amounts of fuel in the oil as well as experiments with base oils are considered to better characterize the effect of oxygenated compounds on the engine oil.

The presented findings support Thesis 1.

6   In-use engine oil aging experiment on an engine testbed

In order to confirm the validity of the artificial aging method and the usability of the developed apparatus, a reference for in-use engine oil degradation is necessary. This section describes the results of data analysis conducted on an empirical dataset of used engine oil properties, average coefficient of friction values and average wear scar diameter values. Engine testing, sample collection and tribometrology was carried out independently from this thesis work at Audi Hungaria Zrt. and the Department of Internal Combustion Engines and Propulsion Technology. Oil analysis was performed by MOL-Lub Kft.

6.1   The applied test method in detail

Engine oil samples were collected from three identical series production turbocharged direct injection diesel engines with a specific power of 60 kW/l, which were investigated on a fired engine test bed. Each engine was subjected to a different test cycle with moderate to high loads and engine speeds. The engines were filled with SAE 0W-30 grade fully synthetic lubricant. Oil samples were taken every 50 hours for oil condition monitoring purposes. Although structurally identical, the three engines spent varying amounts of time in test (ELh) before this study.

The three selected test cycles are internally standardised procedures. Cycle 1 (C1) is intended to simulate the conditions of real-life driving and consist of mixed loads and engine speeds. The second test cycle (C2) is designed to stress the exhaust gas recirculation (EGR) system of the engine and consists of discrete steps with varying engine speeds and throttle positions. Cycle three (C3) is designed to stress the engine to its limits and consist of differing engine speeds with WOT and half-load conditions.

As part of the prior investigation a total of 43 oil samples were collected and sent to oil analysis in order to characterize the state of used engine oils. Kinematic viscosity at 40°C (KV40) and 100°C (KV100) were determined according to ASTM D 7279-16 [130]. Total acid number (TAN) and total base number (TBN) were determined through potentiometric titration according to ASTM D 664-11a [131] and ASTM D 2896-15 [132], respectively. Trace elements of additive depletion (Ca, Mg, Na, Zn, P, S, B) were determined through inductively decoupled plasma atomic emission spectroscopy according to ASTM D 5185-13e1 [133]. Soot content (ST) was determined through

infrared spectrometry according to DIN 51452 [134]. Wear metal content (Fe, Al, Cr, Cu, Si) was determined through analytical ferrography. A general oil condition indicator (OCI) was also calculated from the measured parameters. Oil samples were homogenised before analysis.

Selected oil samples were subjected to friction and wear measurements on a high frequency reciprocating rig in order to determine their lubricating performance. Sample selection was based on oil service life (OAh), since not all analysed oils were available for friction testing. To have a representation of in-engine oil degradation a complete series of samples were chosen from each test cycle, which corresponds to 1 sample of 50, 100, 150, 200 and 250 hours oil service life from the same oil charge of each engine. A ball-on-disc model system was utilized with a steel sliding pair for the measurements. Each sample was tested under the same circumstances in two consecutive measurements. To minimize measurement error and maximize reproducibility the testing of the aged oil samples was carried out according to the ISO 19291:2016 standard (for details see Chapter 5.1). Ball and disc test specimens were supplied by Optimol Instruments with material properties and dimensions according to ISO 19291-2016 and ISO 683-17 [135]. In addition to the registered coefficient of friction curves the averaged wear scar diameter of each ball specimen was determined through optical microscopy as an average of two perpendicular diameter measurements. Mean values were determined as an arithmetic mean of the friction curve after the run-in period.

6.2 Data analysis and results

A linear correlation analysis according to Pearson was carried out on the data in order to assess the significance of measured oil properties in relation to the condition and lubricating performance of the oil samples (Figure 35). Oil properties were correlated to service life. Subsequently, the properties of the oil samples subjected to friction and wear measurements were correlated to the mean coefficient of friction and the mean averaged wear scar diameter. The calculated correlation coefficients or r-values lie in the range of [-1, 1]. A strong linear relationship is characterized by an r-value close to |1|, whereas an r-value of 0 suggests no linear relationship between the variables. The p-value determines if the r-value is significantly different from 0. A p-value less than or equal to the significance level signifies that the correlation is different from 0. A level of significance of 0.05 was chosen for the evaluation of the correlation coefficients based

on the corresponding p-values. Any oil property with a corresponding p-value greater than the level of significance was considered as non-determinate for this study.
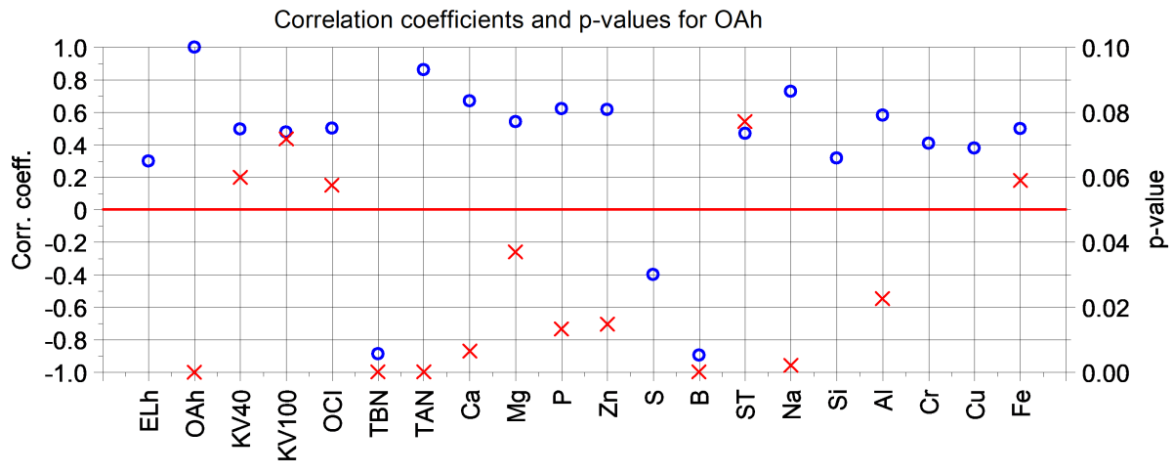
Figure 35. Correlation of measured values to oil service life (OAh); blue circles represent correlation coefficients, red crosses represent p-values, red line represents level of significance (p=0.05)

The correlation analysis suggests that the main indicators of engine oil fitness are TBN, TAN and boron quantity (B) in the oil, signified by low p-values and relatively high absolute correlation coefficients (>= 0.8). A detailed analysis of said values depicted on Figure 36 shows a coherent decrease of TBN and boron content as well as a steady increase of TAN with service life of measured samples regardless the test cycle. In contrast to this behaviour there is noticeable separation in values of the kinematic viscosity of samples from different test cycles. These results are in-line with the expectations, based on the work of other researchers. A mean value from the coefficient of friction curve as well as the averaged wear scar diameter of each measurement was calculated and correlated to the values from the lubricant analysis (Figure 37). The analysis shows a strong correlation between the boron content, soot content and TBN of the samples to the mean coefficient of friction during friction and wear testing. As for the amount of wear a similar trend can be observed. Boron content and TBN show a remarkable correlation alongside with TAN. These findings seem to be in accordance with the results of used oil analysis in relation to service life. To determine the relation between said properties the CoF and AWSD values of individual samples were plotted against boron content, soot content, TAN and TBN respectively. Apart from CoF and soot content, the relation between values appears to be linear. Although it should be noted, that the correlation between the measured coefficient of friction and oil condition is the most apparent on the CoF vs. soot content plot.
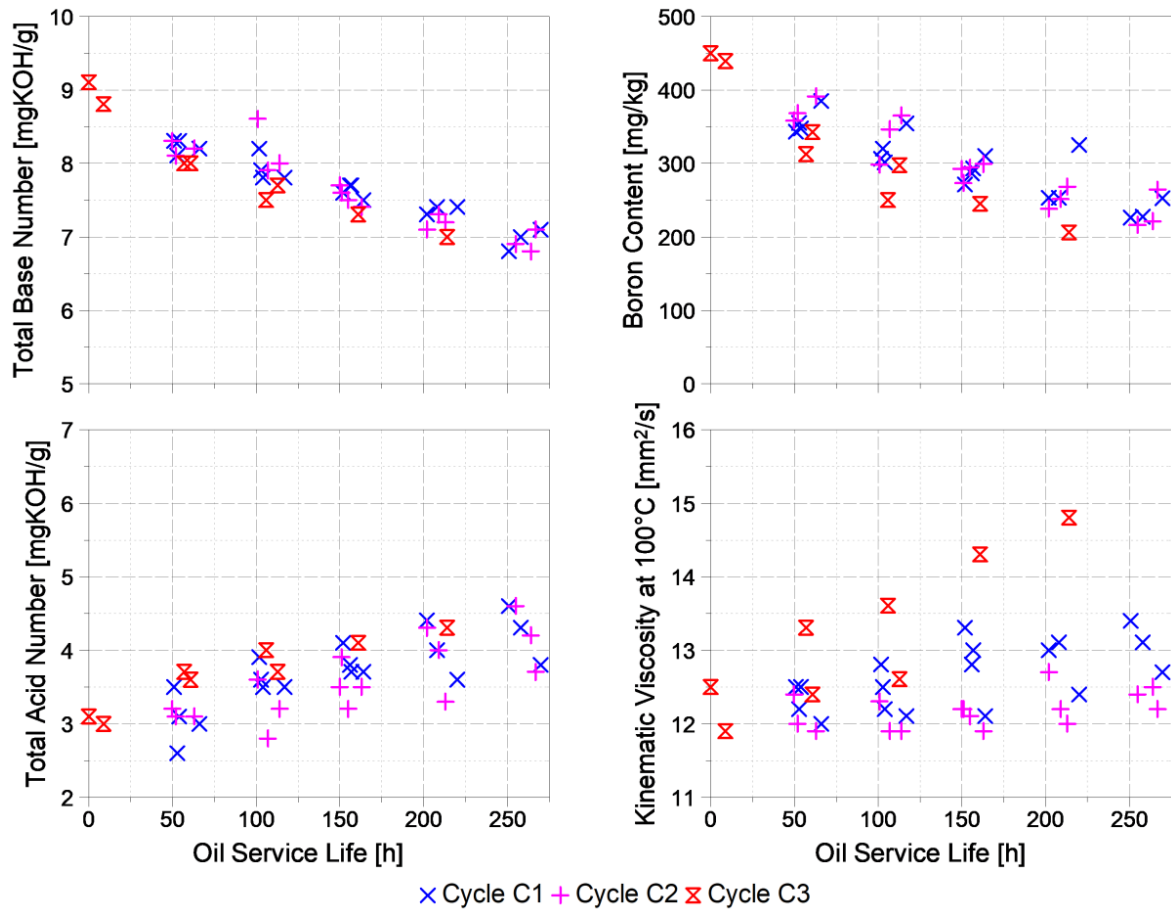
Figure 36. Measured TAN, TBN, boron content and kinematic viscosity of different samples
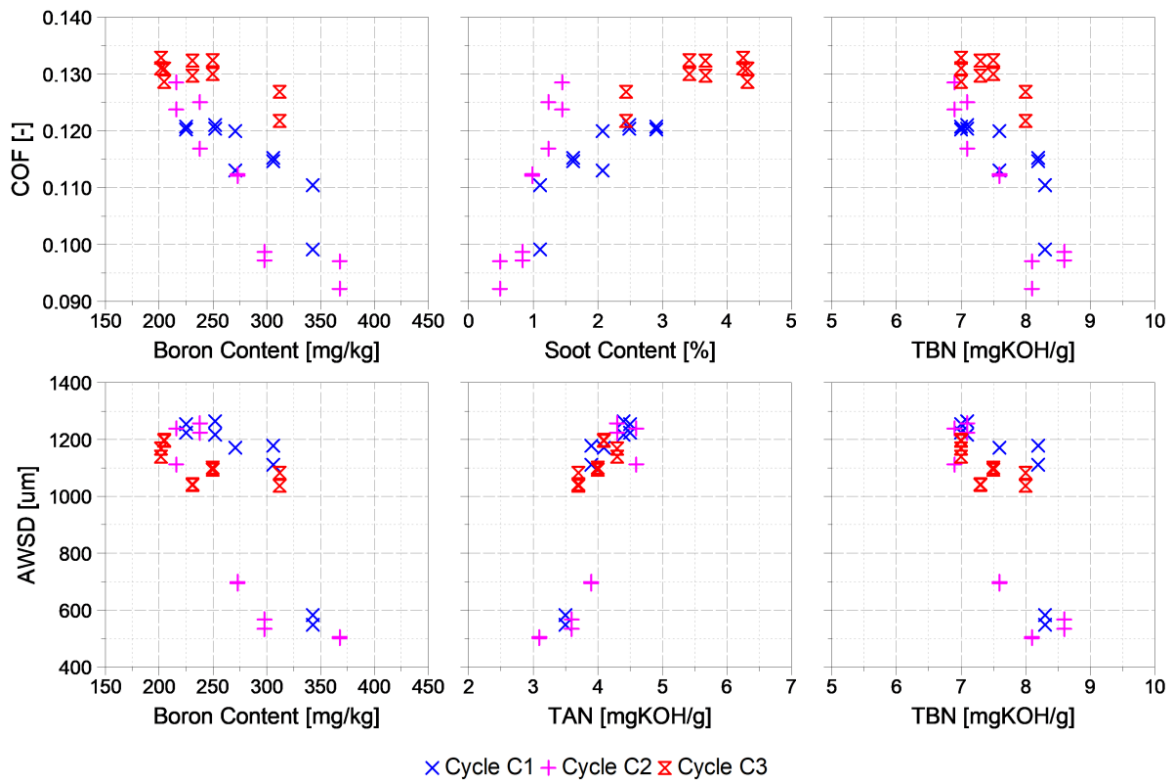

Figure 37. Graphic analysis of the relation between used oil properties and their performance during friction and wear testing

Based on the presented data, the boron content of the sample together with another independent property with significant correlation could be used to describe the fitness of the lubricant in terms of friction reduction and wear protection.

6.3 Summary and conclusion

The presented results presume a significant correlation between TAN, TBN and boron content of a used engine oil and its service life. The acid number is used to measure the concentration of acidic species present in the engine oil. Lean oil has an initial acidity which will increase during service due to acid formation as a result of oxidation and the presence of acidic compounds formed during combustion. The base number measures the alkaline reserve of the lubricant which serves as a neutralizing agent to hinder the effect of weak acids. Therefore, the initial base number of a lean oil will decrease during the service [34]. Boron esters are used in modern formulations as an antioxidant additive or as replacement to ZDDP. Boron can also be used as a solid lubricant nano-additive to successfully reduce friction and wear in a sliding pair as discussed in [136], [137], [138] and [139]. In both cases the initial boron content of the lubricant will decrease with time as experienced. This phenomenon takes place due to degrading chemical reactions and boundary layer formation, which reduce the amount of boron additives in the oil. Hence, the presented results are in accordance with the scientific literature. The conducted correlation analysis assumed a linear correlation between the investigated properties and service life, as well as coefficient of friction and averaged wear scar diameter. This assumption disregards the possibility of non-linear correlation, which can explain why only a weak fit was achievable with the wear scar diameter. Taking only linear correlations into account was a decision in favour of simplicity, as non-linear behaviour would demand finer sampling of the used oils which was not in the scope of this study.

Further experimentation should be considered regarding the dependence of oil properties from the test cycle. Treating this factor as an inherent property of the dataset can introduce an error in the model. A detailed study with real-life driving conditions conducted on a diverse vehicle fleet would be necessary to address this flaw.

These findings underline the necessity of a comprehensive aging study under realistic conditions for creating a baseline for artificial aging experiments.

# 7   In-use engine oil aging experiment on a vehicle fleet

As concluded in Chapter 6.3, a comprehensive assessment of oil aging under realistic conditions is necessary, in order to clarify the dependence of lubricant degradation from the test cycle. This section summarizes the results of a large-scale experiment on a vehicle fleet focused on in-use engine oil aging. The fleet study was conducted with generous help from Audi Hungaria Zrt. Engine oil analysis was carried out in partnership with the Austrian Excellence Centre for Tribology. Findings presented in this chapter are published in {6} and {8}.

7.1   Fleet usage characteristics

A fleet study was conducted according to the methodology outlined in Chapter 4.5. Details regarding vehicle usage are summarized on Figure 38, which presents a clear separation of short-range and long-range vehicles as expected. Further analysis reveals that vehicles with similar characteristics tend to exhibit similar usage profiles.
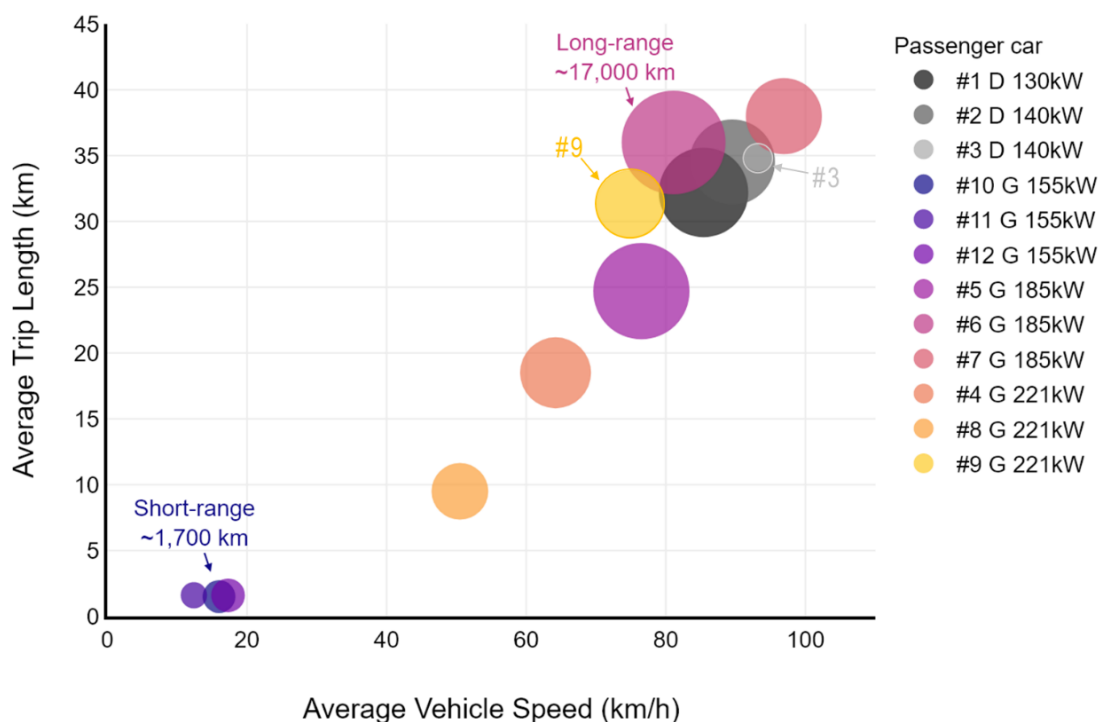
Figure 38. Vehicle usage through the course of the fleet study. Bubble size represents mileage, legend colours signalize engine type (G – Gasoline, D- Diesel) and power

Vehicles with a diesel engine or a 185 kW gasoline engine are larger passenger cars (E-segment and J-segment according to ISO 3833:1977 [140]), which show higher average speed and trip length values and a high mileage during the sampling period. These vehicles have comparably more passenger and luggage space, hence were

taken for long trips involving highways more often. Vehicles with a 221 kW gasoline engine have a smaller chassis (C-segment [140]) and show a mixed usage. Vehicles of this group have a fairly high performance variant of the gasoline engine, but lack luggage space, therefor were rather taken for shorter trips. Two outliers can be identified based on Figure 38:

- Vehicle 3 is a long-range vehicle, which had to undergo maintenance during the fleet study, hence only registered a mileage of 1300 km.
- Vehicle 9 has the largest luggage space from the three C-segment cars, hence it was taken for longer trips for a comparable number of times to large vehicles.
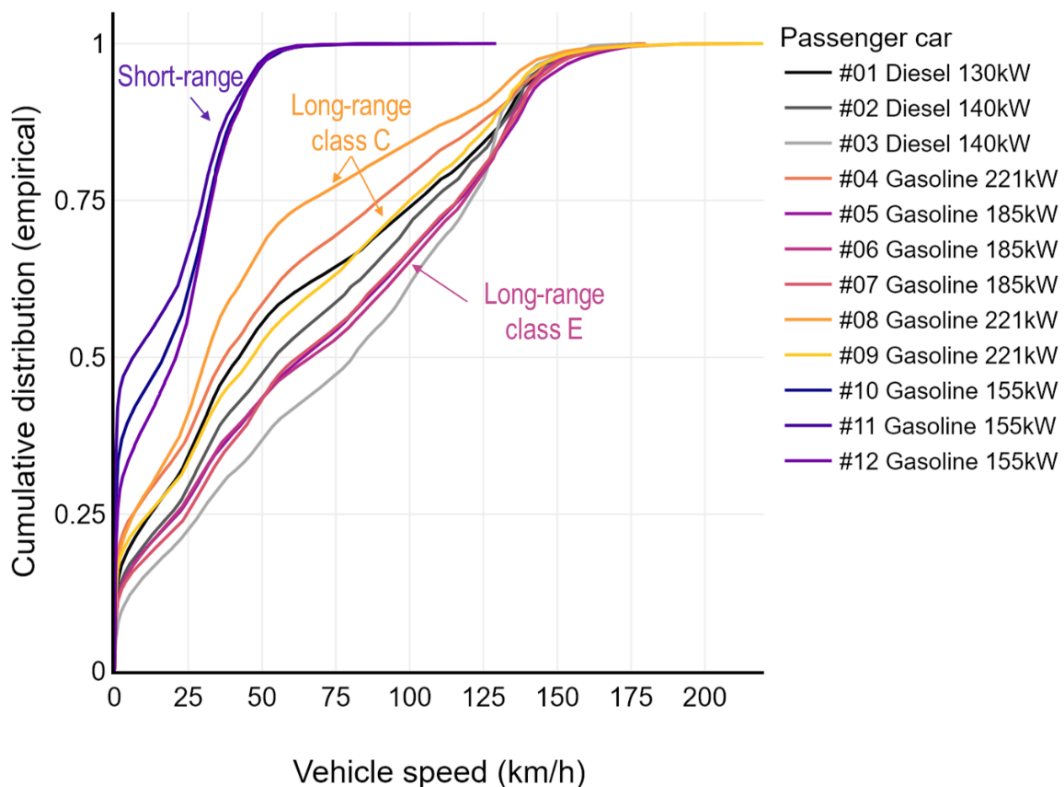
Figure 39. Empirical cumulative distribution plot of the collected vehicle speed data, presenting a clear separation between short-range and long-range vehicle utilization.

Calculating the empirical cumulative distribution of each vehicle gives a detailed look into vehicle utilization. Figure 39 presents the empirical cumulative distribution curves, which underlines a fundamental difference between short-range and long-range vehicles. Vehicle #03 (rightmost light grey curve) for instance was driven under ~30 km/h for a quarter of the duration of the study, operated between ~30 and 80 km/h half of the time, and only went over 120 km/h for a quarter of the test period. In general, short-range vehicles were driven under ~30 km/h for 75% of the time during the

sampling period, whereas for long-range vehicles this value ranges between ~60 and ~120 km/h. Amongst long-range vehicles the 185 kW gasoline variants (class E) show the least variation compared to each other. In contrast, compact high performance cars (221kW class C) display a larger variety in their speed distribution curves. Based on the speed values for the 3rd quartile (75%) it can be concluded, that drivers preferred to take large, moderate performance vehicles for longer trips involving high-speed road infrastructure (i.e. highway > 100km/h), whereas high performance compact vehicles were rather used in urban areas and on main roads (up to 100 km/h).

7.2 Determining engine oil degradation by conventional analytic methods

Analysing key oil properties of in-use samples gives insight into the main aspects of engine oil aging and degradation. Both for development and diagnostics purposes, engine wear is a critical indicator in terms of longevity and reliable operation.

Figure 40 presents key physical and chemical properties of the collected engine oil samples plotted against their mileage. The amount of iron in used oils (Figure 40 d) is a good representation of wear in an internal combustion engine. Diesel engine samples show higher amounts of wear metal content compared to gasoline engines, although a clear distinction can be seen between long-range (noted simply as gasoline) and short-range gasoline samples. Short-range samples with a mileage under 2 000 km exhibit similar amounts of Fe as long-range gasoline samples around 8 000 km. This difference can be understood by looking at the ZDDP antiwear additive content (Figure 40 b) and the kinematic viscosity (Figure 40 a) plots. Both viscosity and ZDDP content show a stark decline in case of short-range vehicles, with values of the former indicating a nearly depleted additive reserve after 2 000 km. As discussed in {6}, the change in viscosity can be explained by fuel dilution in the engine oil, which can also interact with the boundary layer formed by ZDDP and lead to increased wear [141]. Interestingly, diesel samples still possess around 50% of their ZDDP content well after a mileage of 10 000 km. To understand the cause of comparably high wear metal content in diesel engine oils, soot loadings for each sample are plotted on Figure 40 subplot c), which shows identical tendencies of soot and iron content. Soot acts as a mechanical polishing agent in the lubricant, resulting in increasing amounts of wear with increasing soot content.

Chapter 4.3 gives a detailed description of analysis techniques and methods to measure numerous chemical and physical properties of used engine oils. The conducted measurements determined nearly 20 properties e.g. TBN, viscosity, oxidation, nitration, soot loading, water content, as well as the amount of numerous wear metals, degradation products and contaminants in the investigated used oils.
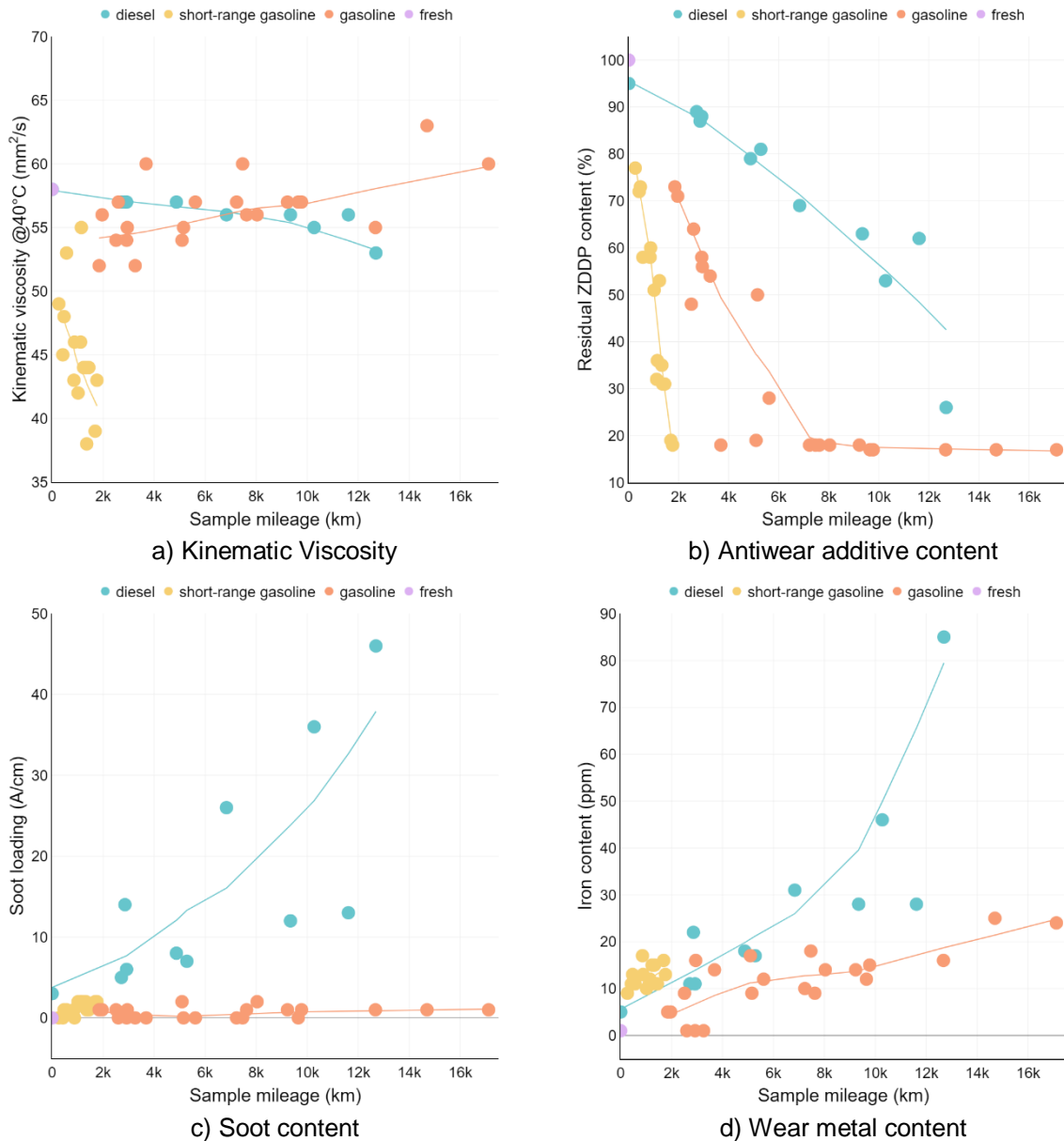
Figure 40. Key physical and chemical properties of used engine oil samples plotted against vehicle mileage.

Results of these analyses in relation to mileage are published and discussed in {6} in detail. However, several other influencing factors can be taken into account when characterising is-use engine oil degradation, e.g. engine power, vehicle utilization, speed metrics, or the number of cold starts. An in-depth analysis of all analysed

properties and influencing factors requires an approach, which is capable of reducing the dimensionality of the dataset without losing valuable information. Hence, principal component analysis was utilized to discover trends and correlations in the data.

7.3 Characterizing engine oil degradation through Principal Component Analysis of quantified oil properties

As detailed in Chapter 4.6, principal component analysis can be interpreted as a means of dimension reduction, which can be used to visually outline correlations in a dataset. PCA achieves this by calculating scores for each original observation, that represent the position of said n-dimensional observation in a 2-dimensional space. This method is applied to measured quantitative oil properties (features) described in Table 10. Each listed value for all collected samples (observations) were normalized (scaled and centred) before the PCA. Additional data (descriptors) – i.e. vehicle properties and utilization metrics presented in Chapters 4.5 and 7.1 – are used to facilitate visualization and discover correlations in the dataset.

Table 10. Measured engine oil properties considered in the PCA

1	**Oxi**	oxidation	2	**Nit**	nitration
3	**ZDDP**	antiwear additive amount	4	**pheAO**	phenolic antioxidant amount
5	**amiAO**	aminic antioxidant amount	6	**TBN**	total base number
7	**NN**	neutralisation number	8	**V40**	kinematic viscosity at 40°C
9	**V100**	kinematic viscosity at 100°C	10	**VI**	viscosity index
11	**H2O**	water content	12	**CC**	soot loading
13	**B**	boron content	14	**Ca**	calcium content
15	**Fe**	iron content	16	**Mg**	magnesium content
17	**P**	phosphorous content	18	**S**	sulphur content
19	**Zn**	zinc content			

Figure 41 presents a visualization of the calculated scores for each object coloured by fuel type and utilization on subplot a), total mileage on subplot b), and engine power on subplot c). Considering utilization, a clear separation of short-range gasoline vehicles can be observed, alongside a mild segregation of diesels from gasoline vehicles. A variance in the data due to utilization was anticipated, since average speed and average trip length (Figure 38), as well as the empirical cumulative distributions of speed (Figure 39) show clearly distinctive utilization tendencies. Mileages show a clear transition along the horizontal axis (PC1), whereas no clear distinction is visible along

the vertical axis (PC2). No clear separation is shown after colouring the objects by engine power, the clustering of 155 kW vehicles on the upper middle section of the image is believed to be mainly a result of the stark difference in utilization. This assumption is backed by the fact, that long-range petrol vehicles are equipped with two significantly different performance classes of the same engine (185 and 221 kW), but show no clear clustering inside their performance class. Figure 41 also includes a loading plot (d), which shows the contribution of each feature to principal component 1 and 2.
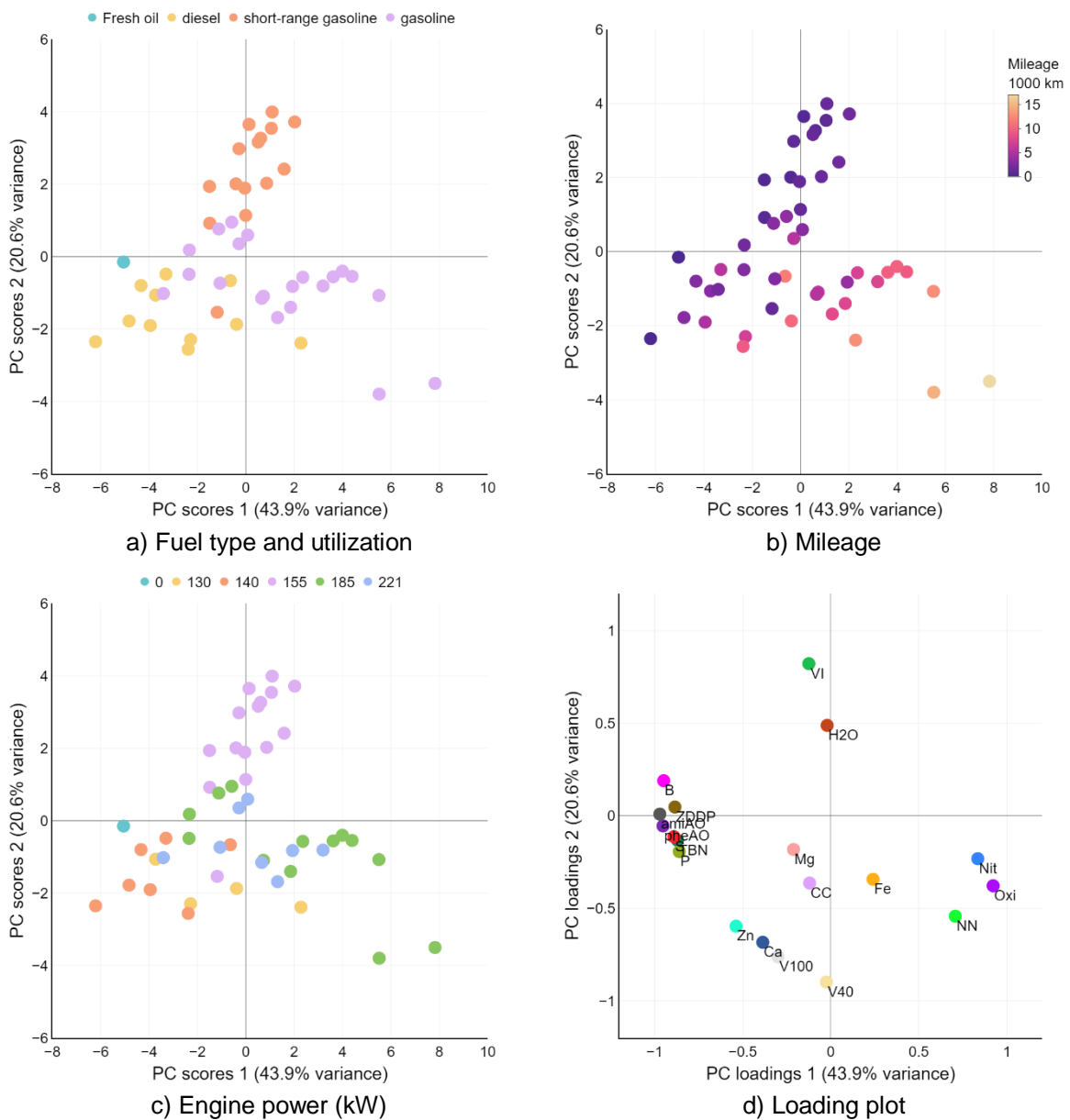

Figure 41. Visualization of PCA results from quantitative oil properties. Score plots are coloured by fuel type and utilization (a), sample mileage (b), and engine power (c), to show the effect of these influencing factors on the variance of the dataset. Loading plot (d) shows the contribution of each property to the principal components.

The closer the calculated loading of a feature is to $|1|$, the stronger the linear correlation is between said feature and the corresponding principal component. Considering the position of the features it can be concluded, that the position of an object along PC1 is mostly influenced by oxidation and nitration (Oxi, Nit, amiAO and pheAO), as well as parameters strongly affected by oxidation e.g. antiwear additive content (ZDDP), neutralisation number (NN), or total base number (TBN). Scattering of objects along PC2 is largely a function of measured oil viscosity, but is also strongly influenced by the amount of degradation products (Zn, Ca) and water content (H_2O). Interpreting the loadings as vectors also explains the direction of change of each feature along the principal components, e.g. the amount of oxidation (Oxi) for an observation is rising along PC1 and is slightly decreasing along the PC2. After understanding how the measured oil properties (features) influence the position of the objects in the coordinate system of the principal components, a general interpretation of the score plots can be achieved:

- long-range utilization of gasoline vehicles results in an increase in viscosity, and together with increased mileage contributes to a higher oxidation,
- short-range utilization allows the accumulation of water in the oil samples, and presumably also results in higher fuel dilution, which is shown by a decrease in viscosity, and an increase in viscosity index along PC2.

7.4 Characterizing oil degradation through PCA of FT-IR spectra

As shown in Chapter 7.3, principal component analysis can be carried out on quantified oil properties, which requires numerous analytical methods to be utilized. On the other hand, the FT-IR spectrum of a sample itself carries a vast amount of information regarding oil chemistry. This chapter presents a different approach to oil condition analysis based on principal component analysis of Fourier transformed infrared spectra, suggested by the Austrian Excellence Centre for Tribology. Results gained through this analysis approach are published in {8}.

Two additional PC analyses were conducted on FT-IR spectra collected from the previously analysed used engine oil samples. Samples from all participating vehicles were included in the first PCA, in order to get an overview on the influence of fuel type, mileage, engine power and utilization on engine oil degradation. The resulting scores from the first PCA are plotted on Figure 42, together with the loadings of each PC.
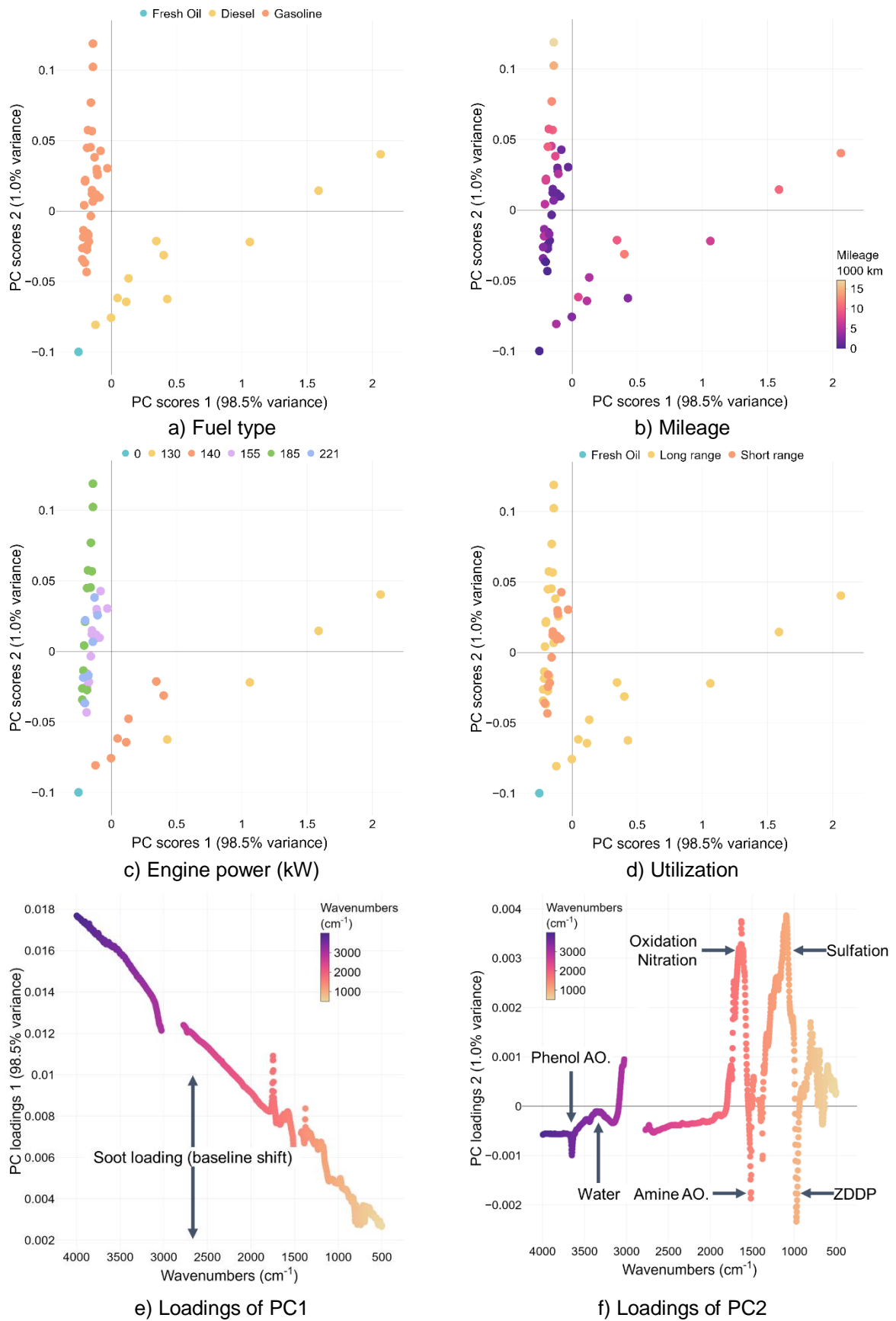
Figure 42. Visualization of PCA results from FT-IR spectra (all samples). Observations are coloured by fuel type (a), sample mileage (b), engine power (c) and vehicle utilization (d). Loading plots (e and f) show the contribution of wavenumbers in the IR spectra to the corresponding PC.

Subplot a) presents all objects coloured by fuelling, showing the mild separation of gasoline and diesel vehicles observed on Figure 41 a) in a more pronounced manner. Diesel vehicles are clearly forming an independent group along PC 1 on the score plot. The separation along PC 2 can be correlated to the total distance travelled, based on Figure 42 b). Regarding the influence of engine power an interesting trend can be seen on Figure 42 c): samples of the 130 kW diesel vehicle are split from 140 kW diesel samples. In terms of utilization (Figure 42 d) the objects from long-range and short-range vehicles are mixed together.

An inspection of the loading plots on Figure 42 facilitates the interpretation of the previously observed tendencies. Loadings are plotted against wavenumbers of the collected spectra. The characteristic wavelengths corresponding to various indicators of oil aging are detailed in Chapter 4.3. PC 1 is strongly related to soot loading, which is visible through a baseline shift on subplot e). This phenomenon has an overwhelming effect on the scores, and singlehandedly accounts for 98.5% variance in the dataset. Subplot f) shows, that PC 2 is influenced by multiple characteristic wavelengths corresponding to oxidation, nitration, sulfation, antioxidant and antiwear additives, and water content. Unfortunately, PC 2 only accounts for 1% variance in this analysis, which means no conclusion can be made regarding the influence of wavelengths on scattering along PC 2.

On the other hand, the separation of diesel vehicles along PC 1 is clearly a result of the differences in soot loading. Gasoline vehicles produce significantly less soot during operation, hence the diversification of gasoline and diesel vehicles is obvious. The split between 130 kW and 140 kW diesel samples can be accounted for the differences in engine technology. Although both performance classes are built around the same short engine, there is a major difference in aftertreatment technology between the two classes. The lower performance engine conforms to the EURO 5 norm, whereas the 140 kW variants are fitted to meet the EURO 6 standard. EURO 6 prescribes a more stringent limit for NO_x and soot emissions, which can only be achieved by applying a Selective Catalytic Converter (SCR). An SCR mixes a urea-solution into the exhaust, in order to achieve the conversion of NO_x into N_2 and O_2. Accordingly, the 130 kW variant utilizes a different approach and reduces NO_x through a lower peak firing temperature (hence, lower performance), which is achieved through higher exhaust gas recirculation (EGR) rates. This results in a higher amount of soot being

reintroduced into the combustion chamber, and consequently into the engine oil. Presumably, the 130 kW diesel vehicle being equipped with a manual transmission also has an influence on the operating ranges of the engine, which together with high EGR rates results in the split between diesel samples. Revisiting Figure 40 c) and d) further confirms this theory. Figure 43 shows soot content (a) and wear metal content (b) of used engine oil samples from 130 kW and 140 kW diesel vehicles plotted against mileage. It is apparent, that the separation of the performance classes on the score plots of Figure 42 is in correlation with soot content, which directly affects wear in the engine as stated in Chapter 7.2.

c) Soot content   d) Wear metal content
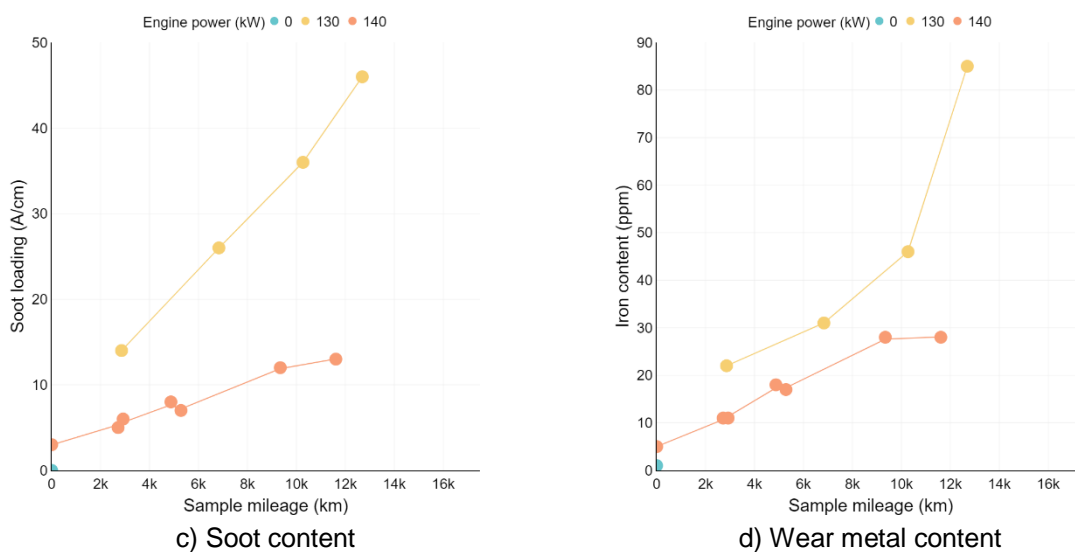
Figure 43. Soot content and wear metal content of used engine oil samples from 130 kW and 140 kW diesel vehicles plotted against mileage.

To better understand the behaviour of gasoline vehicles a secondary PCA was conducted, where diesel samples were excluded from the calculation. Furthermore, additional utilization parameters were computed from the collected vehicle speed data. Number of cold starts was determined by counting the occurrences where at least 60 minutes have passed between consecutive trips. The interquartile range (IQR) of speed was also calculated from all registered speed readings, based on the empirical cumulative distribution curves from Figure 39.

Figure 44 presents score plots and loading plots based on results of the secondary PCA. Subplot a) shows objects coloured by number of cold starts, which depicts a general increase of occurrences along PC 1. Colouring objects by mileage (Figure 44 b) shows an apparent increase in total distance travelled along the vertical axis (PC2).
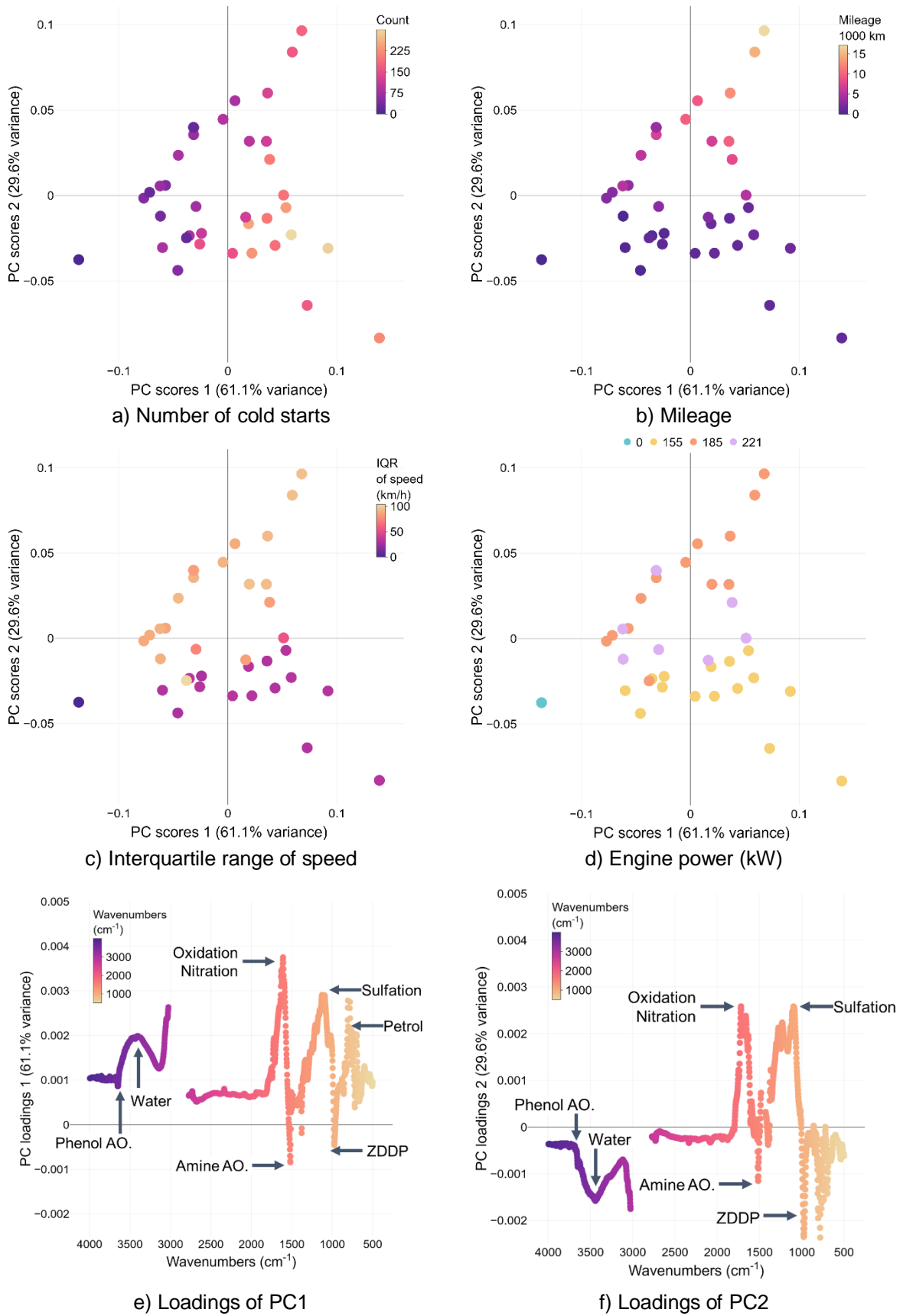
Figure 44. Visualization of PCA results from FT-IR spectra (gasoline samples). Observations are coloured by number of cold stars (a), mileage (b), IQR of speed (c), and power (d). Loading plots (e and f) show the contribution of wavenumbers in the IR spectra to the corresponding PC.

Comparing subplot c) and d), which show objects coloured by IQR and engine power respectively, presents an additional method of diversifying short-range and long-range vehicles. In {6} as well as in Chapter 7.1, vehicle utilization is determined based on the mean trip length and mean vehicle speed readings averaged for the entire test period. This approach confirms the restricted utilization of vehicles with a 155 kW engine, that were confined to a controlled speed area. Comparing vehicles by their respective IQR of speed values yields identical groupings in terms of utilization to the previous approach. All passenger cars previously nominated as short-range (155 kW on Figure 44 d) exhibit IQR values under 50 km/h, meaning that said vehicles were operated in a velocity range of 50 km/h for 50 % of the test period. Considering the general shape of empirical distribution curves on Figure 39 it can be concluded, that vehicles with IQR values under 50 km/h were operated in a short-range fashion, whereas objects with IQR values over 50 km/h belong to long-range vehicles. This consideration also intuitively dictates, that traffic conditions resembling those in cities (short-range) contribute to a shift along the negative PC 2 direction on the score plot, whereas highway traffic conditions (long-range) lead to a shift along the positive PC 2 direction.

Looking at the loadings (Figure 44 e and f) for PC 1 and PC 2 presents a more refined picture of engine oil degradation in gasoline fuelled passenger cars. In contrast to the previous analysis, no single dominant loading can be identified for PC 1 or PC 2. Water and fuel aggregation in the investigated samples contribute to PC 1, but also affect PC 2 as well: increasing amounts of moisture and gasoline push objects in the lower-right region of the score plot (positive loading on PC 1 and negative loading on PC 2). Oxidation, nitration, sulfation, residual ZDDP content and residual antioxidant content act on the positive diagonal, pushing objects towards the upper-right region of the score plot. Objects exhibit increasing values of oxidation, nitration, and sulfation the further away they lie from the origin (positive loading on both PCs), while residual additive content decreases in this direction (negative loading on both PCs).

Revisiting individual oil properties published in {6} presented on Figure 42 further supports the previous interpretation of score plots on Figure 44. All samples exhibit increased oxidation with an increase in total sample mileage, as presented on Figure 42 a). Plotting water content as a function of the number of cold starts shows a decrease in case of samples from a 185 kW long-range vehicle. 155 kW short-range

vehicles present a stagnating value regarding water content, however trend around 700 ppm, with outliers as high as 2226 ppm.

a) Oxidation over mileage   b) Water content over the number of cold starts
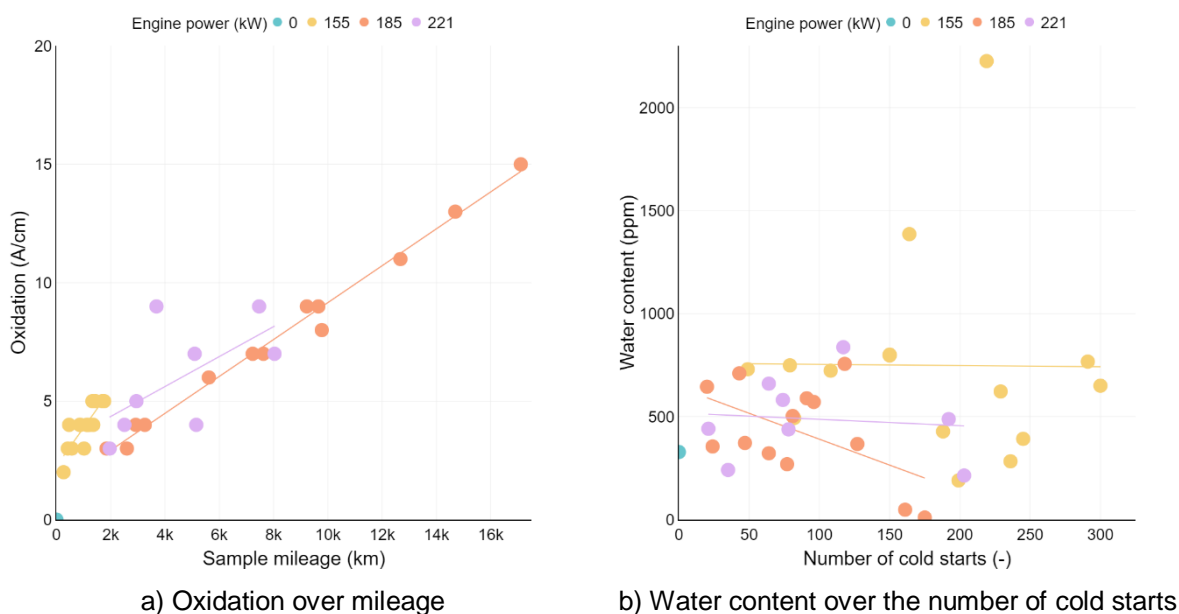
Figure 45. Oxidation and water content of used engine oil samples from 155 kW (short-range), 185 kW and 221 kW gasoline vehicles plotted against mileage.

This alone would not account for the variance along PC2, hence a correlation of conventional quantitative oil parameters with the resulting scores from the FT-IR PCA was also carried out. The two score plots on Figure 46 are presented using quantitative oil analysis results (detailed in Chapter 7.3) from potentiometric titration (TAN) and Stabinger viscometry (kinematic viscosity) as the descriptors (colour dimension). Total acid number gives a good estimation regarding oxidation of the lubricant (as presented in {8}), whereas kinematic viscosity can indicate thickening due to excess polymerization, or thinning due to shear forces (transmissions) or dilution (engines).

Investigating the score plot coloured by total acid number (Figure 46 a) gives clear indication, that an increasing mileage (derived from Figure 44 b) leads to a moderate increase in acidity, which is in accordance with the inferred (Figure 44 e and f) and observed (Figure 42 a) increase in oxidation.

Using kinematic viscosity values to distinguish the objects on Figure 46 b) indicates that an increasing number of cold starts causes a decrease in viscosity. A decreasing viscosity in cease of an in-use engine oil sample is a result of fuel dilution and water accumulation, which are also suggested by loading plots Figure 41 e and f. Despite

fuel dilution only being determined for selected engine oil samples, the encountered values suggest a similar tendency as suggested by the previously presented results.

a) Neutralisation Number (~TAN)   b) Kinematic Viscosity at 40°C
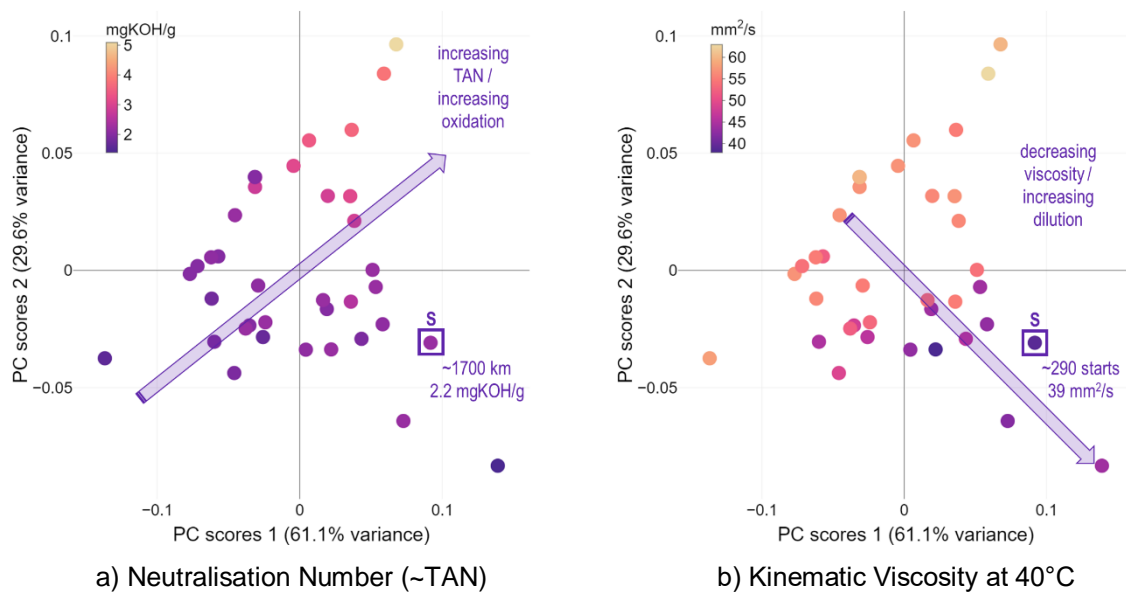
Figure 46. Visualization of PCA results from FT-IR spectra (gasoline samples), with sample *S* highlighted; objects coloured according to quantitative properties from Chapter 7.3

Fuel dilution results of ~3.7% were reported in {6} for a selected short-range gasoline vehicle, whereas for the selected long-range gasoline passenger car a fuel dilution level of ~0.6% was measured. Correlating a relatively high number of ~290 cold starts under a low mileage of ~1700 km (S on Figure 46) with the ~3.7% dilution presents an increase in acidity from 1.6 to 2.2 mgKOH/g and a significant drop in kinematic viscosity from 58 to 39 mm^2/s. Considering fuel dilution, viscosity, and TAN acknowledges the assumptions made earlier, which are in accordance with the observations of the comprehensive PCA presented in Chapter 7.3.

7.5 Summary and conclusion

Chapter 8 summarizes the core findings of a field test with the participation of 12 passenger cars, which focused on engine oil aging in modern internal combustion engines. Researching lubricant aging in relation to utilization, and technical solutions and constraints resulting from environmental regulations – i.e. aftertreatment technologies, alternative fuels, hybrid powertrains – can help in understanding degradation processes and increasing robustness of powertrains, while decreasing emissions.

Two different approaches were discussed for oil condition monitoring, both relying on principal component analysis to correlate utilization characteristics with used lubricant properties.

A more comprehensive approach through the analysis of quantitative oil properties showed a good separation of oil samples from short-range and long-range vehicles, and also gave insight on the influence of mileage and utilization.

An analysis of FT-IR spectra as a cost-effective solution to oil condition monitoring is widely used, the presented PCA approach can lead to valuable knowledge in addition to quantitative properties for comparison. Studying spectra from all collected samples revealed an interesting grouping between samples from diesel engines, which was traced back to a fundamental difference in aftertreatment technology. Since soot loading proved to be highly influential on FT-IR measurement results, a separate analysis was also carried out focusing on gasoline samples. This investigation revealed how utilization, more precisely the number of cold starts and total mileage affect engine oil properties, further proving observations of the comprehensive analysis:

- long-range utilization of gasoline vehicles contributes to a higher oxidation due to increased mileage,
- short-range utilization of gasoline vehicles results in higher fuel dilution and a decrease in viscosity due to a high number of cold starts.

Furthermore, the analysis of EURO 5 and EURO 6 diesel engine samples revealed the influence of aftertreatment technology on soot loading in the lubricant. Due to EURO 6 engines utilizing a urea solution for NO_x reduction, a high exhaust gas recirculation (EGR) to decrease peak combustion temperatures can be avoided. Decreased EGR has a positive effect on soot accumulation, which subsequently causes a decrease of wear metal traces present in the oil.

Based on the presented results, the approach of FT-IR PCA suggested by the Austrian Excellence Centre for Tribology proved to be a powerful and efficient method for correlating engine oil condition and vehicle utilization data.

The above findings support Thesis 4.

8 New scientific results

This section summarizes new scientific results, which were discovered during the research.

Thesis 1 − Friction and wear with alternative fuel contaminated oils

I have demonstrated the effect of OME_{3-5} on the degradation of a modern fully synthetic multi-grade engine oil through friction and wear testing on a model system with artificially aged engine oil samples. Experiments according to ISO 19291 on a ball-on-disc setup have shown, that adding 7 wt% OME_{3-5} to a commercially available SAE 0W-20 engine oil during artificial aging results in increased wear and an alteration in the dominant wear process on 100Cr6 bearing steel test samples compared to regular diesel fuel. Surface analysis results after friction and wear testing with a 96 hour old artificially aged sample including 7 wt% EN 590 regular diesel fuel have shown predominantly abrasive wear marks. In contrast, surfaces after testing with a 96 hour old artificially aged sample containing identical amounts of OME_{3-5} exhibit an increased amount of fatigue wear. In addition to the apparently distinct wear mode, OME_{3-5} as a contaminant contributed to ~6% increase in the averaged wear scar diameter.

Golyó-tárcsa modellen elvégzett tribológiai modellkísérletek által bebizonyítottam, hogy az OME_{3-5} hatással van a kereskedelmi forgalomban kapható modern motorolajok degradációjára. A 7 m% OME_{3-5}-tel szennyezett mesterségesen öregített kereskedelmi fogalomban kapható SAE 0W-20 motorolaj az ISO 19291 szabvány szerinti kopásvizsgálatok során a 100Cr6 minőségű csapágyfém tribológiai mintákon a hagyományos gázolajhoz képest a kopás megnövekedését, valamint a domináns kopásfolyamat megváltozását idézte elő. A kísérleteket követő felületanalízis alapján a 7m% EN 590 előírásnak megfelelő gázolajjal szennyezett 96 órán át mesterségesen öregített kenőanyaggal kent felületeken jellemzően abrazív kopásnyomok keletkeztek, az azonos mennyiségű OME_{3-5} alternatív tüzelőanyaggal szennyezett 96 órán át mesterségesen öregített olajjal kent felületeken ezzel szemben jellemzően fáradásod kopás (pitting) volt megfigyelhető. A jól láthatóan eltérő kopásjelleg mellet az OME_{3-5} szennyező az átlagos kopásnyom átmérő ~6%-os növekedéséhez járult hozzá.

Related personal publications: {1}, {2}, {3}; related chapters: 5

Thesis 2 – Artificial oil aging without contamination

I have demonstrated that thermo-oxidative aging for 96-hours at 160°C with 1 l/min air throughput has a significant effect on the antioxidant and antiwear additive reserves of the investigated engine oil. 150 ml SAE 0W-20 samples exhibited a 17% drop in aminic and phenolic antioxidant content on average, due to the thermal load and reactions with O_2 from the constant agitated airflow during the procedure, which is quantifiable through a 4.1 A/cm average oxidation. An average 89.2% decrease in ZDDP antiwear additive content was also established as a result of the thermal degradation of ZDDP.

Kimutattam, hogy 96 órán át, 160°C-on, 1 l/min levegő átfolyatása mellett történő termo-oxidatív öregítés szignifikáns hatással van a kenőolaj antioxidáns és kopásgátló adalék tartalmára. A vizsgált 150 ml–es SAE 0W-20 osztályú motorolaj minták átlagosan 17%-os aminos és fenolos antioxidáns adaléktartalom csökkenést szenvedtek el az öregítés során fellépő hőterhelés és az átáramoltatott levegő oxigéntartalmával való reakciók következtében, amely 4.1 A/cm átlagos oxidációval számszerűsíthető. Átlagosan 89.2% csökkenés került kimutatásra a ZDDP kopásgátló adalék mennyiségében, amely a ZDDP termikus degradációjának eredménye.

Related personal publications: {4}, {5}, {7}; related chapters 4.4, Appendix A

Thesis 3 – Artificial aging with alternative fuel contamination

I have concluded in a follow-up aging experiment on Shell Helix 0W-30 engine oil, that the previously experienced transition in wear processes can be explained with the change in engine oil chemistry due to an increased oxidation in the presence of OME_{3-5}, which is quantifiable through the decrease of aminic antioxidants in the aged sample.

További, Shell Helix 0W-30 motorolajon végzett kísérletek során kimutattam, hogy a meghatározó kopásfolyamat előzőekben részletezett módosulása a vizsgált kenőolajban az OME_{3-5} jelenlétében lezajló kémiai reakciók következményeként fellépő megnövekedett oxidációval magyarázható, amely számszerűen kimutatható az aminos oxidációgátló adaléktartalom csökkenésének vizsgálatával.

Related personal publications: {4}, {5}, {7}; related chapters 4.4, Appendix A

Thesis 4 – Engine oil aging under real-life conditions

I have demonstrated through principal component analysis of experimental data, that in a vehicle fleet comprising of a selection of passenger cars with various performance classes of the same base motorization, the physical and chemical deterioration of the lubricant is mainly dependent on the attributes of vehicle usage. A strong correlation was found between the number of cold starts and the severity of engine oil degradation as a result of real-life short-range utilization of identical passenger cars. A relatively high number of ~290 cold starts under a low mileage of ~1700 km contributed to quantifiable increase in acidity based on the neutralisation number from 1.6 to 2.2 mgKOH/g and a significant drop in kinematic viscosity from 58 mm^2/s to 39 mm^2/s. This phenomenon can be attributed to a 3.7% dilution of the engine oil with fuel. No strong correlation can be found between the differences in engine performance and the physical and chemical properties of the used engine oils in a test fleet.

Empirikus adatgyűjtés és főelem-analízis alkalmazásával kimutattam, hogy azonos alapmotorra épülő hajtáslánccal rendelkező, különböző teljesítményosztályú és felépítményű járművek esetén a kenőolaj kémiai és fizikai tulajdonságainak járműhasználatból adódó megváltozását legnagyobb mértékben a járműhasználat jellege határozza meg. Valós körülmények között, rövid utakon használt járművek esetén erős korrelációs áll fenn a hidegindítások száma és a kenőolaj degradációjának mértéke között. Alacsony ~1700 km futásteljesítmény és viszonylag magas számú ~290 hidegindítás mellett a savasság a neutralizációs szám alapján 1,6 mgKOH/g-ról 2,2 mgKOH/g-ra emelkedik, a kinematikai viszkozitás pedig 58 mm^2/s-ról 39 mm^2/s-ra csökken. Ez a jelenség a hajtóanyag által okozott 3,7%-os kenőolaj hígulásnak tudható be. Nem áll fenn erős korreláció a járművek között tapasztalható motorteljesítmény különbségek és a kenőolaj kémiai és fizikai tulajdonságainak járműhasználatból adódó megváltozása között.

Related personal publications: {6}, {8}; related chapters: 7

9   Summary

Concluding my research, I have established a methodology to evaluate the long-term effect of alternative fuels on engine oil aging and the consequent alteration in friction and wear. I have evaluated the state-of-the-art through literature review and identified the lack of friction and wear experiments of oil samples contaminated with alternative fuels. I have conducted an exploratory study of artificial engine oil aging promoted by fuel contamination on a ball-on-disc model system and showed that OME_{3-5} contamination contributes to a change in the dominant wear process. I have developed a controlled procedure and apparatus for artificial aging of engine oil samples and validated the artificial aging procedure through comparing the physical and chemical properties of artificially aged engine oil samples to in-use oil samples from internal combustion engines. To achieve this, I have organized a field test with 12 participating passenger cars – 9 general use and 3 constrained to a city-like environment –, collected oil samples and utilization data for 6 months, and through the principal component analysis of gathered data I have identified key correlations between engine oil oxidation and mileage, as well as between a drop in viscosity (i.e. dilution through fuel) and the number of cold starts. I have published my findings in ranked scientific journals, and disseminated my research on international conferences.

Results presented in the dissertation suggest, that the proposed methodology is suitable for artificial aging of engine oils in order to simulate in-use aging. The developed process and apparatus can serve as a basis for follow-up research on lubricant degradation in the presence of alternative fuels. Various additional scenarios, e.g. commercial and heavy-duty vehicles, or hybrid powertrains can be taken into account. Furthermore, extending artificial aging and oil analysis with advanced friction and wear measurements on a piston ring – cylinder liner experimental model could provide valuable data regarding boundary layer formation and wear. Additionally, the presented correlative analysis of fleet data and engine oil condition could be implemented by fleet operators or OEMs to continuously monitor both oil and powertrain fitness and effectively preserve a good operating condition without unnecessary, or late oil changes.

Appendix A – Validity and applicability of the artificial aging procedure

This section presents experimental results regarding the validity and applicability of the artificial engine oil aging apparatus introduced in Chapter 4.4. Details of the aging experiments are presented in. Engine oil samples were collected and sent for chemical analysis to determine the effect of artificial aging on key oil properties. Presented findings are published in {7}.

An oil aging experiment including 8 distinct thermo-oxidative load cases was performed on Shell Helix Ultra ECT C2/C3 0W-30 engine oil samples. A fractional-factorial parametric study was set up using 4 variables at 2 levels each according to Table 11. Sample temperature, air flow rate and sample volume were varied independently, with aging time being confounded to temperature and flow rate. Sample names correspond to the levels of independent variables. Samples were subjected to a cyclic thermal degradation process composed of 12 h heating and 12 h accumulation phases. This cyclic thermo-oxidative aging procedure is based on a procedure developed by Singer et al. [117]. The system reaches a stable set point temperature under 120 min and is able to keep sample temperatures within ± 1.5 °C.

Table 11. Sample identifiers and corresponding parameter values
for the parametric engine oil aging experiment

Sample	Temperature (°C)	Air flow rate (l/min)	Sample volume (ml)	Aging time (h)
A4.122	160	2.5	96	200
A4.121	160	2.5	96	100
A4.112	160	1	192	200
A4.111	160	1	192	100
A4.212	180	1	96	200
A4.211	180	1	96	100
A4.222	180	2.5	192	200
A4.221	180	2.5	192	100

A secondary study was carried out involving 5 contaminating agents (conventional fuels and novel automotive fuel candidates) with an identical initial oil quality to the parametric study. Contaminants were identified and selected based on a prior literature review on alternative fuels. Artificial aging was conducted on 200 ml samples at 160

°C with 2 l/min air flow rate. After a 96 h preliminary aging procedure the samples were contaminated with 5 mL of the corresponding fuels. An additional 96-hour aging procedure was executed, where a further 15 ml of the corresponding contaminant was added to each sample in three 5 ml doses after 24, 48 and 72 h. Sample identifiers and corresponding contaminants are given in Table 12.

Table 12. Sample identifiers and corresponding contaminants
for the contaminated engine oil aging experiment.

Sample	Contaminating agent	Target concentration (wt%)
A3.NOC	No contamination	0
A3.DMC	Dimethyl carbonate (DMC)	10
A3.OME	Oxymethylene dimethyl ether 3-5 (OME_{3-5})	10
A3.MTH	Methanol (MTH)	10
A3.E25	EN228 gasoline with 25% ethanol (E25)	10
A3.R95	EN228 gasoline, RON 95	10

One major limitation of the presented experimental investigation is the lack of repetition of the artificial aging experiments. As presented in Chapter 4.4.3, a good reproducibility with a relative deviation under 5% was achieved using the same reference oil, which was deemed to be acceptable. Hence, to maximize the achievable gain of experience with the budgetary constraints of the study, variety was chosen over repetition. A limitation of the presented methodology is the lack of mechanical shear load, and the absence of metallic reagents during aging. These could contribute to a more realistic aging procedure, which can also consider viscosity changes due to shear thinning and the depletion of additives due to surface bonding and boundary layer development.

Conventional oil analysis was performed on all samples after the completion of the aging experiments. Chemical analysis was carried out by the Austrian Excellence Center for Tribology (AC2T) in Wiener Neustadt. Details regarding oil analysis methods are presented in Chapter 4.3.

Parametric engine oil aging results

Oxidation based on absorption peak height (Figure 47 a) shows a clear increasing tendency with increasing temperature, aging time and air flow rate. Increasing the sample volume causes a drop in specific thermal and oxidative load, which also leads to decreased oxidation. As anticipated, no nitration or soot content was perceived by

the FTIR measurement. Residual zinc dialkyldithiophosphate (ZDDP) antiwear additive content (Figure 47 b) shows a significant drop in all cases compared to the reference sample (100%).
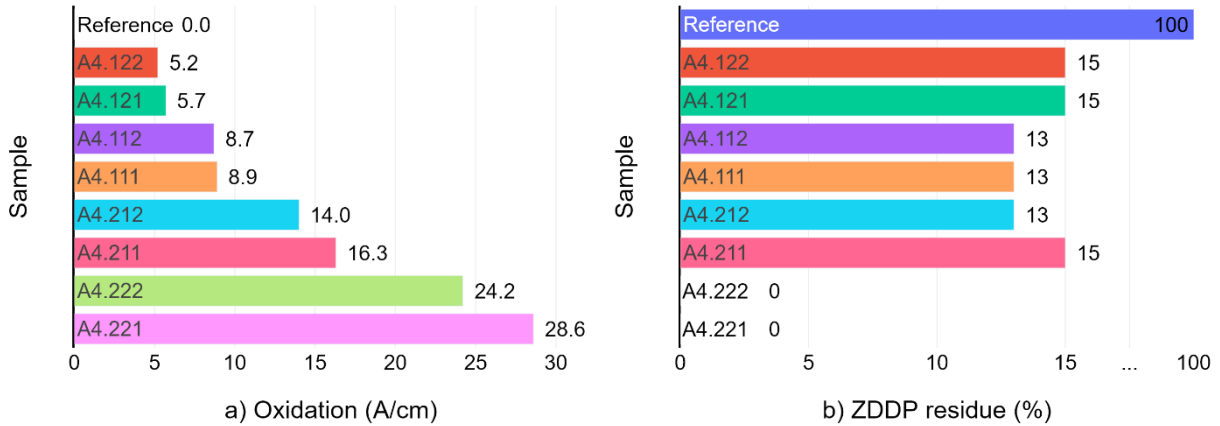

Figure 47. Oxidation (left) and ZDDP content (right) of parametric oil aging samples.

All samples exhibit a value of around 13-15% antiwear content aside from the ones with the highest load (180 °C for 192 h). These extreme load cases appear to completely deplete the antiwear additive content of the samples, with no measurable amount of ZDDP left in the samples after aging.
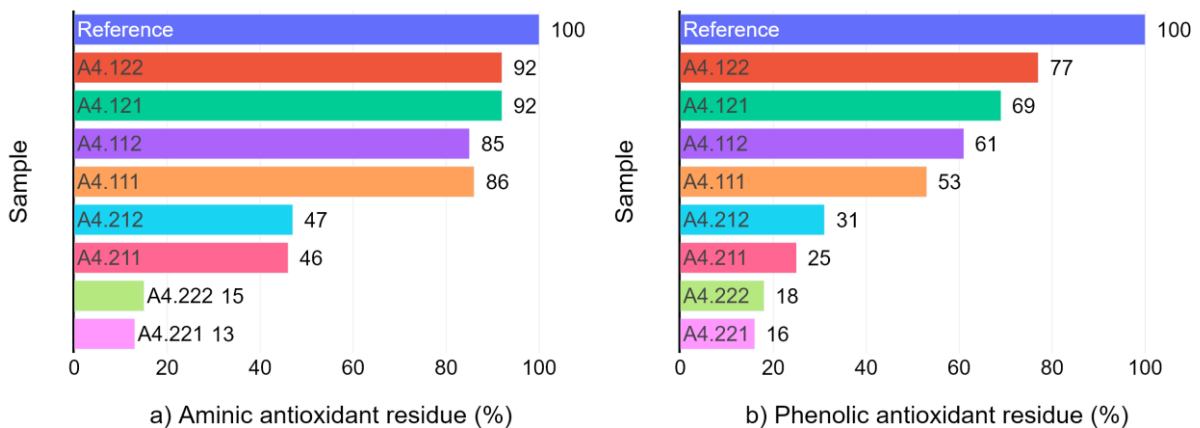

Figure 48. Aminic (left) and phenolic (right) antioxidant content of parametric oil aging samples.

Residual antioxidant content shows a gradual decrease compared to the reference oil sample. The amount of phenolic antioxidant residue (Figure 48 b) is in accordance with the previous observation of overall oxidation and shows correlating tendencies for all samples. Regarding aminic antioxidant residues (Figure 48 a), a slightly different trend can be observed. Sample volume and air flow rate appear to have less of an impact, while aging time causes seemingly minor variance at 160 °C. At 180 °C aging time

appears to be a prominent influencing factor, with around a 40% drop in values compared to 160 °C and another 30% variance between 96 and 192 h samples.
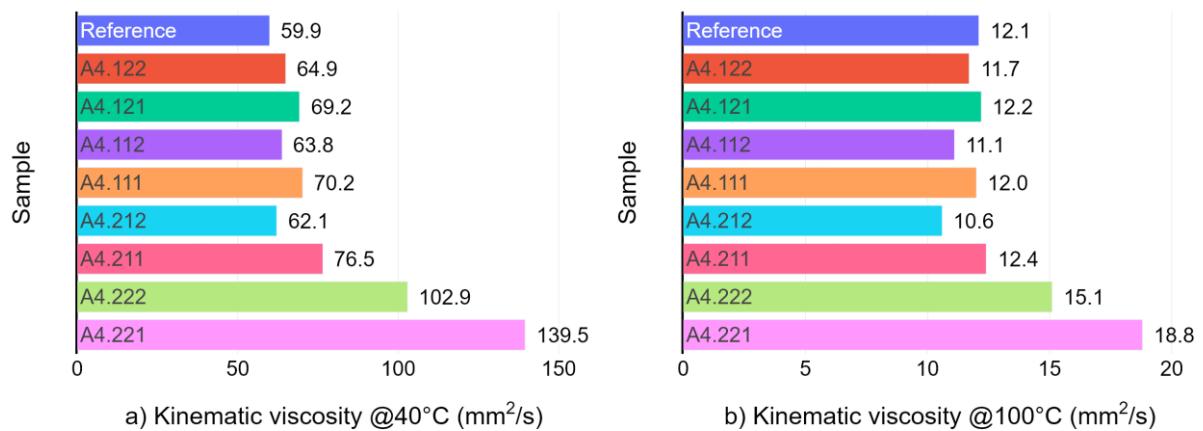
Figure 49. Kinematic viscosity at 40°C (left) and 100°C (right) of parametric oil aging samples.

Regarding kinematic viscosity at 40 °C (Figure 49 a) each sample displays an increased value compared to the reference. Samples aged at 160 °C for 96 and 192 h show comparable values. Samples aged at 180 °C for 96 h exhibit similar values, whereas samples aged at 180 °C for 192 h show 71% to 132% increases. At 100 °C (Figure 49 b) most values lie slightly below or around the reference oil's viscosity, whereas the two samples with the highest specific thermal load and longest aging time exhibit significant increases in kinematic viscosity values. Regarding viscosity index (Figure 50 a), a highly similar tendency to aminic residual additives was established.
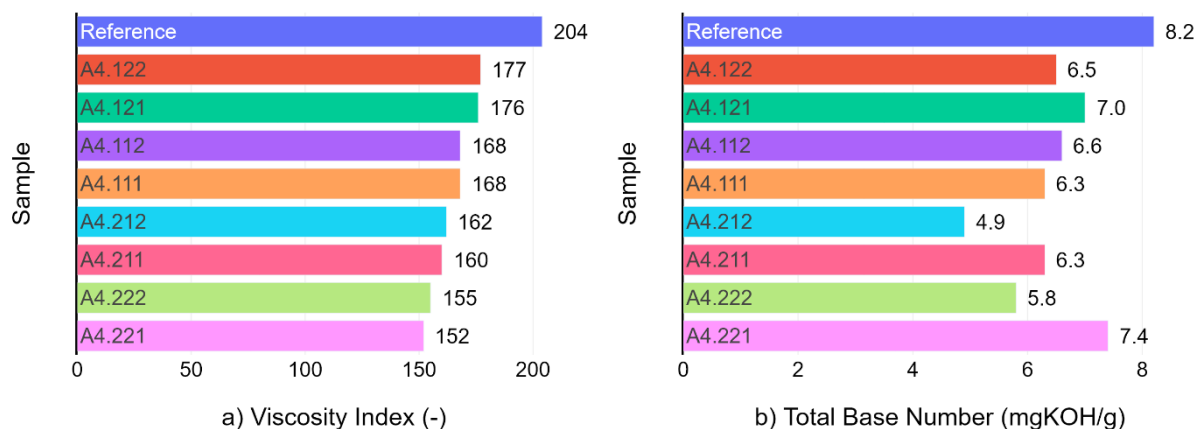

Figure 50. Viscosity index (left) and TBN (right) of parametric oil aging samples.

Total base number values display a moderate decrease (Figure 50 b), with the most significant change of around 41% at 180 °C after 96 h. One aged sample shows an

interesting outlier regarding TBN, with the lowest comparable decrease in TBN after 192 h at 180 °C.

Contaminated engine oil aging results

Contaminant type appears to have little effect on general oxidation (Figure 51 a), with negligible differences between samples. Similarly to the previously presented results, no nitration or soot content was perceived by the FTIR measurement. Residual ZDDP content (Figure 51 b) shows comparable values for all contaminated samples, which are in accordance with the findings of the parametric aging experiment.
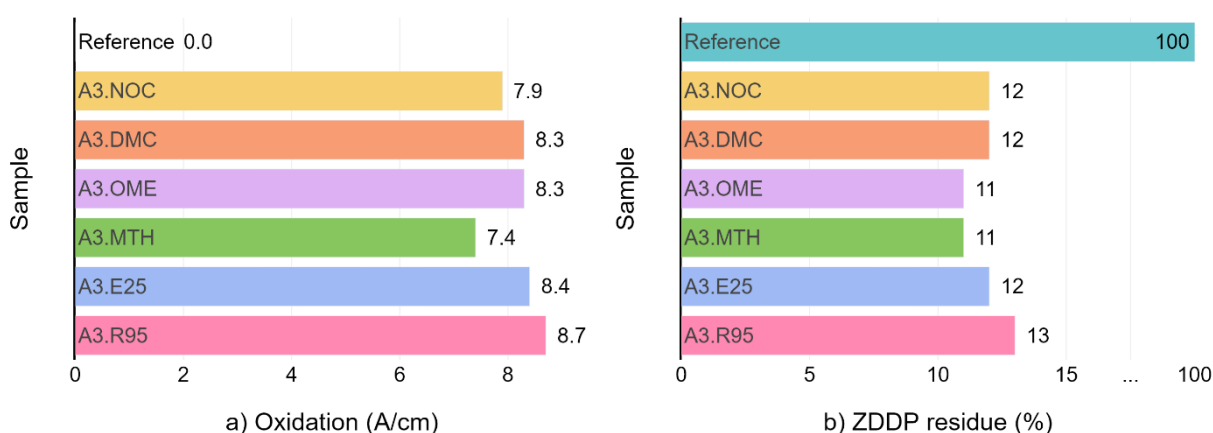
Figure 51. Oxidation (left) and ZDDP content (right) of contaminated oil aging samples.

Aminic (Figure 52 a) and phenolic (Figure 52 b) antioxidant content dropped in all samples during aging. A maximal difference of 5% phenolic antioxidant content can be established between samples with contaminants OME_{3-5} and methanol, which is marginal. Interestingly, contaminating the oil with OME_{3-5} during the experiment resulted in a significant drop in aminic antioxidant content compared to other samples. Oxymethylene ethers are known oxidizers and are investigated as diesel fuel additives [142], [78] for their ability to reduce the NO_x-soot trade-off in CIDI engines. The oxidative nature of OME_{3-5} could lead to a faster depletion of certain antioxidants in the engine oil. This phenomenon needs further investigation to understand the reaction pathways and products of OME-antioxidant interactions.

A general increase in kinematic viscosity was measured at 40 °C (Figure 53 a). The sample contaminated with OME_{3-5} shows the highest value in comparison, with a rather significant ~30% increase over the reference sample. This difference is similarly pronounced at 100 °C (Figure 53 b), with a ~10% higher value than the reference. A

nearly identical tendency can be observed with DMC contamination, with slightly lower absolute increase over the reference. This increase in viscosity could be attributed to increased polymerization due to the catalytic effect of OME_{3-5} and DMC.
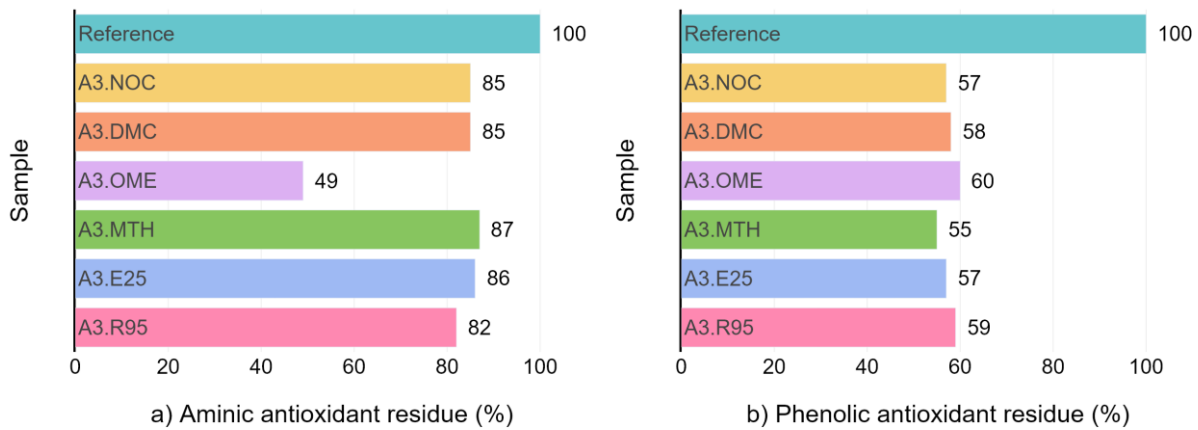

Figure 52. Aminic (left) and phenolic (right) antioxidant content of contaminated oil aging samples.

Regarding viscosity index (Figure 54 a), all samples measured around 172 units, which denotes a ~15% decrease compared to the reference. There seems to be no distinguishable effect of contaminant type on viscosity index. TBN values show (Figure 54 b) an identical trend to residual aminic antioxidants. OME_{3-5} contamination leads to a noticeable reduction in total base number compared to other fuel types.
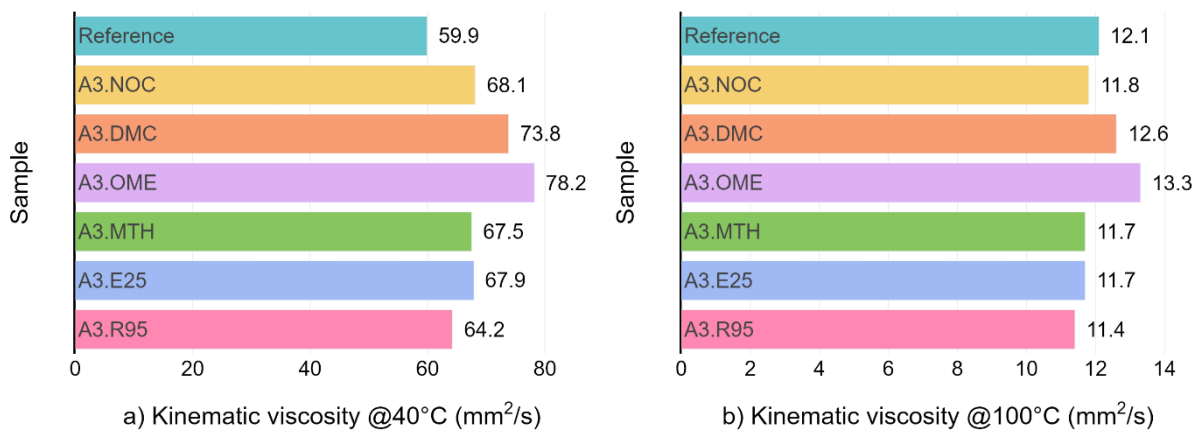
Figure 53. Kinematic viscosity at 40°C (left) and 100°C (right) of contaminated oil aging samples.

Overall, the aging study involving alternative fuels as contaminants in the oil during aging yielded interesting results regarding the amount of residual aminic antioxidant and kinematic viscosity values for the sample contaminated with OME_{3-5}. The experienced drop in antioxidant content and elevated kinematic viscosity at both 40 °C

and 100 °C suggest an underlying chemical reaction, which needs further attention and detailed analysis, but exceeds the scope of the current study.
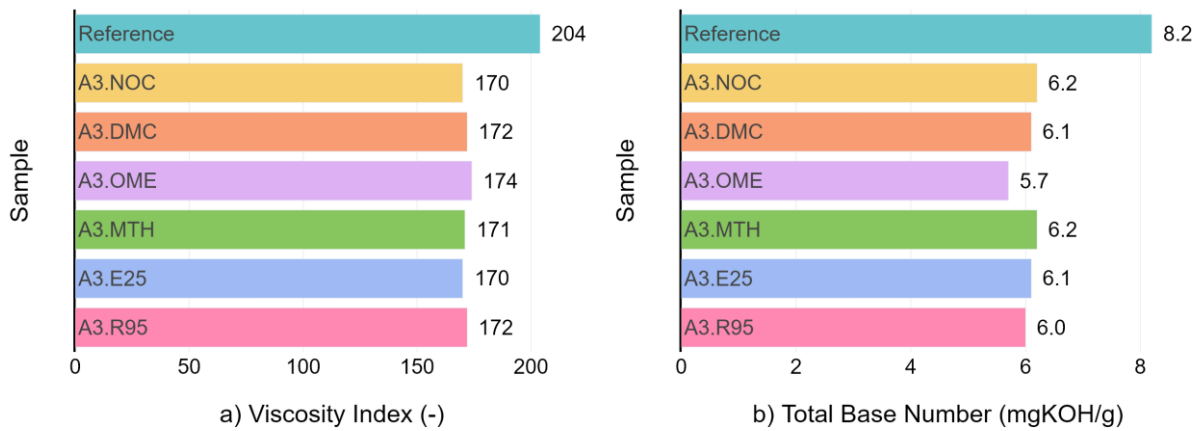

Figure 54. Viscosity index (left) and TBN (right) of contaminated oil aging samples.

Comparison and analysis of field aged and artificially aged engine oils

Principal component analysis (PCA) was utilized to identify the main contributing factors and visualize relations between collected samples. A similar approach was taken to incorporate artificially aged samples into the analysis and determine the suitability of the aging procedure and apparatus for simulating in-vehicle engine oil degradation. Since only conventional oil analysis was conducted on the laboratory-aged samples, the following variables (features) were included in the PCA: oxidation, residual antiwear additive content (ZDDP), residual antioxidant additive content (phenolic and aminic), TBN, kinematic viscosity (at40 °C and at100 °C) and viscosity index (VI).

Results of the PCA are presented on Figure 55. The contribution of each feature to the principal components is shown on a loading plot (Figure 55 a). Samples from the fleet study are shaded by mileage (Figure 55 b) and power (Figure 55 c) on the respective score plots. Artificially aged samples are marked with upward (parametric study) and downward (contaminant study) facing triangles (Figure 55 d). Reference oil samples are marked for both the fleet (circle) and artificial aging (triangle) experiments. A total explained variance of 87.56% was established, with the 1st principal component (PC1) contributing to 64.61% of the explained variance. The 2nd principal component (PC2) explains 22.95% of variance in the measured values in this analysis. PC1 and PC2 are interpreted as linear combinations of previously mentioned features.
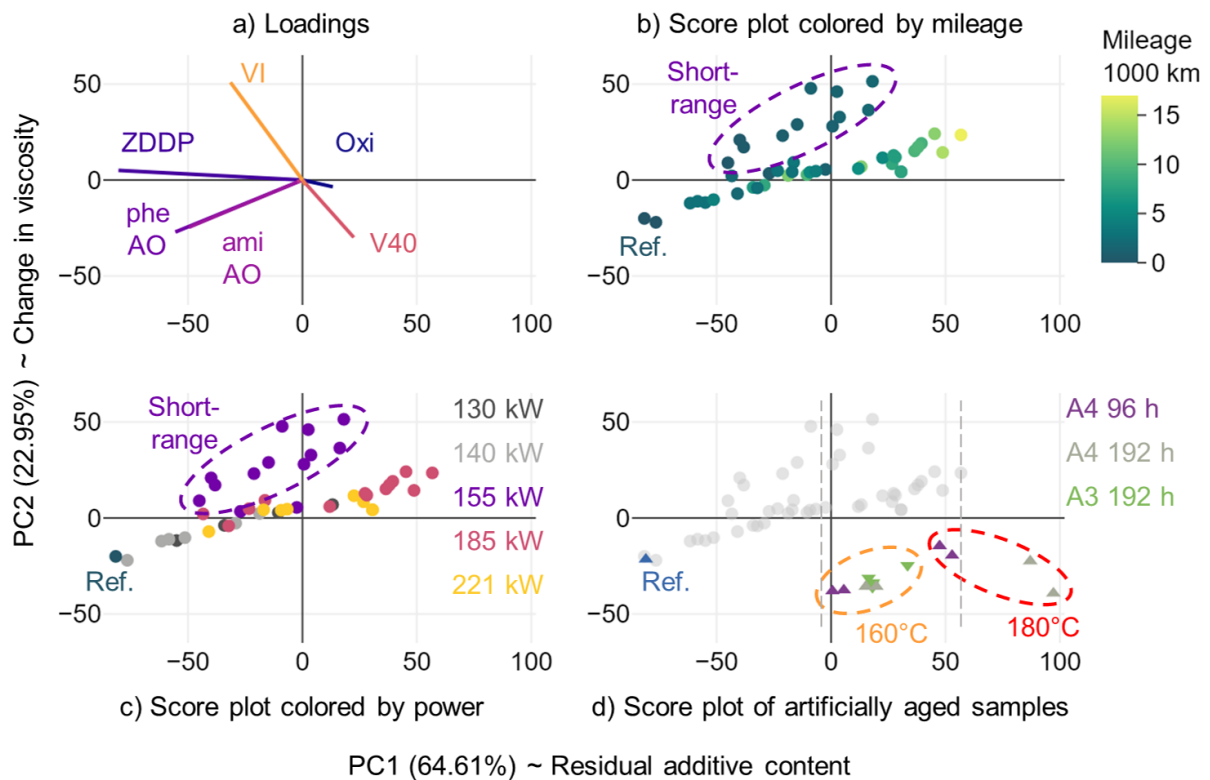
Figure 55. Score plot of the principal component analysis conducted on in-use and artificially aged engine oil samples.

A deeper insight into the nature of in-use and artificial oil degradation can be gained by taking a look at the loadings for each feature and the corresponding loading plot (Figure 55 a). The direction of each plotted vector shows how the corresponding feature correlates to the two principal components. The length of each plotted vector signifies the strength of correlation between each feature and the principal components. For PC1 the first three features in the order of strength of correlation are residual antiwear additive content (ZDDP, r = 0.687), residual phenolic antioxidant additive content (pheAO, r = 0.475) and residual aminic antioxidant additive content (amiAO, r = 0.424). The first three features for PC2 in order of correlation strength are viscosity index (VI, r = 0.729), kinematic viscosity at 40 °C (V40, r = 0.429) and residual phenolic antioxidant additive content (pheAO, r = 0.389).

According to the loadings it can be concluded that PC1 corresponds to residual additive content, whereas PC2 corresponds to the change in oil viscosity. Taking into account the previously presented values of the reference sample as well as the artificially aged samples, it is reasonable to assume that PC1 is inversely proportional to the amount

of antioxidant and antiwear additive residues, while PC2 is inversely proportional to viscosity.

As anticipated, higher mileage (Figure 55 b) contributes to a significant decrease in additive content and a mild-to-moderate decrease in kinematic viscosity, which is in accordance with overall expectations. Interestingly, short-range and long-range vehicles show a clear separation in terms of chemical properties in the PCA. Samples from vehicles with low average trip length and average vehicle speed (short-range, Figure 38) show distinct PC2 values from long-range vehicles.

However, more nuanced differences between vehicles – e.g., engine power – seem to have negligible effects on the investigated parameters (Figure 55 c). The largest change in viscosity was registered by a 155 kW short-range vehicle with around 2000 km mileage, whereas the most significant drop in additive content was reported from a 185 kW long-range vehicle with approx. 17,000 km mileage. Most reported values scatter below these extrema, regardless of engine performance. This apparent discrepancy of engine power affecting oil degradation can be attributed to the fact that every engine derivate includes slight modifications to ensure long-term operation without failure. A 221 kW derivate in general has improved oil cooling and a slightly higher oil charge compared to a 155 kW derivate, in order to avoid overloading the lubricant. As presented in Chapter 7.3, incorporating soot and wear metal content into the PCA leads to a clear separation of diesel vehicles. Diesel samples were ignored in the current study, since the presented aging method is incapable of producing such properties.

Figure 55 d presents PCA score values for the artificially aged samples in relation to the fleet study. This representation of the data gives a basic understanding of how artificially aged samples compare to in-use samples. In terms of antiwear and antioxidant additive residue (PC1) the artificially aged samples show comparable values, with a large number of observations from both studies falling into the region marked by dotted lines. Viscosity change (PC2), however, shows consistently higher values after the artificial aging procedure. This can be attributed to the fact that in-engine oil aging is highly influenced by fuel dilution, which was not considered in the case of the parametric aging experiments. The elevated temperature during artificial aging contributes to the evaporation of lighter-end hydrocarbons and results in an

increase in kinematic viscosity. As for the contaminated samples, the addition of fuels occurred at the start of each heating phase during the second stage of the experiment. It is theorized that most of the contaminant evaporates during the high temperature phase, hence a dilution at the end of the experiment cannot be measured by determining the viscosity of the sample. The mechanism of in-use fuel dilution follows a different pathway, where contamination occurs continuously and under moderate temperature (approx. 110 °C) inside the oil sump. Higher fuel dilution values are reported when a shorter test cycle is applied to an engine in a cold (~0 °C) environment, while continuous operation for longer time periods yields equilibrium fuel dilution levels around 4% [38], [143], [41].
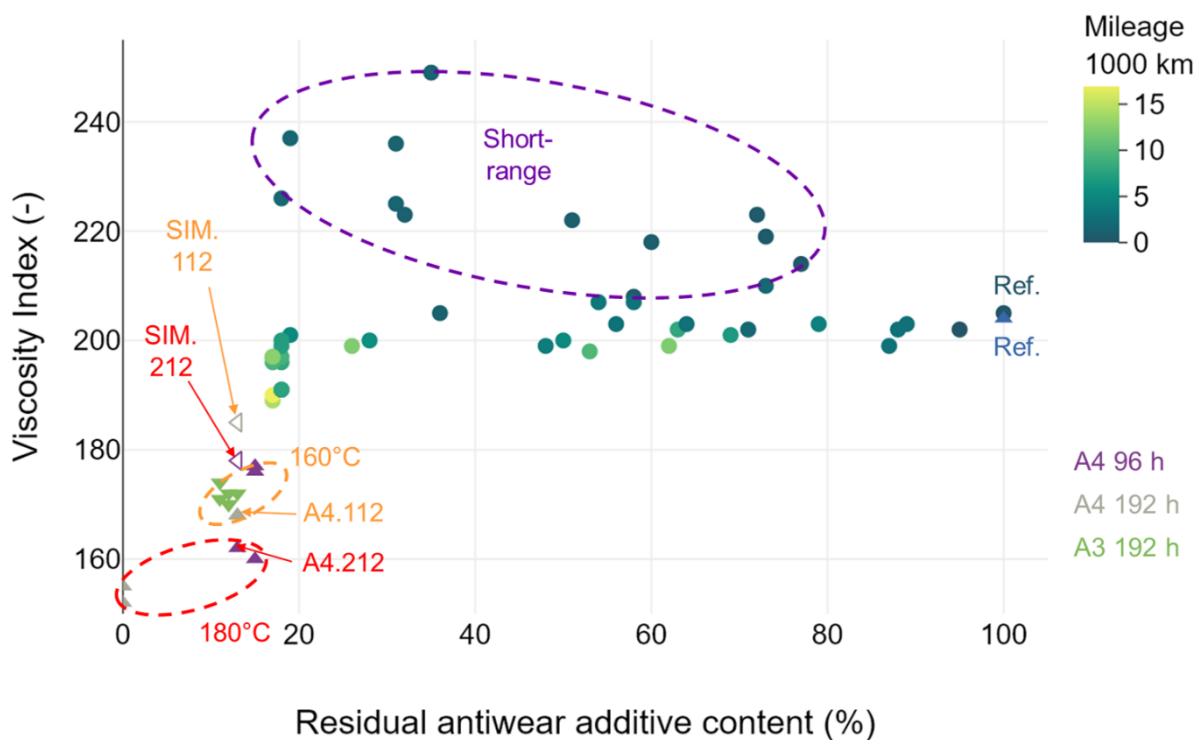
Figure 56. Viscosity Index plotted against residual antiwear additive (ZDDP) content for in-use and artificially aged oil samples.

Figure 56 presents viscosity index values plotted against residual antiwear additive content. A similar separation to Figure 55 can be established, with artificially aged samples showing a lower viscosity index. All artificially aged samples register slightly below the in-use samples for antiwear additive content. This result is in accordance with the thermal decomposition phenomenon of ZDDP antiwear additives reported by Jones et al [144], Peng et al [145] and Ferguson et al [146]. In-use samples can exhibit temperatures well over 180 °C in an operating internal combustion engine (e.g., piston ring and cylinder wall interaction in the TDC region [147], however, these

circumstances affect a restricted amount of lubricant at a time. Oil is in constant flow inside the engine between higher temperature (200 - 250 °C) load bearing regions (e.g., top piston ring nut) and accumulates in lower temperature (<110 °C) relief regions (i.e., the oil sump). According to the presented results the specific thermo-oxidative load during the artificial aging procedure appears to be moderately higher as exhibited by the lubricant under its common operating conditions.
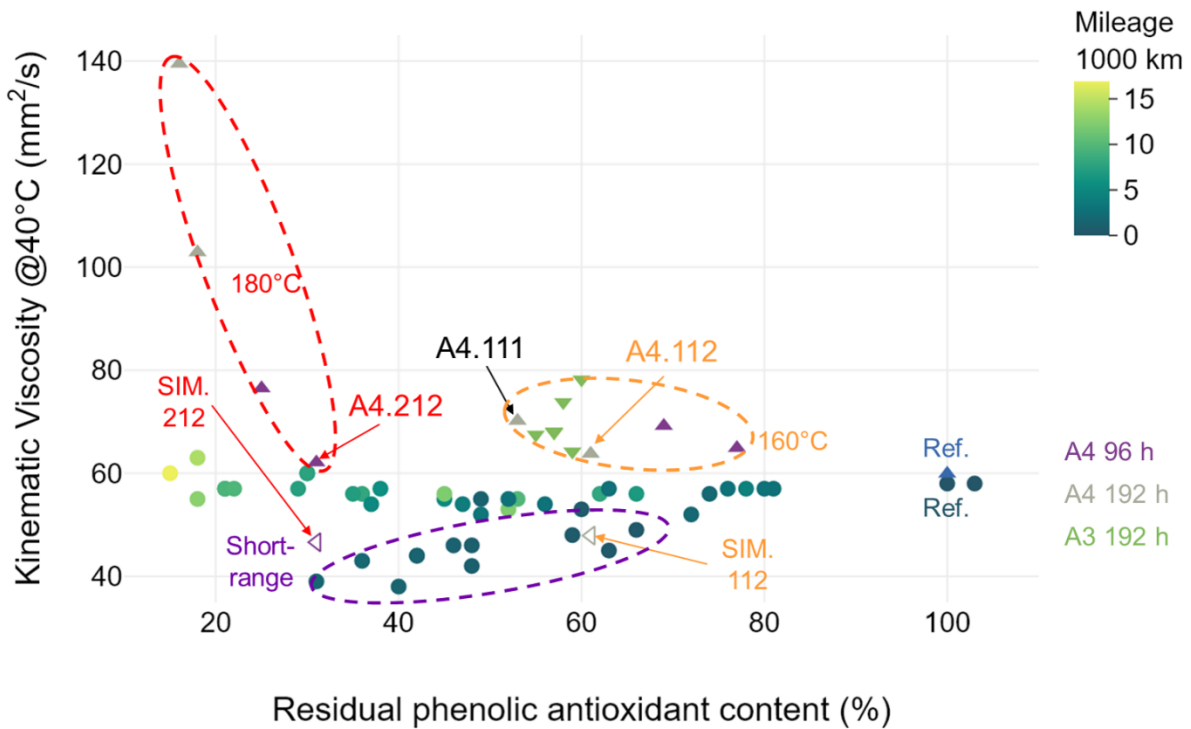
Figure 57. Kinematic viscosity at40°C plotted against residual phenolic antioxidant additive content for in-use and artificially aged oil samples.

A discernible variation in values and a better overall correlation of artificially aged and in-use samples can be seen on Figure 57. Regarding residual phenolic antioxidant content, all artificial aging samples exhibit values in the range of the in-use samples. Taking into account viscosity as well, samples from the A3 series (contaminated) all scatter between A4.111 and A4.112 (parametric). This further proves the reproducibility aspect of the aging procedure, since these samples were exposed to nearly identical conditions in the sense of temperature, air flow rate and initial sample volume during the corresponding experiments. Furthermore, a strong resemblance can be found between A4.212 and multiple in-use samples with around 7000 km mileage.

As presented in {6}, a fuel dilution of around 3.7 m% was found in selected samples of short-range vehicles. Furthermore, it was shown in a simple dilution experiment [148]

that mixing 3.7 m% RON 95 gasoline into the reference oil results in comparable kinematic viscosity and viscosity index values to the corresponding properties of a selected in-use sample with identical dilution. This further suggests that the change in viscosity in the case of field study samples can be partly attributed to fuel dilution. Hence, the differences between in-use and artificial samples in terms of PC2, viscosity index and kinematic viscosity can be explained by contrasting boundary conditions in the fuel dilution process for the artificial and real-life scenarios. In order to simulate the accumulation of fuel in the lubricant and the resulting change in viscosity, values of A4.112 and A4.212 were offset by a factor of 1.1 for viscosity index and 0.75 for kinematic viscosity at 40 °C, based on experimental results presented in {6}. The resulting simulated values are plotted on Figure 56 and Figure 57, labelled as SIM.112 and SIM.212. The simulated higher permanent dilution (i.e., fuel administered after the aging, thus not evaporated due to the thermal load) reduces viscosity and improves viscosity index. With this consideration, both simulated samples present values that are close to the observations of the fleet study in terms of viscosity index, with SIM.112 showing fairly good correlation to short-range samples regarding phenolic antioxidants and kinematic viscosity as well. This suggests that parameter set A4.112, with a post-aging fuel dilution of 3.7 m%, could be utilized to create batches of artificially aged oil with similar properties to used oils from short-range vehicles.

Regarding oil aging in long-range vehicles, the parameter set A4.212 could be applicable for creating small batches of artificially aged lubricant samples from SAE 0W-30 engine oils under laboratory conditions, which represent a used engine oil condition of around 7000 km mileage in terms of kinematic viscosity at 40°C and residual phenolic antioxidant content, and resemble used oil conditions regarding residual ZDDP antiwear additive content.

Section summary

The following observations were made based on the presented results:

- The parametric aging study showed that the main contributor to engine oil oxidation is aging temperature, followed by aging time. Sample volume, therefore specific thermal load, also has a discernible effect; however, air flow rate during aging appears to have only a minor impact.

- Both temperature levels of the parametric aging study appear to cause nearly identical degradation of ZDDP antiwear additives, with comparable levels of residual content at 160 °C and 180 °C after 96 h of aging. Samples still showed similar values after 192 h at 160 °C, whereas no residual antiwear additive content was found after 192 h at 180 °C. This can be explained with the lack of temperature stability above 120 °C of ZDDP [149] as an engine oil additive.

- Kinematic viscosity increased during the parametric aging experiment, which could be a result of polymerized oxidation products and/or thermal polymerization of the engine oil. This observation is in accordance with [125], and is briefly mentioned in [118]. However, a more detailed analysis is necessary to prove this assumption.

- The contaminated aging study yielded interesting results regarding the amount of residual aminic antioxidant and kinematic viscosity values for the sample contaminated with OME_{3-5}. The experienced drop in antioxidant content and elevated kinematic viscosity at both 40 °C and 100 °C suggest an underlying chemical reaction, which needs further attention and detailed analysis, but exceeds the scope of the current study.

- Compared to in-use engine oil samples, both artificial aging studies show comparable results in terms of residual phenolic antioxidant content. Based on the presented results the parameter set A4.212 (180 °C, 1 l/min, 200 ml, 96 h) can be recommended for small-scale artificial aging of engine oils. This aging procedure can create an oil condition similar to an in-use engine oil sample after 7000 km of mixed on-road usage in terms of kinematic viscosity at 40 °C, residual phenolic antioxidant content and residual ZDDP antiwear additive content.

The above findings support Theses 2 and 3.

Appendix B – Scientific outlook

This section gives a brief summary of experimental results that were not incorporated into the thesis due to their incompleteness.

As detailed in Chapter 4, numerous friction and wear experiments were conducted on a selection of model system throughout the research phase, although only results from the ball-on-disc setup were presented. The main goal of utilizing experimental setups in addition to the ball-on-disc was to investigate the effects – a transition from abrasive wear to fatigue wear – detailed in Chapter 5 under mild-to-moderate loads and larger contact areas as well. However, decreasing the contact stress through enlarging the contact area introduced an increased repeatability error in the measurements, which hindered wear quantification through optical measurement techniques, as well as compromised the comparability. The reason behind an increased error lies in the precision of sample placement and fastening at the start of each experiment. Cylinder-on-disc experiments exhibited a large variance in the length and placement of the wear scar along the disc surface, which was caused by misalignment introduced trough the fastening mechanism. The disc specimen is fastened with a metric bolt, that has no guiding aside from a tapped bore in the sample holder. This permits a slight sideway displacement of the bolt, which translates up to a 0.05 mm raise of the disc in the holder. Additionally, the friction between the tail end of the bolt and the sample holding jaw introduces a slight moment, which tilts the disc specimen in the sample holder. Finding the root cause of the problem and elaborating a solution lead to a delay in the research process, hence results from these experiments remained unpublished.

Experiments on the piston ring – cylinder liner model system were also in preparation. The uniqueness of this experimental setup compared to ball-on-disc or cylinder-on-disc tests is the fact, that both bodies in the experimental setup are manufactured from series production parts, i.e. real, mass produced engine parts, with production material properties, surface hardness and topology. Using real-life parts in a model investigation aids the transferability and generalization of research results to real-life applications and conditions. This advantage also carries an inherent weakness compared to a tailor-made solution, that it needs a sophisticated sample preparation routine to ensure good repeatability. In case of the cylinder liner, the suggested 18 mm wide sample size together with the deformation of the samples due to residual stresses

in the cast part lead to a large variation in effective contact area during measurement. Since with the SRV 5 system the effective contact stress is determined by the effective contact area, the comparability of measurements was compromised. A careful setting of the ring segment pretension can mitigate this problem, although only when an applicable pretension technique is applied before each experiment. Figure 58 presents irregularities of the cylinder liner contact area after friction and wear testing. An excessive distortion of the cylinder liner leads to an asymmetric contact area (Figure 58 a), which is difficult to compensate for with the alignment of the piston ring. Setting up the curvature of the ring segment incorrectly can lead either to an intermittent contact area (Figure 58 b) if the ring is under insufficient tension, or to an incomplete contact area (Figure 58 c), if the ring is overtensioned.

a) asymmetric contact   b) contact under insufficient tension   c) contact under excessive tension
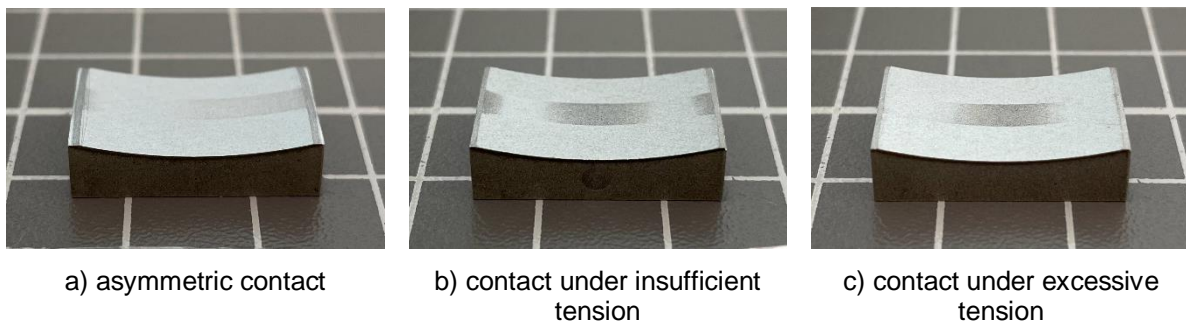
Figure 58. Irregular contact area on the cylinder liner surface due to an alignment error of the piston ring segment.

A guide rig is being developed to alleviate these issues stemming from misalignment during setting up the experiment. The guide rig comprises of a baseplate, which holds the cylinder liner in place during the procedure. A movement system is fastened to the baseplate, which guides a vertically moving carriage. The carriage supports the sample holder for the piston ring segment. To set the desired curvature the samples are fastened in the guide rig, the carriage is set under 50 N compression and the adjustment setscrew is tightened or loosened until no light can be seen passing through the gap between the piston ring and the cylinder liner. A 3D printed rapid prototype version of the guide rig is pictured on Figure 59. The prototype is not intended to simulate in-test loads through compression, and the vertical movement of the carriage is overconstrained. However, the guide rig is already a step forward to a repeatable, precise sample pretension technique in its current form.

Furthermore, a set of experiments were also carried out to determine a reasonable load collective for friction and wear testing of aged engine oil samples in a piston ring

– cylinder liner experimental environment. All experiments were conducted with a 3 mm long stroke at 50 Hz oscillation frequency. A variation of test loads, sample temperatures, lubrication types, test times and preload scenarios were investigated in order to select a load set, which produces measurable alterations on the sample surface under a manageable time period.
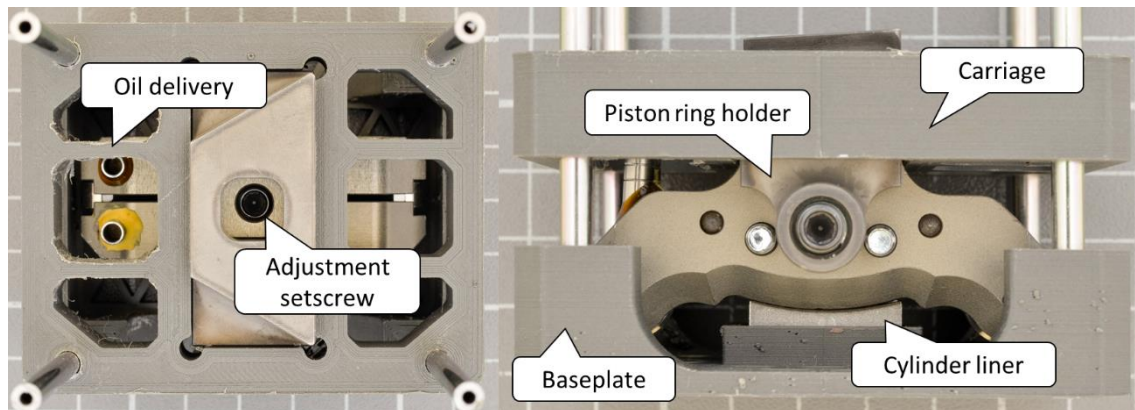

Figure 59. Top view (left) and side view (right) of the guide rig prototype.

Three different scenarios were examined regarding preload and test load:

A. 5 minutes of 50 N preload followed by a 200 N test load shifted during 5 minutes
B. 5 minutes of 50 N preload shifted during 5 minutes to a 350 N overload, shifted back to a 200 N test load under another 5 minutes
X. 5 minutes of 50 N preload followed by a 400 N test load shifted during 5 minutes

It was theorized, that utilizing an increased load during the run-in process (scenario B) could help in establishing a uniform contact area. An overload (scenario X) was considered to investigate lubrication and wear under severe contact pressure.

In terms of lubrication, a continuous flow setup and a one-time dosing approach were investigated. The continuous flow setup consists of a closed-loop oil circuit driven by a two-stage peristaltic pump. The loop incorporates an electric heater for individual temperature conditioning of the test lubricant. One-time dosing is carried out at the start of the experiment, with 0.1 ml lubricant being spread over the contact surface of the cylinder liner. This approach produces less single-use waste, but also represents a more severe environment for the lubricant. Since no oil replenishment takes place during the test run, the specific thermal and mechanical load acting on the lubricant is considerably higher. After several preliminary test runs, the continuous flow setup was

ruled out, due to providing superior lubrication, hence resulting in immeasurable wear on the cylinder liner surface even under severe load conditions.

Test time and sample temperature combinations are summarized in Table 13.

Table 13. Sample temperatures and test times for different load scenarios

Load scenario	Temperature (°C)	Test time (min)	Test runs
A	120	120	1 & 2
		240	3
B	120	480	4
	150	240	5
	180		6
X	150	240	7
	180		8

Test run 1 was carried out as reference using an unadulterated batch of the Shell Helix 0W-30 engine oil. Consecutive tests were all conducted with an artificially aged oil batch with identical aging properties to sample A3.NOC presented in Chapter 0.
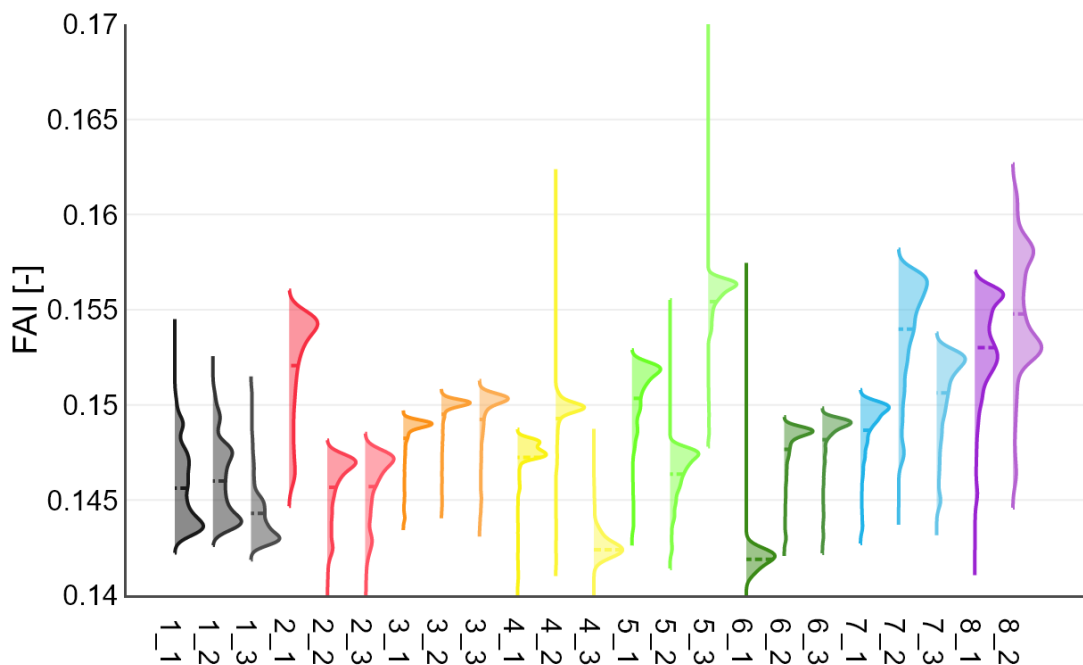

Figure 60. Probability density plot of friction absolute integral (friction coefficient) values registered during testing of piston ring – cylinder liner samples. Originally published in [150].

Figure 60 summarizes coefficient of friction results from the test series on piston ring – cylinder liner samples. The probability density plot presents a means of informed

comparison through incorporating information regarding the distribution of values in addition to their means and extrema. Based on the distributions, load scenario A produces comparable tendencies, with one outlier experiment (2_1). Tests with the reference oil (1_#) produce comparable distributions and scatter in a tight band. Test with the aged oil sample show acceptable results with load case A, cases B and X on the other hand present an unstable system.
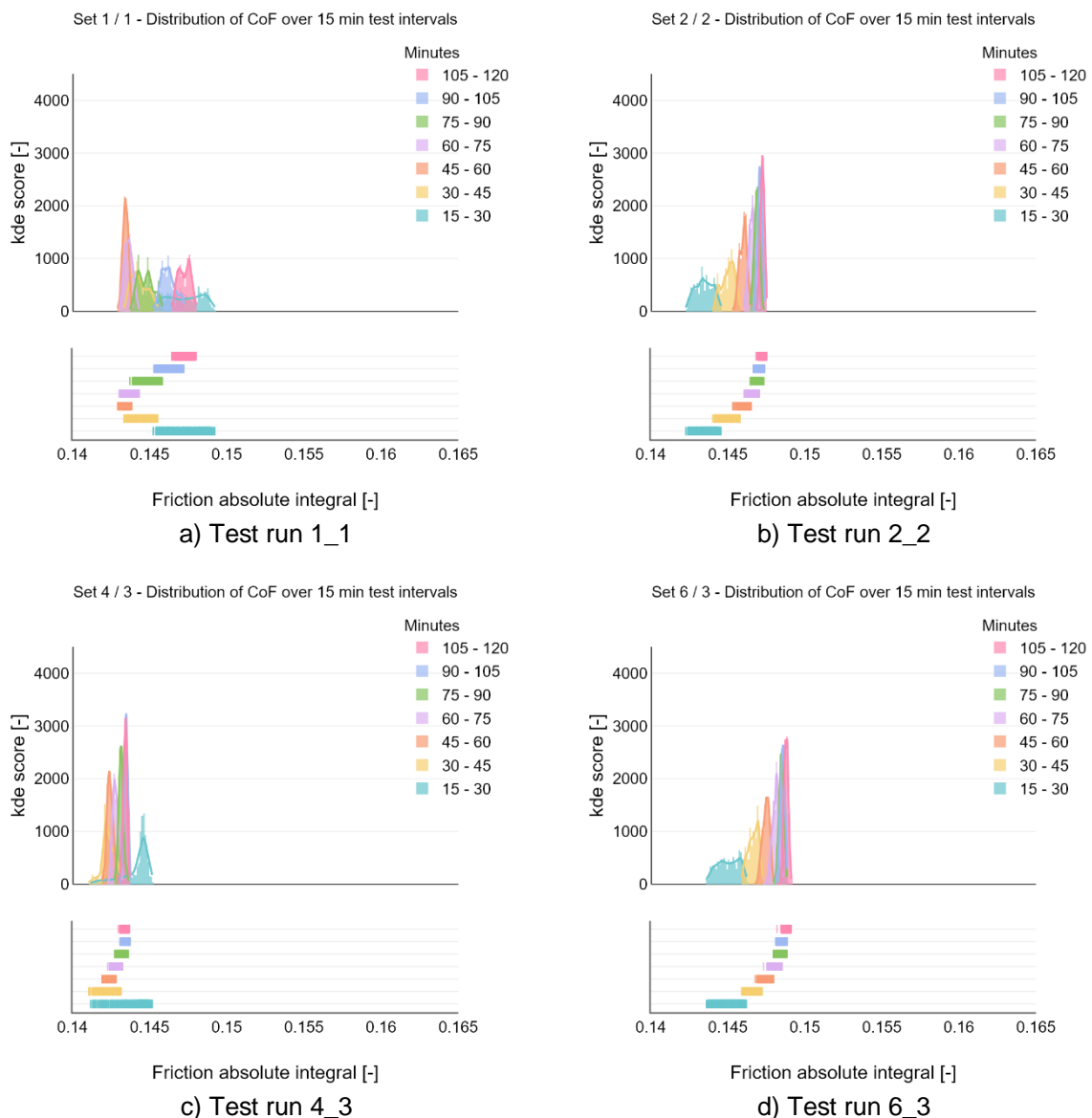

Figure 61. Distribution of friction coefficient values over 15 minute intervals for 4 selected experiments.

At this point it is unclear how severely the instability of the results is influenced by the overload of the tribological system at loads over 200 N, or if it's a direct consequence of sample misalignment. A historic analysis reveals how coefficient of friction values

are distributed during the first 120 minutes of the presented test cases. Figure 61 presents the distribution of friction coefficient values over 15 minute intervals for 4 selected experiments. As noted on Figure 60, there is a basic difference in tendencies with the reference sample and aged samples. Test run 1_1 (Figure 61 a) shows a high initial value in the first interval, which drops down and rises back up after 60 minutes. In comparison, 2_2 (Figure 61 b) and 6_3 (Figure 61 c) show a steady rise over the intervals of the test. Interestingly, the latter two test runs are not identical in terms of load cases, despite presenting highly similar behaviour in the first two hours of the test. Test run 4_3 (Figure 61 d) shows an example for a severely misaligned experimental setup, with a distribution unlike the previous two tendencies.

a) Test run 1_1	b) Test run 2_2
c) Test run 4_3	d) Test run 6_3
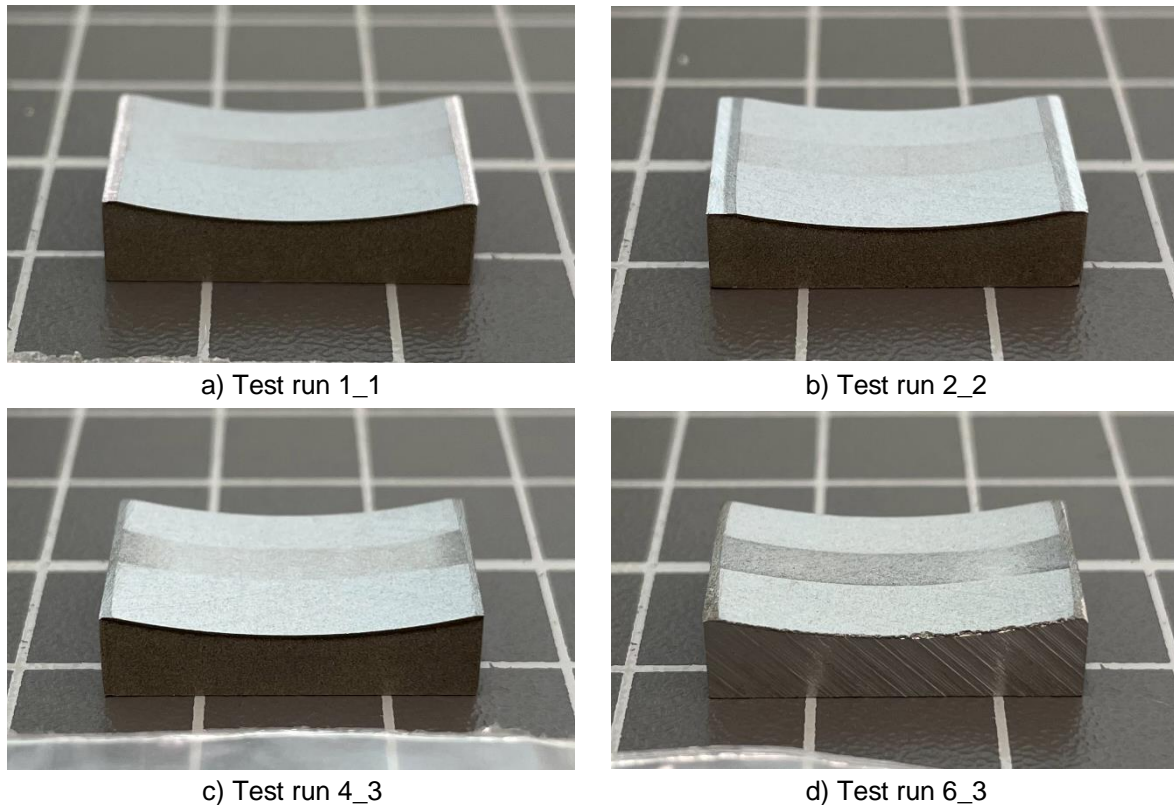
Figure 62. Wear scar on selected cylinder liner samples after testing.

Looking at the wear scars on the corresponding cylinder liners after testing (Figure 62) reveals a fairly homogeneous effective contact area for samples 1_1, 2_2 and 6_3. Test sample 4_3 has a severely intermittent wear scar (mild wear in the middle, pronounced wear near the edges), which is a clear signs of inadequate piston ring tension. Based on these findings it seems reasonable to assume, that the poor repeatability is caused by the sample misalignment. Ongoing activities related to further development of the procedure include a revised guiding rig prototype, as well

as a revised design of the cylinder liner sample itself. A narrower sample geometry could contribute to a larger room for error, as well as slightly overtensioning the piston ring, which appears to be easier to replicate.

Finally, surface topography measurements were also carried out on each tested cylinder liner sample, which lead to ambiguous results. The utilized engine type is equipped with a thermal spray coating on its cylinders, which leads to a porous structure with a sporadic distribution of void shape, volume and density. Since a sampling approach (i.e. taking measurements from worn and pristine parts of the same test sample surface) was utilized to compare before and after conditions, the actual porosity in the investigated area had a strong influence over the calculated roughness parameters. The measured values are applicable to show a tendency of change due to wear, but too sensitive to porosity and not sensitive enough to changes in load case or lubricant. Utilizing a backtracking measurement strategy with a suitable means of marking the surface before friction and wear testing and measuring the same area before and after the test runs could reduce the influence of porosity.

Further research is in preparation with a revised methodical approach based on the experiences and lessons learned with piston ring and cylinder liner experiments. In addition to the presented techniques, an in-depth analysis of the boundary layer on piston ring and cylinder liner samples after testing with various aged oils is also proposed.

Personal publications

{1}   **A. L. Nagy**, J. Knaup and I. Zsoldos, "A Review on the Effect of Alternative Fuels on the Friction and Wear of Internal Combustion Engines," *In: Jármai, K., Bolló, B., Eds.; Vehicle and Automotive Engineering 2,* pp. 42–55, 2018

{2}   **A. L. Nagy**, J. Knaup and I. Zsoldos, "A friction and wear study of laboratory aged engine oil in the presence of diesel fuel and oxymethylene ether," *Tribology-Materials, Surfaces & Interfaces*, vol. 13 (1), pp. 20-30, 2019, doi: 10.1080/17515831.2018.1558026

{3}   **A. L. Nagy**, J. Knaup and I. Zsoldos, "Investigation of Used Engine Oil Lubricating Performance Through Oil Analysis and Friction and Wear Measurements," Acta Technica Jaurinensis, vol. 12, no. 3, pp. 237-251, 2019, doi: https://doi.org/10.14513/actatechjaur.v12.n3.495

{4}   **A. L. Nagy**, "Development of an artificial aging process for automotive lubricants," *Spring Wind 2019*, pp. 771–775, 2019

{5}   **A. L. Nagy** and I. Zsoldos, "Artificial Aging of Ultra-low Viscosity Lubricant Samples on a Programmable Oil Aging Rig," VAE 2020: Vehicle and Automotive Engineering 3; pp. 139–147, 2021, doi: 10.1007/978-981-15-9529-5_12

{6}   A. Agocs, **A. L. Nagy**, Z. Tabakov, J. Perger, J. Rohde-Brandenburger, M. Schandl, C. Besser and N. Dörr, "Comprehensive assessment of oil degradation patterns in petrol and diesel engines observed in a field test with passenger cars—Conventional oil analysis and fuel dilution," Tribology International, 2021, doi: 10.1016/j.triboint.2021.107079.

{7}   **A. L. Nagy**, J. Rohde-Brandenburger, I. Zsoldos, "Artificial Aging Experiments of Neat and Contaminated Engine Oil Samples," Lubricants, vol. 9, no. 63, 2021, doi: https://doi.org/10.3390/lubricants9060063

{8}   **A. L. Nagy**, A. Agocs et al, "Rapid Fleet Condition Analysis through Correlating Basic Vehicle Tracking Data with Engine Oil FT-IR Spectra," Lubricants, vol. 9, no. 12, 2021, https://doi.org/10.3390/lubricants9120114

References

[1] "Worldwide harmonized Light vehicles Test Procedure (ECE/TRANS/180/Add.15)." United Nations Global Registry, 2014, [Online]. Available: https://unece.org/fileadmin/DAM/trans/main/wp29/wp29r-1998agr-rules/ECE-TRANS-180a15e.pdf.

[2] "Commission Regulation (EU) 2017/1151 of 1 June 2017 supplementing Regulation (EC) No 715/2007 of the European Parliament and of the Council on type-approval of motor vehicles with respect to emissions from light passenger and commercial vehicles (Euro 5 a." 2017, [Online]. Available: https://eur-lex.europa.eu/legal-content/EN/ALL/?uri=CELEX:32017R1151.

[3] "European Vehicle Market Statistics: Pocketbook 2019/20." International Council on Clean Transportation (ICCT), p. 56, 2019, [Online]. Available: https://theicct.org/sites/default/files/publications/European_vehicle_market_statistics_20192020_20191216.pdf.

[4] M. Scheidt, C. Brands, M. Lang, M. Kratzsch, and M. Günther, "Kombinierte Miller- / Atkinson-Strategie für zukünftige Downsizing-Konzepte," 2014, doi: https://doi.org/10.1007/978-3-658-05016-0_16.

[5] S. Kojima, S. Kiga, K. Moteki, E. Takahashi, and K. Matsuoka, "Development of a New 2L Gasoline VC-Turbo Engine with the World's First Variable Compression Ratio Technology," 2018, doi: https://doi.org/10.4271/2018-01-0371.

[6] J. J. López, A. García, J. Monsalve-Serrano, V. Cogo, and K. Wittek, "Potential of a two-stage variable compression ratio downsized spark ignition engine for passenger cars under different driving conditions," *Energy Convers. Manag.*, vol. 203, p. 112251, 2020, doi: https://doi.org/10.1016/j.enconman.2019.112251.

[7] E. Schutting *et al.*, "Miller- und Atkinson-Zyklus am aufgeladenen Dieselmotor," *MTZ - Mot. Zeitschrift*, vol. 68, no. 6, pp. 480–485, 2007, doi: 10.1007/BF03227416.

[8] J. Zhao, "Research and application of over-expansion cycle (Atkinson and Miller)

engines – A review," *Appl. Energy*, vol. 185, pp. 300–319, 2017, doi: https://doi.org/10.1016/j.apenergy.2016.10.063.

[9] M. Böhm, W. Mährle, H.-C. Bartelt, and S. Rubbert, "Funktionale Integration einer Wassereinspritzung in den Ottomotor," *MTZ - Mot. Zeitschrift*, vol. 77, no. 1, pp. 38–43, 2016, doi: 10.1007/s35146-015-0151-4.

[10] "Nissan's new VCR engine: worth the effort?," *SAE International*, 2018. https://www.sae.org/news/2018/05/2019-infiniti-qx-50-w-vc-turbo-review.

[11] "Fuel-efficient micro-hybrid for the Golf New 130 PS petrol engine is as efficient as a diesel," *Volkswagen-Newsroom*, 2018. https://www.volkswagen-newsroom.com/en/press-releases/fuel-efficient-micro-hybrid-for-the-golf-new-130-ps-petrol-engine-is-as-efficient-as-a-diesel-1997.

[12] "5 Liter Wasser für 500 Pferde," *BMW-M Magazin*, 2015. https://www.bmw-m.com/de/topics/magazine-article-pool/5-liter-wasser-fuer-500-pferde.html.

[13] H. T. Xu, Z. Q. Luo, N. Wang, Z. G. Qu, J. Chen, and L. An, "Experimental study of the selective catalytic reduction after-treatment for the exhaust emission of a diesel engine," *Appl. Therm. Eng.*, vol. 147, pp. 198–204, 2019, doi: https://doi.org/10.1016/j.applthermaleng.2018.10.067.

[14] C. McCaffery *et al.*, "On-road gaseous and particulate emissions from GDI vehicles with and without gasoline particulate filters (GPFs) using portable emissions measurement systems (PEMS)," *Sci. Total Environ.*, vol. 710, p. 136366, 2020, doi: https://doi.org/10.1016/j.scitotenv.2019.136366.

[15] Y. Chen *et al.*, "Emissions of automobiles fueled with alternative fuels based on engine technology: A review," *J. Traffic Transp. Eng. (English Ed.*, vol. 5, no. 4, pp. 318–334, 2018, doi: https://doi.org/10.1016/j.jtte.2018.05.001.

[16] P. Aakko-Saksa *et al.*, "Comprehensive emission characterisation of exhaust from alternative fuelled cars," *Atmos. Environ.*, vol. 236, p. 117643, 2020, doi: https://doi.org/10.1016/j.atmosenv.2020.117643.

[17] A. Kontses, G. Triantafyllopoulos, L. Ntziachristos, and Z. Samaras, "Particle

number (PN) emissions from gasoline, diesel, LPG, CNG and hybrid-electric light-duty vehicles under real-world driving conditions," *Atmos. Environ.*, vol. 222, p. 117126, 2020, doi: https://doi.org/10.1016/j.atmosenv.2019.117126.

[18] J. M. Luján, A. García, J. Monsalve-Serrano, and S. Martínez-Boggio, "Effectiveness of hybrid powertrains to reduce the fuel consumption and NOx emissions of a Euro 6d-temp diesel engine under real-life driving conditions," *Energy Convers. Manag.*, vol. 199, p. 111987, 2019, doi: https://doi.org/10.1016/j.enconman.2019.111987.

[19] S. Ou, D. Gohlke, and Z. Lin, "Quantifying the impacts of micro- and mild- hybrid vehicle technologies on fleetwide fuel economy and electrification," *eTransportation*, vol. 4, p. 100058, 2020, doi: https://doi.org/10.1016/j.etran.2020.100058.

[20] D. Zi, L. Zhang, B. Chen, and Q. Zhang, "Study of the electric-booster and turbo-generator system and its influence on a 1.5 L gasoline engine," *Appl. Therm. Eng.*, vol. 162, p. 114236, 2019, doi: https://doi.org/10.1016/j.applthermaleng.2019.114236.

[21] B. Chen, L. Zhang, J. Han, and Q. Zhang, "A combination of electric supercharger and Miller Cycle in a gasoline engine to improve thermal efficiency without performance degradation," *Case Stud. Therm. Eng.*, vol. 14, p. 100429, 2019, doi: https://doi.org/10.1016/j.csite.2019.100429.

[22] A. García, J. Monsalve-Serrano, S. Martínez-Boggio, and K. Wittek, "Potential of hybrid powertrains in a variable compression ratio downsized turbocharged VVA Spark Ignition engine," *Energy*, vol. 195, p. 117039, 2020, doi: https://doi.org/10.1016/j.energy.2020.117039.

[23] G. Schmaltz, *Technische Oberflächenkunde*, 1st ed. Berlin: Springer Verlag Berlin Heidelberg, 1936.

[24] "ISO 25178-2:2012 Geometrical product specifications (GPS) — Surface texture: Areal — Part 2: Terms, definitions and surface texture parameters." International Organization for Standardization, Geneva, 2012, [Online]. Available: https://www.iso.org/obp/ui/#iso:std:iso:25178:-2:ed-1:v1:en.

[25] "ISO 13565-2:1996 Geometrical Product Specifications (GPS) — Surface texture: Profile method; Surfaces having stratified functional properties — Part 2: Height characterization using the linear material ratio curve." International Organization for Standardization, Geneva, 1996, [Online]. Available: https://www.iso.org/standard/22280.html.

[26] H. Czichos and K.-H. Habig, *Tribologie-Handbuch*, 4th ed. Wiesbaden: Springer Vieweg, 2015.

[27] K.-H. Zum Gahr, *Microstructure and Wear of Materials*. Amsterdam: Elsevier B.V., 1987.

[28] K. Hokkirigawa and K. Kato, "An experimental and theoretical investigation of ploughing, cutting and wedge formation during abrasive wear," *Tribol. Int.*, vol. 21, no. 1, pp. 51–57, 1988, doi: 10.1016/0301-679X(88)90128-4.

[29] A. J. Gant, M. G. Gee, D. D. Gohil, H. G. Jones, and L. P. Orkney, "Use of FIB/SEM to assess the tribo-corrosion of WC/Co hardmetals in model single point abrasion experiments," *Tribol. Int.*, vol. 68, pp. 56–66, 2013, doi: 10.1016/j.triboint.2012.11.008.

[30] L. R. Rudnick, *Lubricant Additives*, 2nd ed. Third edition. | Boca Raton : CRC Press, Taylor & Francis Group, 2017.: CRC Press, 2017.

[31] M. Torbacke, Å. K. Rudolphi, and E. Kassfeldt, *Lubricants*. Chichester, UK: John Wiley & Sons, Ltd, 2014.

[32] "Viscosity index," *wiki.anton-paar.com*, 2021. https://wiki.anton-paar.com/hu-hu/viszkozitasi-index/.

[33] "SAE J300 - Engine Oil Viscosity Classification." Society of Automotive Engineers, 2021, doi: https://doi.org/10.4271/J300_202104.

[34] E. Richard Booser, *CRC Handbook of Lubrication and Tribology, Volume III*. 1993.

[35] R. M. Mortier, M. F. Fox, and S. Orszulik, Eds., *Chemistry and Technology of Lubricants*, 3rd ed. Dordrecht: Springer Netherlands, 2010.

[36] "Different oil question," *bimmerfest.com*, 2008. https://www.bimmerfest.com/threads/different-oil-question.1333525/.

[37] C. Bruce, "Watch The Oil Pour Out Of This Engine Like Peanut Butter," *motor1.com*, 2021. https://www.motor1.com/news/465984/oil-sludge-chevy-tahoe-video/.

[38] T. Sagawa, H. Fujimoto, and K. Nakamura, "Study of fuel dilution in direct-injection and multipoint injection gasoline engines," *SAE Tech. Pap.*, no. 724, 2002, doi: 10.4271/2002-01-1647.

[39] P. J. Shayler, L. D. Winborn, and A. Scarisbrick, "Fuel transport to the crankcase, oil dilution and HC return with breather flow during the cold operation of a SI engine," *SAE Tech. Pap.*, no. 724, 2000, doi: 10.4271/2000-01-1235.

[40] H. L. Costa and H. Spikes, "Effects of Ethanol Contamination on Friction and Elastohydrodynamic Film Thickness of Engine Oils," *Tribol. Trans.*, vol. 58, no. 1, pp. 158–168, 2015, doi: 10.1080/10402004.2014.957369.

[41] M. Hakeem, J. Anderson, G. Surnilla, and S. S. Yamada, "Characterization and speciation of fuel oil dilution in gasoline direct injection (DI) engines," in *ASME 2015 Internal Combustion Engine Division Fall Technical Conference, ICEF 2015*, 2015, vol. 1, doi: 10.1115/ICEF2015-1072.

[42] T. Hu, H. Teng, X. Luo, and B. Chen, "Impact of Fuel Injection on Dilution of Engine Crankcase Oil for Turbocharged Gasoline Direct-Injection Engines," *SAE Int. J. Engines*, vol. 8, no. 3, 2015, doi: 10.4271/2015-01-0967.

[43] P. Haenel, R. De Bruijn, D. Tomazic, and H. Kleeberg, "Analysis of the impact of production lubricant composition and fuel dilution on stochastic pre-ignition in turbocharged, direct-injection gasoline engines," *SAE Tech. Pap.*, vol. 2019-April, no. April, pp. 1–22, 2019, doi: 10.4271/2019-01-0256.

[44] P. I. Lacey, S. Gunsel, M. D. Ferner, M. Pozebanchuk, and A. Alim, "Effect of oil drain interval on crankcase lubricant quality," *SAE Tech. Pap.*, 2003, doi: 10.4271/2003-01-1957.

[45]   S. A. G. Watson and V. W. Wong, "The effects of fuel dilution with biodiesel and low sulfur diesel on lubricant acidity, oxidation and corrosion - A bench scale study with CJ-4 and CI-4+ lubricants," *2008 Proc. STLE/ASME Int. Jt. Tribol. Conf. IJTC 2008*, pp. 233–235, 2009, doi: 10.1115/ijtc2008-71221.

[46]   X. He, A. Williams, E. Christensen, J. Burton, and R. McCormick, "Biodiesel Impact on Engine Lubricant Dilution During Active Regeneration of Aftertreatment Systems," *SAE Int. J. Fuels Lubr.*, vol. 4, no. 2, pp. 158–178, Dec. 2011, doi: https://doi.org/10.4271/2011-01-2396.

[47]   S. K. Kurre, R. Garg, and S. Pandey, "A review of biofuel generated contamination, engine oil degradation and engine wear," *Biofuels*, vol. 8, no. 2, pp. 273–280, 2017, doi: 10.1080/17597269.2016.1224291.

[48]   L. S. Khuong *et al.*, "A review on the effect of bioethanol dilution on the properties and performance of automotive lubricants in gasoline engines," *RSC Adv.*, vol. 6, no. 71, pp. 66847–66869, 2016, doi: 10.1039/c6ra10003a.

[49]   A. Banerji, M. J. Lukitsch, and A. T. Alpas, "Friction reduction mechanisms in cast iron sliding against DLC: Effect of biofuel (E85) diluted engine oil," *Wear*, vol. 368–369, pp. 196–209, 2016, doi: 10.1016/j.wear.2016.09.001.

[50]   L. S. Khuong *et al.*, "Effect of gasoline-bioethanol blends on the properties and lubrication characteristics of commercial engine oil," *RSC Adv.*, vol. 7, no. 25, pp. 15005–15019, 2017, doi: 10.1039/c7ra00357a.

[51]   C. Besser, N. Dörr, F. Novotny-Farkas, K. Varmuza, and G. Allmaier, "Comparison of engine oil degradation observed in laboratory alteration and in the engine by chemometric data evaluation," *Tribol. Int.*, vol. 65, pp. 37–47, Sep. 2013, doi: 10.1016/j.triboint.2013.01.006.

[52]   P. Singh, V. Goel, and S. R. Chauhan, "Impact of dual biofuel approach on engine oil dilution in CI engines," *Fuel*, vol. 207. pp. 680–689, 2017, doi: 10.1016/j.fuel.2017.06.110.

[53]   H. L. Fang, S. D. Whitacre, E. S. Yamaguchi, and M. Boons, "Biodiesel Impact on Wear Protection of Engine Oils," 2007, doi: https://doi.org/10.4271/2007-01-

4141.

[54] A. K. Agarwal, J. Bijwe, and L. M. Das, "Effect of biodiesel utilization of wear of vital parts in compression ignition engine," *J. Eng. Gas Turbines Power*, vol. 125, no. 2, pp. 604–611, 2003, doi: 10.1115/1.1454114.

[55] M. Andreae, H. Fang, and K. Bhandary, "Biodiesel and Fuel Dilution of Engine Oil," 2007, doi: https://doi.org/10.4271/2007-01-4036.

[56] S. Sripad and V. Viswanathan, "Performance Metrics Required of Next-Generation Batteries to Make a Practical Electric Semi Truck," *ACS Energy Lett.*, vol. 2, no. 7, pp. 1669–1673, Jul. 2017, doi: 10.1021/acsenergylett.7b00432.

[57] "Chart library: Passenger vehicle fuel economy," *theicct.org*, 2021. https://theicct.org/chart-library-passenger-vehicle-fuel-economy.

[58] I. Ridjan, B. V. Mathiesen, D. Connolly, and N. Duić, "The feasibility of synthetic fuels in renewable energy systems," *Energy*, vol. 57, pp. 76–84, 2013, doi: 10.1016/j.energy.2013.01.046.

[59] A. Mohr and S. Raman, "Lessons from first generation biofuels and implications for the sustainability appraisal of second generation biofuels," *Effic. Sustain. Biofuel Prod. Environ. Land-Use Res.*, vol. 63, pp. 281–310, 2013, doi: 10.1016/j.enpol.2013.08.033.

[60] S. N. Naik, V. V. Goud, P. K. Rout, and A. K. Dalai, "Production of first and second generation biofuels: A comprehensive review," *Renew. Sustain. Energy Rev.*, vol. 14, no. 2, pp. 578–597, 2010, doi: 10.1016/j.rser.2009.10.003.

[61] R. E. Teixeira, "Energy-efficient extraction of fuel and chemical feedstocks from algae," *Green Chem.*, vol. 14, no. 2, pp. 419–427, 2012, doi: 10.1039/C2GC16225C.

[62] H. Shokravi *et al.*, "Fourth generation biofuel from genetically modified algal biomass: Challenges and future directions," *Chemosphere*, vol. 285, p. 131535, 2021, doi: https://doi.org/10.1016/j.chemosphere.2021.131535.

[63] B. Abdullah *et al.*, "Fourth generation biofuel: A review on risks and mitigation

strategies," *Renew. Sustain. Energy Rev.*, vol. 107, pp. 37–50, 2019, doi: https://doi.org/10.1016/j.rser.2019.02.018.

[64] S. Schemme, R. C. Samsun, R. Peters, and D. Stolten, "Power-to-fuel as a key to sustainable transport systems – An analysis of diesel fuels produced from CO 2 and renewable electricity," *Fuel*, vol. 205, pp. 198–221, Oct. 2017, doi: 10.1016/j.fuel.2017.05.061.

[65] N. Schmitz, J. Burger, E. Ströfer, and H. Hasse, "From methanol to the oxygenated diesel fuel poly(oxymethylene) dimethyl ether: An assessment of the production costs," *Fuel*, vol. 185, pp. 67–72, 2016, doi: 10.1016/j.fuel.2016.07.085.

[66] F. S. Zeman and D. W. Keith, "Carbon neutral hydrocarbons," *Philos. Trans. R. Soc. A Math. Phys. Eng. Sci.*, vol. 366, no. 1882, pp. 3901–3918, 2008, doi: 10.1098/rsta.2008.0143.

[67] S. Brynolf, M. Taljegard, M. Grahn, and J. Hansson, "Electrofuels for the transport sector: A review of production costs," *Renew. Sustain. Energy Rev.*, vol. 81, no. May, pp. 1887–1905, 2018, doi: 10.1016/j.rser.2017.05.288.

[68] H. Xiao, B. Hou, P. Zeng, A. Jiang, X. Hou, and J. Liu, "Combustion and emission characteristics of diesel engine fueled with 2,5-dimethylfuran and diesel blends," *Fuel*, vol. 192, pp. 53–59, 2017, doi: https://doi.org/10.1016/j.fuel.2016.12.007.

[69] P. Tamilselvan, N. Nallusamy, and S. Rajkumar, "A comprehensive review on performance, combustion and emission characteristics of biodiesel fuelled diesel engines," *Renew. Sustain. Energy Rev.*, vol. 79, no. May, pp. 1134–1159, 2017, doi: 10.1016/j.rser.2017.05.176.

[70] R. Sakthivel, K. Ramesh, R. Purnachandran, and P. Mohamed Shameer, "A review on the properties, performance and emission aspects of the third generation biodiesels," *Renew. Sustain. Energy Rev.*, vol. 82, no. 5, pp. 2970–2992, 2018, doi: 10.1016/j.rser.2017.10.037.

[71] B. Li, Y. Li, H. Liu, F. Liu, Z. Wang, and J. Wang, "Combustion and emission characteristics of diesel engine fueled with biodiesel/PODE blends," *Appl.*

Energy, vol. 206, pp. 425–431, 2017, doi: 10.1016/j.apenergy.2017.08.206.

[72] S. Manzetti and O. Andersen, "A review of emission products from bioethanol and its blends with gasoline. Background for new guidelines for emission control," *Fuel*, vol. 140, pp. 293–301, 2015, doi: 10.1016/j.fuel.2014.09.101.

[73] S. K. Thangavelu, A. S. Ahmed, and F. N. Ani, "Review on bioethanol as alternative fuel for spark ignition engines," *Renew. Sustain. Energy Rev.*, vol. 56, pp. 820–835, 2016, doi: 10.1016/j.rser.2015.11.089.

[74] A. K. Pandey, M. Nandgaonkar, P. Sivakumar, A. Veerabhadrappa, and A. Kumarasamy, "Comparison and evaluation of performance, emission and wear analysis of diesel, JP-8 and pura karanja biodiesel in a military 780 HP CIDI engine," in *Proceedings of the ASME 2013 International Mechanical Engineering Congress and Exposition*, 2013, pp. 1–9.

[75] M. Devitt, D. W. Drysdale, I. Macgillivray, A. J. Norrisf, R. Thompsonft, and J. W. Twidell, "Biofuel for transport: An investigation into the viability of rape methyl ester (RME) as an alternative to diesel fuel," *Int. J. Ambient Energy*, vol. 14, no. 4, pp. 195–218, 1993, doi: 10.1080/01430750.1993.9675617.

[76] A. Zare *et al.*, "The influence of oxygenated fuels on transient and steady-state engine emissions," *Energy*, vol. 121, no. 2017, pp. 841–853, 2017, doi: 10.1016/j.energy.2017.01.058.

[77] A. Zare *et al.*, "Diesel engine emissions with oxygenated fuels: A comparative study into cold-start and hot-start operation," *J. Clean. Prod.*, vol. 162, pp. 997–1008, 2017, doi: 10.1016/j.jclepro.2017.06.052.

[78] S. E. Iannuzzi, C. Barro, K. Boulouchos, and J. Burger, "POMDME-diesel blends: Evaluation of performance and exhaust emissions in a single cylinder heavy-duty diesel engine," *Fuel*, vol. 203, pp. 57–67, 2017, doi: 10.1016/j.fuel.2017.04.089.

[79] M. A. Costagliola *et al.*, "Performances and emissions of a 4-stroke motorcycle fuelled with ethanol/gasoline blends," *Fuel*, vol. 183, no. 2016, pp. 470–477, 2016, doi: 10.1016/j.fuel.2016.06.105.

[80]   S. López-Aparicio and C. Hak, "Evaluation of the use of bioethanol fuelled buses based on ambient air pollution screening and on-road measurements," *Sci. Total Environ.*, vol. 452–453, no. 2013, pp. 40–49, 2013, doi: 10.1016/j.scitotenv.2013.02.046.

[81]   "ASTM D6078-04(2016), Standard Test Method for Evaluating Lubricity of Diesel Fuels by the Scuffing Load Ball-on-Cylinder Lubricity Evaluator (SLBOCLE)." ASTM International, West Conshohocken, 2016, doi: 10.1520/D6078-04R16.

[82]   "ASTM D6079-11(2016), Standard Test Method for Evaluating Lubricity of Diesel Fuels by the High-Frequency Reciprocating Rig (HFRR)." ASTM International, West Conshohocken, 2016, doi: 10.1520/D6079-11R16.

[83]   "ISO 12156-1:2018 Diesel fuel—Assessment of lubricity using the high-frequency reciprocating rig (HFRR)—Part 1: Test method." International Organization for Standardization, Geneva, p. 14, 2018, [Online]. Available: https://www.iso.org/standard/72481.html.

[84]   "ASTM D975-20c, Standard Specification for Diesel Fuel." ASTM International, West Conshohocken, 2020, doi: 10.1520/D0975-20C.

[85]   "EN 590:2013+A1:2017 - Automotive fuels - Diesel - Requirements and test methods." European Committee For Standardization, 2017, [Online]. Available: https://standards.cen.eu/dyn/www/f?p=204:110:0::::FSP_PROJECT,FSP_ORG _ID:64612,6003&cs=1002EF349397DF1DD4B165A4BA1679FE0.

[86]   A. K. Agarwal, J. Bijwe, and L. M. Das, "Wear assessment in a biodiesel fueled compression ignition engine," *J. Eng. Gas Turbines Power*, vol. 125, no. 3, pp. 820–826, 2003, doi: 10.1115/1.1501079.

[87]   D. X. Peng, "Tribological performance of various types of biodiesel," *Mater. Trans.*, vol. 56, no. 12, pp. 1953–1959, 2015, doi: 10.2320/matertrans.M2015263.

[88]   M. M. Rahman, M. Rasul, and N. M. S. Hassan, "Study on the tribological characteristics of Australian native first generation and second generation biodiesel fuel," *Energies*, vol. 10, no. 1, 2017, doi: 10.3390/en10010055.

[89] Y. Xu, X. Hu, K. Yuan, G. Zhu, and W. Wang, "Friction and wear behaviors of catalytic methylesterified bio-oil," *Tribol. Int.*, vol. 71, pp. 168–174, 2014, doi: 10.1016/j.triboint.2013.11.018.

[90] M. A. Fazal, A. S. M. A. Haseeb, and H. H. Masjuki, "Investigation of friction and wear characteristics of palm biodiesel," *Energy Convers. Manag.*, vol. 67, pp. 251–256, 2013, doi: https://doi.org/10.1016/j.enconman.2012.12.002.

[91] K. C. Corkwell and M. M. Jackson, "Lubricity and Injector Pump Wear Issues with E diesel Fuel Blends," 2002, doi: https://doi.org/10.4271/2002-01-2849.

[92] A. S. M. A. Haseeb, M. A. Fazal, M. I. Jahirul, and H. H. Masjuki, "Compatibility of automotive materials in biodiesel: A review," *Fuel*, vol. 90, no. 3, pp. 922–931, 2011, doi: 10.1016/j.fuel.2010.10.042.

[93] B. Singh, J. Korstad, and Y. C. Sharma, "A critical review on corrosion of compression ignition (CI) engine parts by biodiesel and biodiesel blends and its inhibition," *Renew. Sustain. Energy Rev.*, vol. 16, no. 5, pp. 3401–3408, 2012, doi: 10.1016/j.rser.2012.02.042.

[94] K. A. Sorate and P. V. Bhale, "Biodiesel properties and automotive system compatibility issues," *Renew. Sustain. Energy Rev.*, vol. 41, pp. 777–798, 2015, doi: 10.1016/j.rser.2014.08.079.

[95] E. Hu, Y. Xu, X. Hu, L. Pan, and S. Jiang, "Corrosion behaviors of metals in biodiesel from rapeseed oil and methanol," *Renew. Energy*, vol. 37, no. 1, pp. 371–378, 2012, doi: 10.1016/j.renene.2011.07.010.

[96] D. L. Cursaru, G. Brănoiu, I. Ramadan, and F. Miculescu, "Degradation of automotive materials upon exposure to sunflower biodiesel," *Ind. Crops Prod.*, vol. 54, pp. 149–158, 2014, doi: 10.1016/j.indcrop.2014.01.032.

[97] J. Burger, M. Siegert, E. Ströfer, and H. Hasse, "Poly(oxymethylene) dimethyl ethers as components of tailored diesel fuel: Properties, synthesis and purification concepts," *Fuel*, vol. 89, no. 11, pp. 3315–3319, 2010, doi: 10.1016/j.fuel.2010.05.014.

[98] L. Lautenschütz, D. Oestreich, P. Seidenspinner, U. Arnold, E. Dinjus, and J. Sauer, "Physico-chemical properties and fuel characteristics of oxymethylene dialkyl ethers," *Fuel*, vol. 173, pp. 129–137, 2016, doi: 10.1016/j.fuel.2016.01.060.

[99] E. Hu, X. Hu, X. Wang, Y. Xu, K. D. Dearn, and H. Xu, "On the fundamental lubricity of 2,5-dimethylfuran as a synthetic engine fuel," *Tribol. Int.*, vol. 55, pp. 119–125, 2012, doi: 10.1016/j.triboint.2012.06.005.

[100] E. Sukjit, P. Poapongsakorn, K. D. Dearn, M. Lapuerta, and J. Sánchez-Valdepeñas, "Investigation of the lubrication properties and tribological mechanisms of oxygenated compounds," *Wear*, vol. 376–377, pp. 836–842, 2017, doi: 10.1016/j.wear.2017.02.007.

[101] L. G. R. Lopreato, E. J. De Oliveira, and M. V. E. Duarte, "Gasoline lubricity: An exploratory evaluation," *SAE Tech. Pap.*, no. October, 2012, doi: 10.4271/2012-36-0502.

[102] P. Arkoudeas, D. Karonis, E. Lois, and F. Zannikos, "Lubricity assessment of gasoline fuels," *Fuel Process. Technol.*, vol. 122, p. 12, 2014.

[103] D. P. Wei, H. A. Spikes, and S. Korcek, "The Lubricity of Gasoline," *Tribol. Trans.*, vol. 42, no. 4, pp. 813–823, 1999, doi: 10.1080/10402009908982288.

[104] M. Oguma, M. Matsuno, M. Kaitsuka, and K. Higurashi, "Evaluation of Hydrous Ethanol Fuel Lubricity by HFRR," 2016, doi: https://doi.org/10.4271/2016-01-2260.

[105] T. Dubois, L. Abiad, and P. Caine, "Investigating the Impact of Ethanol on the Lubricity of Gasoline and on the Lubricity Improvers Efficiency," 2017, doi: https://doi.org/10.4271/2017-01-2297.

[106] F. Gustavsson, P. Forsberg, and S. Jacobson, "Friction and wear behaviour of low-friction coatings in conventional and alternative fuels," *Tribol. Int.*, vol. 48, pp. 22–28, 2012, doi: 10.1016/j.triboint.2011.06.001.

[107] F. F. Rovai, D. K. Tanaka, and A. Sinatora, "Wear and Corrosion Evaluation of

Electric Fuel Pumps with Ethanol/Gasoline Blends," in *2005 Brasil Fuels & Lubricants Meeting and Exhibition*, 2005, p. 12.

[108] "ISO 19291:2016, Lubricants — Determination of tribological quantities for oils and greases — Tribological test in the translatory oscillation apparatus." International Organization for Standardization, Geneva, 2016, [Online]. Available: https://www.iso.org/standard/64298.html.

[109] N. Dörr, A. Agocs, C. Besser, A. Ristić, and M. Frauscher, "Engine Oils in the Field: A Comprehensive Chemical Assessment of Engine Oil Degradation in a Passenger Car," *Tribol. Lett.*, vol. 67, no. 3, 2019, doi: 10.1007/s11249-019-1182-7.

[110] "ASTM D7042-21, Standard Test Method for Dynamic Viscosity and Density of Liquids by Stabinger Viscometer (and the Calculation of Kinematic Viscosity)." ASTM International, West Conshohocken, 2021.

[111] "ASTM D2270-10(2016), Standard Practice for Calculating Viscosity Index from Kinematic Viscosity at 40 °C and 100 °C." ASTM International, West Conshohocken, 2016.

[112] "ISO 3771:2011 Petroleum products — Determination of base number — Perchloric acid potentiometric titration method." International Organization for Standardization.

[113] "ASTM E2412-10(2018), Standard Practice for Condition Monitoring of In-Service Lubricants by Trend Analysis Using Fourier Transform Infrared (FT-IR) Spectrometry." ASTM International, West Conshohocken, 2018, doi: 10.1520/E2412-10R18.

[114] "DIN 51777 Petroleum products - Determination of water content using titration according to Karl Fischer." Deutsches Institut Fur Normung E.V., p. 30, 2020, doi: 10.31030/3120598.

[115] "ASTM D3525-20, Standard Test Method for Gasoline Fuel Dilution in Used Gasoline Engine Oils by Wide-Bore Capillary Gas Chromatography." ASTM International, West Conshohocken, 2020, doi: 10.1520/D3525-20.

[116] "ASTM D3524-14(2020), Standard Test Method for Diesel Fuel Diluent in Used Diesel Engine Oils by Gas Chromatography." ASTM International, West Conshohocken, 2020, doi: 10.1520/D3524-14R20.

[117] A. Singer, W. Ruck, and J. Krahl, "Influence of Different Biogenic Fuels on Base Oil Aging," *SAE Tech. Pap.*, vol. 2014-Octob, 2014, doi: 10.4271/2014-01-2788.

[118] C. Besser *et al.*, "Generation of engine oils with defined degree of degradation by means of a large scale artificial alteration method," *Tribol. Int.*, vol. 132, pp. 39–49, 2019, doi: https://doi.org/10.1016/j.triboint.2018.12.003.

[119] J. A. Rice, *Mathematical Statistics and Data Analysis*, 3rd ed. Hampshire: Cengage Learning, 2007.

[120] "NIST/SEMATECH e-Handbook of Statistical Methods," *2012*, 2021. http://www.itl.nist.gov/div898/handbook/.

[121] R. A. FISHER, "THE USE OF MULTIPLE MEASUREMENTS IN TAXONOMIC PROBLEMS," *Ann. Eugen.*, vol. 7, no. 2, pp. 179–188, 1936, doi: https://doi.org/10.1111/j.1469-1809.1936.tb02137.x.

[122] M. Morcos, G. Parsons, F. Lauterwasser, M. Boons, and W. Hartgers, "Detection Methods for Accurate Measurements of the FAME Biodiesel Content in Used Crankcase Engine Oil," Nov. 2009, doi: https://doi.org/10.4271/2009-01-2661.

[123] O. O. Ajayi, C. Lorenzo-Martin, G. Fenske, J. Corlett, C. Murphy, and S. Przesmitzki, "Bioderived Fuel Blend Dilution of Marine Engine Oil and Impact on Friction and Wear Behavior," *J. Tribol.*, vol. 138, no. 2, pp. 1–11, 2016, doi: 10.1115/1.4031781.

[124] K. Mori, N. Sugimoto, K. Yamane, and K. Kawasaki, "Influence of Biodiesel Fuel on Lubricant Oil Oxidative Degradation," 2015, doi: https://doi.org/10.4271/2015-01-2030.

[125] M. D. Johnson, S. Korcek, R. K. Jensen, A. K. Gangopadhyay, and E. A. Soltis, "Laboratory assessment of the oxidation and wear performance capabilities of low phosphorus engine oils," *SAE Tech. Pap.*, no. 724, 2001, doi: 10.4271/2001-

01-3541.

[126] J. Kral, B. Konecny, J. Kral, K. Madac, G. Fedorko, and V. Molnar, "Degradation and chemical change of longlife oils following intensive use in automobile engines," *Measurement*, vol. 50, pp. 34–42, 2014, doi: https://doi.org/10.1016/j.measurement.2013.12.034.

[127] A. Yaguchi and K. Inoue, "Development and field test performance of fuel efficient SAE 5W-20 oils," 1995, doi: 10.4271/952341.

[128] C. S. Koh and J. B. Butt, "Experimental and Modeling Study of Kinetics and Selectivity in the Oxidation of a Poly(α-olefin) Lubricant," *Ind. Eng. Chem. Res.*, vol. 34, no. 2, pp. 524–535, 1995, doi: 10.1021/ie00041a013.

[129] M. Wattrus, "Fuel Property Effects on Oil Dilution in Diesel Engines," *SAE Int. J. Fuels Lubr.*, vol. 6, no. 3, pp. 794–806, 2013, doi: 10.4271/2013-01-2680.

[130] "ASTM D7279 - 16, Standard Test Method for Kinematic Viscosity of Transparent and Opaque Liquids by Automated Houillon Viscometer." ASTM International, West Conshohocken, 2016, doi: 10.1520/D7279-16.

[131] "ASTM D664-11a, Standard Test Method for Acid Number of Petroleum Products by Potentiometric Titration." ASTM International, West Conshohocken, 2011, doi: 10.1520/D0664-11A.

[132] "ASTM D2896-15, Standard Test Method for Base Number of Petroleum Products by Potentiometric Perchloric Acid Titration." ASTM International, West Conshohocken, 2015, doi: 10.1520/D2896-15.

[133] "ASTM D5185-13e1, Standard Test Method for Multielement Determination of Used and Unused Lubricating Oils and Base Oils by Inductively Coupled Plasma Atomic Emission Spectrometry (ICP-AES)." ASTM International, West Conshohocken, 2013, doi: 10.1520/D5185-13E01.

[134] "DIN 51452, Testing of lubricants; Determination of the soot content in used diesel engine oils; Infrared Spectrometry." Deutsches Institut Fur Normung E.V., p. 2, 1994, [Online]. Available:

https://global.ihs.com/doc_detail.cfm?document_name=DIN 51452&item_s_key=00252643.

[135] "ISO 683-17:2014, Heat-treated steels, alloy steels and free-cutting steels — Part 17: Ball and roller bearing steels." International Organization for Standardization, Geneva, 2014, [Online]. Available: https://www.iso.org/standard/57231.html.

[136] H. Baş and Y. E. Karabacak, "Investigation of the Effects of Boron Additives on the Performance of Engine Oil," *Tribol. Trans.*, vol. 57, no. 4, pp. 740–748, 2014, doi: 10.1080/10402004.2014.909549.

[137] J. Sahu, K. Panda, B. Gupta, N. Kumar, P. A. Manojkumar, and M. Kamruddin, "Enhanced tribo-chemical properties of oxygen functionalized mechanically exfoliated hexagonal boron nitride nanolubricant additives," *Mater. Chem. Phys.*, vol. 207, pp. 412–422, 2018, doi: https://doi.org/10.1016/j.matchemphys.2017.12.050.

[138] Q. Wan, Y. Jin, P. Sun, and Y. Ding, "Tribological Behaviour of a Lubricant Oil Containing Boron Nitride Nanoparticles," *Procedia Eng.*, vol. 102, pp. 1038–1045, 2015, doi: https://doi.org/10.1016/j.proeng.2015.01.226.

[139] L. Wang, H. Wu, D. Zhang, G. Dong, X. Xu, and Y. Xie, "Synthesis of a novel borate ester containing a phenylboronic group and its tribological properties as an additive in PAO 6 base oil," *Tribol. Int.*, vol. 121, pp. 21–29, 2018, doi: https://doi.org/10.1016/j.triboint.2018.01.033.

[140] "ISO 3833:1977 Road vehicles — Types — Terms and definitions." International Organization for Standardization, Geneva, 1977, [Online]. Available: https://www.iso.org/standard/9389.html.

[141] Y. Zhou, W. Li, B. C. Stump, R. M. Connatser, S. Lazarevic, and J. Qu, "Impact of Fuel Contents on Tribological Performance of PAO Base Oil and ZDDP," *Lubricants*, vol. 6, no. 3, 2018, doi: 10.3390/lubricants6030079.

[142] M. Härtl, P. Seidenspinner, E. Jacob, and G. Wachtmeister, "Oxygenate screening on a heavy-duty diesel engine and emission characteristics of highly

oxygenated oxymethylene ether fuel OME1," *Fuel*, vol. 153, pp. 328–335, 2015, doi: 10.1016/j.fuel.2015.03.012.

[143] F. Kleiner, M. Kaspar, C. Artmann, and H. P. Rabl, "Online Oil Dilution Measurement at GDI Engines," *SAE Tech. Pap.*, vol. 2014-Octob, 2014, doi: 10.4271/2014-01-2591.

[144] R. B. Jones and R. C. Coy, "Chemistry of the Thermal Degradation of Zinc Dialkyldithiophosphate Additives.," *Prepr. - Tribol. Conf.*, no. October 2012, pp. 37–41, 1979.

[145] P. Peng, S.-Z. Hong, and W.-Z. Lu, "The degradation of zinc dialkyldithiophosphate additives in fully formulated engine oil as studied by P-31 NMR spectroscopy," *Lubr. Eng.*, vol. 50, no. 3, pp. 230–235, 1994, [Online]. Available: https://www.osti.gov/biblio/393913-degradation-zinc-dialkyldithiophosphate-additives-fully-formulated-engine-oil-studied-nmr-spectroscopy.

[146] S. Ferguson, J. Johnson, D. Gonzales, C. Hobbs, C. Allen, and S. Williams, "Analysis of ZDDP Content and Thermal Decomposition in Motor Oils Using NAA and NMR," *Phys. Procedia*, vol. 66, pp. 439–444, 2015, doi: 10.1016/j.phpro.2015.05.055.

[147] Mahle GmbH, Ed., *Pistons and engine testing*. Wiesbaden: Vieweg+Teubner Verlag, 2012.

[148] A. Agocs *et al.*, "Feldstudie über die Motorölalterung in Personenkraftwagen," in *Tribologie und Schmierungstechnik*, 2020, vol. 67, no. 5–6, pp. 78–79.

[149] "Safe Handling Guidelines for ZDDP Components and Blends." American Chemistry Council, Washington, 2015.

[150] G. Marton, "Kísérleti módszerfejlesztés mesterségesen öregített kenőolajok tesztelésére súrlódás és kopásmérő próbapadon," Széchenyi István Egyetem, 2021.